2013

Behaviour of shape-modified columns confined with carbon fibre-reinforced polymer under eccentric loading

Viet Le Doan
University of Wollongong, vld143@uowmail.edu.au

UNIVERSITY OF WOLLONGONG

Faculty of Engineering

Behaviour of Shape-Modified Columns Confined with Carbon Fibre-Reinforced Polymer under Eccentric Loading

Le V. Doan, BEng

"This thesis is presented as part of the requirements for the award of the Degree of Master of Engineering (Research) of the University of Wollongong"

June 2013

CERTIFICATION

I, Le V. Doan, declare that this thesis, submitted in partial fulfillment of the requirements for the award of Master of Engineering (Research), in the School of Civil, Mining and Environmental Engineering, Faculty of Engineering, University of Wollongong, is wholly my own work unless otherwise referenced or acknowledged. The document has not been submitted for qualifications at any other academic institution.

Le V. Doan

June 2013

ABSTRACT

Fibre Reinforced Polymer (FRP) has been popularly used to improve the load-carrying capacity and ductility of columns. Early research studies have indicated that confinement enhancement of FRP wrapped circular columns is more efficient than that of square/rectangular RC columns. Most existing columns, however, are square/rectangular in cross-section. This study presents a retrofitting method for square reinforced concrete (RC) columns using shape modification and FRP wrapping. The cross-section of RC columns is changed from a square to a circle before confining them with FRP to maximise the confining pressure of FRP.

Sixteen square RC columns (150 mm in side length by 800 mm in height) were cast with 40 MPa concrete and divided into four groups. The specimens of the first group were tested without further modification and their four specimens served as a reference group. Each column from the twelve remaining square RC columns in the second, third and fourth groups were bonded with four pieces of segmental circular concrete covers, which had nominal compressive strength of 40 MPa, 80 MPa and 100 MPa, respectively. The shape-modified columns were then wrapped with three layers of Carbon FRP (CFRP). From each group, three of the four columns were tested under different eccentric loadings including 0 mm (concentric), 25 mm, 50 mm eccentricity, and the remaining specimen in each group was tested under flexural bending to failure. The effectiveness of the proposed retrofitting using shape modification and CFRP wrapping was investigated.

A theoretical study was then implemented taking into account the interaction between the internal transverse steel reinforcement and the external FRP jacket. The analytical values were validated with the experimental data and good agreement was found.

Conclusions are drawn and recommendations for future research are proposed.

To my parents and sisters

ACKNOWLEDGEMENTS

First and foremost, I would like to express my heartfelt gratitude to Associate Professor Muhammad N. S. Hadi for his endless patience, guidance and enthusiastic support throughout my study. His rigorous approaches to academic research and depth of knowledge in structural engineering have greatly benefitted me to become a mature researcher. I am honoured to have studied with him as my research supervisor.

I wish to acknowledge special contribution from Mr Thong M. Pham, PhD scholar, for participating in the whole experimental program. His advice and assistance is greatly appreciated. Meanwhile, I would like to thank Dr Alisa Percy for her valuable guidance on academic language from the beginning of my study.

I am grateful to both the University of Da Nang and the University of Wollongong for their financial support. I am also grateful to the University of Wollongong for providing the research facilities.

I wish to acknowledge the technical assistance of Messers Alan Grant, Fernando Escribano, Cameron Neilson, Ritchie McLean, Colin Devenish and Ian Laird. Their technical expertise and experience made the testing efficiently and effectively during various stages. I also thank Mr. Eric Lume for his advice on casting HSC.

Last but certainly not least, I am greatly indebted to my parents and two my sisters for their constant understanding, encouragement and love, without which my achievements would have never been able to be accomplished.

PUBLICATION LIST

Conference paper

Le V. Doan., Xu Lei., Thong M. Pham. and Muhammad N.S. Hadi 2013, "Effect of FRP and transverse steel dual confinement on retrofitting square concrete columns." accepted by 4th Asia-Pacific Conference on FRP in Structures, Melbourne, Australia, 11st-13rd December 2013.

Thong M. Pham, Le V. Doan and Muhammad N.S. Hadi (2013), "Behavior of modified RC columns retrofitted with CFRP." accepted by 26th Biennial Conference of the Concrete Institute, Queensland, Australia, 16th-18th October 2013.

Pham, T. M., Doan, L. V., and Hadi, M. N. S. (2013) "Strengthening Square Reinforced Concrete Columns by Shape Modification and CFRP." Proc., Structures Congress 2013, American Society of Civil Engineers, 2602-2613.

Journal Paper

Pham, T. M., Doan, L. V., and Hadi, M. N. S. (2013). "Strengthening square reinforced concrete columns by circularisation and FRP confinement." Construction and Building Materials, 49, 490-499.

TABLE OF CONTENTS

LIST OF FIGURES

LIST OF TABLES

CHAPTER 1. INTRODUCTION

1.1 Overview

Structures are usually designed to a last long time. However, sometimes structures need to be strengthened due to an increase in the applied load or deteriorated structural members, such as concrete columns that have deteriorated due to the corrosion of reinforcing steel. To this end, the use of concrete jackets and fiber reinforced polymer (FRP) wrapping is suitable to improve the performance of columns in terms of the load carrying capacity and ductility. The retrofitting method using the concrete jackets has serious disadvantages compared to the FRP wrapping, including the increase in weight of structure and cross-section size. Being a lightweight material, excellent corrosion resistance and ease of onsite handling are typical properties of FRP that make it ideal for retrofitting application. For these reasons, FRP has been widely used in construction and structural rehabilitation.

FRP has been popularly used to strengthen reinforced and pre-stressed concrete, timber, masonry, and metal structures. FRP has been used for flexural strengthening of beams and slabs, shear strengthening of concrete beams, and axial strengthening and ductility enhancement of concrete columns.

This study investigates a new method for retrofitting square RC columns by modifying the cross-section from a square to circle and confining them with CFRP. The load carrying capacity, load–deflection responses, failure modes and the CFRP strain distribution in the hoop direction of the columns are discussed.

1.2 Significance and Objective

Most existing columns are square/rectangular in cross-section. Early research studies have indicated that confinement enhancement of FRP wrapped rectangular RC columns is less efficient than that of circular columns because of the knife-effect (Hadi et al. 2013; Harries and Carey 2003; Pellegrino and Modena 2010; Pessiki et al. 2001; Silva 2011; Toutanji et al. 2010). Therefore, in order to maximise the confinement of FRP wrapped square and rectangular RC columns, the column's

shape could be modified from a square/rectangular to circular section. Hadi et al. (2013) proposed a successful modification method for strengthening existing square columns. These columns were circularised by bonding four segmental circular plain concrete covers, which had the same concrete strength. In this study, the covers were cast from normal strength concrete (NSC) of 40 MPa to high strength concrete (HSC) of 80 MPa and 100 MPa, while the compressive strength of the square columns was 40 MPa. The higher compressive concrete strength of the segmental covers should give higher load-carrying capacity compared to NSC. The effectiveness of the retrofitting method was examined in this study.

The majority of past research on FRP-confined concrete have examined the behaviour of concentrically loaded columns from small scale to large scale specimens. These tests have been useful as a means of accurately characterizing the stress-strain behaviour of FRP-confined concrete and FRP confinement under concentric load are now reasonably well understood. However, few studies are availabe on eccentrically loaded FRP-confined columns, and recently were design guidelines developed to account for axial load and bending moment (P-M) interaction (Concrete Society 2012; ACI 440.2R 2008). The FRP confinement is less effective when columns are subjected to higher eccentricity (Bisby and Ranger 2010; Fam et al. 2003; Guan et al. 2011; Hadi 2005, 2006, 2007, 2009, 2010; Hadi and Widiarsa 2012; Li and Hadi 2003; Wu and Jiang 2012). The test results of Fam et al. (2003) indicated that increasing the eccentricity results in a strain gradient that subjects a large part of the cross section to tensile strain, which significantly reduces the level of confinement. As the behaviour of columns confined with FRP under eccentric loadings is complicated, very little research studies have focused on this problem.

In this study, sixteen square RC columns were cast with 40 MPa concrete. These specimens consisted of four specimens served as the reference columns and twelve specimens served as the shape-modified columns. The shape-modified specimens were circularised by bonding four pieces of segmental circular concrete covers and

wrapped with CFRP. The concrete covers were made from NSC of 40 MPa to HSC of 80 MPa and 100 MPa. All the specimens were tested to failure under various eccentric loading conditions.

The objective of the research program presented in this study is to investigate the effectiveness of the proposed retrofitting method for square RC columns using the shape modification and FRP wrapping. The specific objectives of this study are as follows:

1. Conduct an experimental and theoretical program to examine the increase in load-carrying capacity and ductility of retrofitted RC columns compared to unconfined RC columns.

2. Examine the effect of eccentricity on the performance of both unconfined and FRP-confined concrete columns.

3. Compare the efficiency of bonding segmental circular plain concrete covers using different grades of concrete in enhanced load-carrying capacity and ductility.

4. Observe the mechanics of confinement for FRP wrapped columns subjected to combined axial and bending moment.

5. Present the proposed approaches to evaluate the axial load-bending moment behaviour of FRP-confined columns and then validate by experimental results.

1.3 Thesis outline

The current chapter presents an overview of the retrofitting method using the shape modification and the external FRP confinement, research significance, and research objectives.

Chapter 2 presents a summary of the current research on confined concrete pertaining to the confined effect of transverse steel, FRP, and both transverse steel and FRP. The characteristics of the confined column wrapped with FRP are introduced to examine the effectiveness of FRP's confinement. The chapter ends with a discussion of research gaps addressed in this study.

Chapter 3 consists of the experimental program, including the processes of modifying square RC columns, wrapping CFRP and testing procedures. Ancillary tests conducted to determine the mechanical properties of various constituent materials used in the current study are also described.

Chapter 4 presents the analysis of experimental results, which include load-carrying capacity, axial and lateral deflection of CFRP confined RC columns. The effects of the compressive strengths of concrete covers on the performance of FRP-confined column are also assessed. Furthermore, the strain distribution in hoop direction of FRP confined columns subjected to various loading conditions is discussed.

Chapter 5 presents the model to predict the axial load-bending moment interaction behaviour of both unconfined and FRP-confined RC columns. Test results from Chapter 4 are used for the purposes of comparison and validation.

The thesis closes with Chapter 6, where the conclusions from previous chapter are reviewed and the recommendations for further research are expressed.

CHAPTER 2. LITERATURE REVIEW

2.1 Introduction

This chapter presents are view of confined concrete considering the effects of transverse steel, Fiber Reinforced Polymer (FRP) and the dual confinement of transverse steel and FRP. It then identifies the key parameters on the behaviour of FRP-confined concrete affecting strength and ductility of confined columns.

2.2 Steel-confined concrete

The confinement of reinforced concrete columns involves the provision of sufficient transverse steel reinforcement in the form of helix or circular hoop or rectangular arrangements to prevent bucking of the longitudinal bars and shear failure. Tests have shown that the strength and ductility of compressive concrete are increased as a result of transverse steel reinforcement confinement. Under the uniaxial load, the cover concrete is unconfined and becomes ineffective after the compressive strength is achieved. However, the core concrete continues to carry load to failure.

There have been a wide variety of steel-confined concrete models proposed (Cedolin et al. 1977; Cusson and Paultre 1995; Hognestad 1951; Imran and Pantazopoulou 1996; Lan and Guo 1997; Légeron and Paultre 2003; Madas and Elnashai 1992; Sfer et al. 2002); however, the models of Richart et al. (1929; 1928) and Mander et al. (1988a, 1988b) have been adopted in engineering practices and employed by many FRP-confined concrete models.

The model of Mander et al. (1988a) is based on the assumption of active confinement, which gives constant and uniform confinement to core concrete. This model uses Popovics' (1973) model of the stress-strain relationship of steel-confined concrete, as illustrated in Figure 2.1. In Popovics' model, for a low strain rate and monotonic loading, the compressive concrete stress f_c is given by:

$$f_c = \frac{f'_{cc}(\varepsilon_c/\varepsilon_{cc})r}{r-1+(\varepsilon_c/\varepsilon_{cc})^r} \tag{2.1}$$

where ε_c is compressive strain of concrete corresponding to axial stress f_c; f'_{cc} and ε_{cc} are compressive strength or peak stress and corresponding compressive strain of confined concrete.

$$r = \frac{E_c}{E_c - E_{sec}} \tag{2.2}$$

where $E_c = 5000\sqrt{f_{co}^{'}}$ MPa is the tangent modulus of elasticity of the concrete.

$E_{sec} = \frac{f_{cc}^{'}}{\varepsilon_{cc}}$ is the second modulus of concrete.

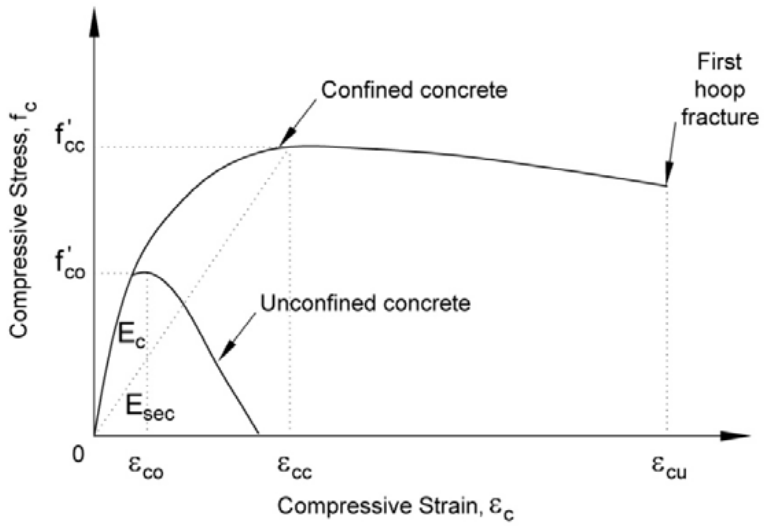

Figure 2.1 Stress-strain curve of confined and unconfined concrete (Mander et al. 1988a)

It can be seen from Figure 2.1 that the compressive strength and the ultimate strain of confined concrete are much higher than that of unconfined concrete.

To determine the compressive strength ($f_{cc}^{'}$) and corresponding axial strain under constant confinement pressure, Richart et al. (1928) presented Equation (2.3) and (2.4) using concrete specimens confined with active hydrostatic pressure:

$$f_{cc}^{'} = f_{co}^{'} + 4.1 f_l \tag{2.3}$$

$$\varepsilon_{cc} = \varepsilon_{co}\left[1 + 5\left(\frac{f_{cc}^{'}}{f_{co}^{'}} - 1\right)\right] \tag{2.4}$$

where $f_{co}^{'}$ and ε_{co} are the compressive strength of unconfined concrete and the corresponding axial strain; f_l is the confining pressure or lateral pressure.

The effective confining pressure is approached in Mander et al. (1988a) model, which is similar to the method investigated by Sheikh and Uzumeri (1980). Figure 2.2 shows the arching action that is assumed to occur between the two levels of transverse circular and rectangular reinforcement. The area in the middle of

transverse reinforcement is the smallest area of confinement due to the arching effect. For this reason, Mander et al. (1988a) proposed the confinement effectiveness coefficient given by Equations (2.5), (2.6) and (2.7) to determine the actual confining pressure.

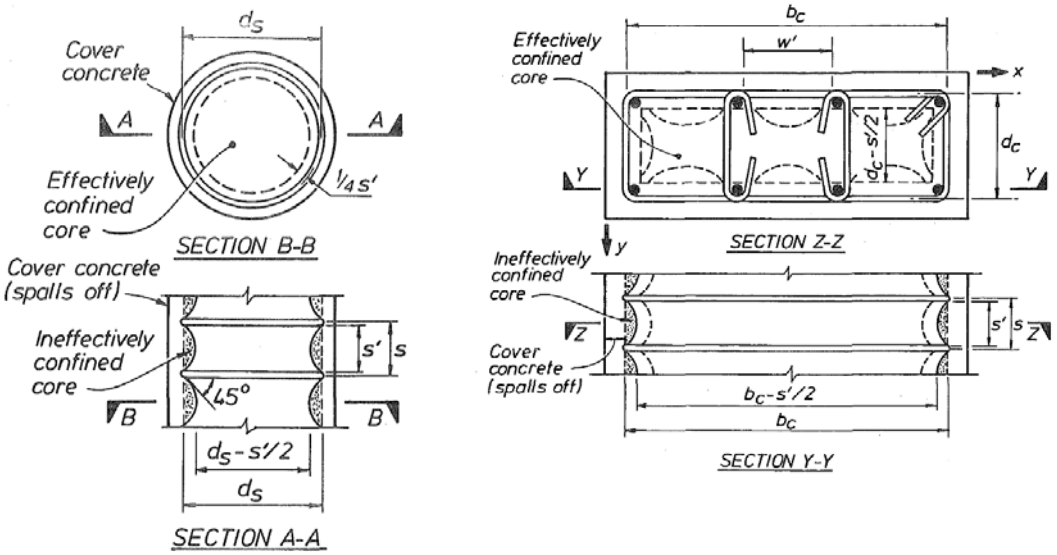

Figure 2.2 Effectively confined area of circular hoop reinforcement

(Mander et al. 1988a)

For circular hoops:

$$k_e = \frac{\left(1 - \frac{s^s}{2d_s}\right)^2}{1 - \rho_{cc}} \tag{2.5}$$

For circular helices:

$$k_e = \frac{1 - \frac{s^s}{2d_s}}{1 - \rho_{cc}} \tag{2.6}$$

For rectangular hoops:

$$k_e = \frac{\left(1 - \sum_{i=1}^{n} \frac{\left(w_i^{'}\right)^2}{6b_c d_c}\right)\left(1 - \frac{s^{'}}{2b_c}\right)\left(1 - \frac{s^{'}}{2d_c}\right)}{1 - \rho_{cc}} \tag{2.7}$$

where ρ_{cc} is ratio of area of longitudinal reinforcement to area of core of section;

$w_i^{'}$ is the i_{th} clear distance between adjacent longitudinal bars; b_c and d_c are core dimensions to centerlines of perimeter hoop in x and y directions, respectively, where $b_c \geq d_c$.

The actual confining pressure or effective confining pressure is given by:

$$f_l^{'} = f_l \, .k_e \tag{2.8}$$

where f_l is the lateral confining pressure found by considering the half body confined by a spiral or circular hoop. Based on the assumption of active confinement, uniform hoop tension was developed by the transverse steel at yield. The lateral stress on the concrete core is derived from the forces of equilibrium:

$$f_l = \frac{2 f_{sy} A_{sp}}{s d_c} \tag{2.9}$$

where s is centre to centre spacing of the spiral or circular hoop; d_c is diameter of concrete core, measured center to centre of the spiral or circular hoop; f_{sy} is steel yield stress; and A_{sp} is area of transverse steel cross section.

Mander et al. (1988a) adopted the equation of compressive strength of William and Warnke (1975) based on the "five parameter" multiaxial failure surface given by Equation (2.10). The solution of the failure criterion is presented in terms of the two lateral confining stresses. When the confined concrete core is placed in triaxial compression with equal effective lateral confining pressure from transverse steel, the confined compressive strength is given as follows:

$$f_{cc}^{'} = f_{co}^{'}(-1.254 + 2.254\sqrt{1 + \frac{7.94 f_l^{'}}{f_{co}^{'}}} - 2\frac{f_l^{'}}{f_{co}^{'}}) \tag{2.10}$$

The axial strain at rupture or ultimate compressive strain, defined as that strain at which first fracture of transverse reinforcement occurs, was developed by Priestley (1996)

$$\varepsilon_{cu} = 0.004 + \frac{1.4 \rho_s f_{sy} \varepsilon_{su}}{f_{cc}^{'}} \tag{2.11}$$

where ρ_s is the ratio of the volume of confinement reinforcement to the volume of confined concrete core; and ε_{cu} is the steel strain of the steel at maximum tensile stress.

2.3 FRP- confined concrete

The characteristics of FRP are different from that of steel; therefore, the model for steel-confined concrete could not be used for FRP-confined concrete (Mirmiran and Shahawy 1996; Samaan et al. 1998; Xiao and Wu 2000). Figure 2.3 shows the dissimilar behavior of stress-strain for the two confinement mechanisms. It can be seen that the steel-confined concrete experiences a might softening before reaching peak stress $f_{cc}^{'}$, followed by a gradually descending branch. At failure, peak stress $f_{cc}^{'}$ is higher than the stress $f_{cu}^{'}$. In contrast, the FRP-confined concrete has a distinct bilinear ascending response; that is, it experiences a sharp softening and a transition zone before the stress reaches unconfined strength $f_{co}^{'}$, followed by tangent stiffness stabilizing at a constant value until achieving the ultimate strength $f_{cu}^{'}$.

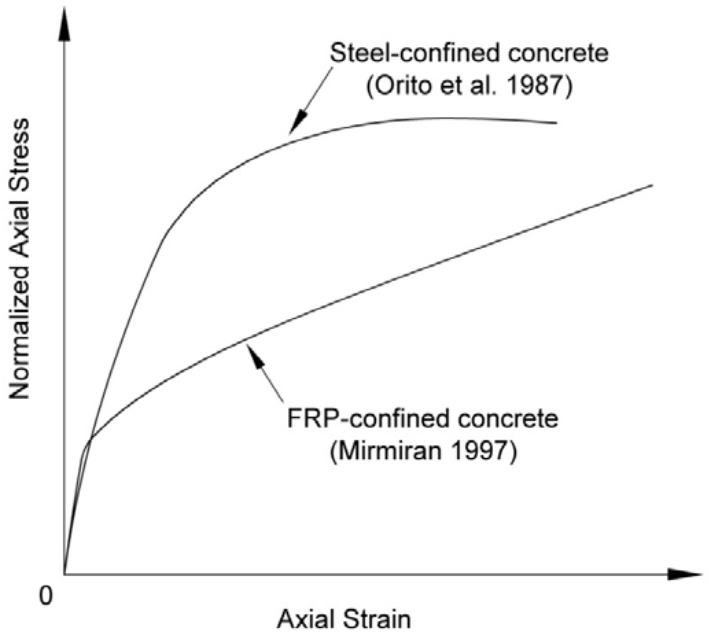

Figure 2.3 Stress-strain curves of FRP-confined concrete and Steel-confined concrete (Samaan et al. 1998)

From the large number of studies on FRP-confined concrete (De Lorenzis and Tepfers 2003; Fardis and Khalili 1981; Fardis and Khalili 1982; Lam and Teng 2003a, b, 2004a, b; Mirmiran and Shahawy 1997; Pessiki et al. 2001; Rochette and Labossière 2000; Spoelstra and Monti 1999; Toutanji 1999), a number of stress-strain models have been classified into two categories: (1) design-oriented models, and (2) analysis-oriented models. Design-oriented models are generally defined

using simple closed form expressions and suitable for practical application. Analysis-oriented models, on the other hand, are more complicated, but have a better predictive capability and are more versatile than design-oriented models because they explicitly account for the interaction between the confining material and the concrete core.

2.3.1 Design-oriented models

Most of the design-oriented models have been proposed based directly on test stress-strain curves of FRP-confined circular concrete specimens (De Lorenzis and Tepfers 2003; Lam and Teng 2003a; Samaan et al. 1998; Xiao and Wu 2000). The Lam and Teng (2003a, 2003b) and Samaan et al. (1998) models were identified as being the more accurate models. The Samaan et al. (1998) model was developed from the four-parameter relationship of Richard and Abbot (1975) to describe the elastic-plastic behaviour of structure system, as shown in Figure 2.4 and Equation (2.12).

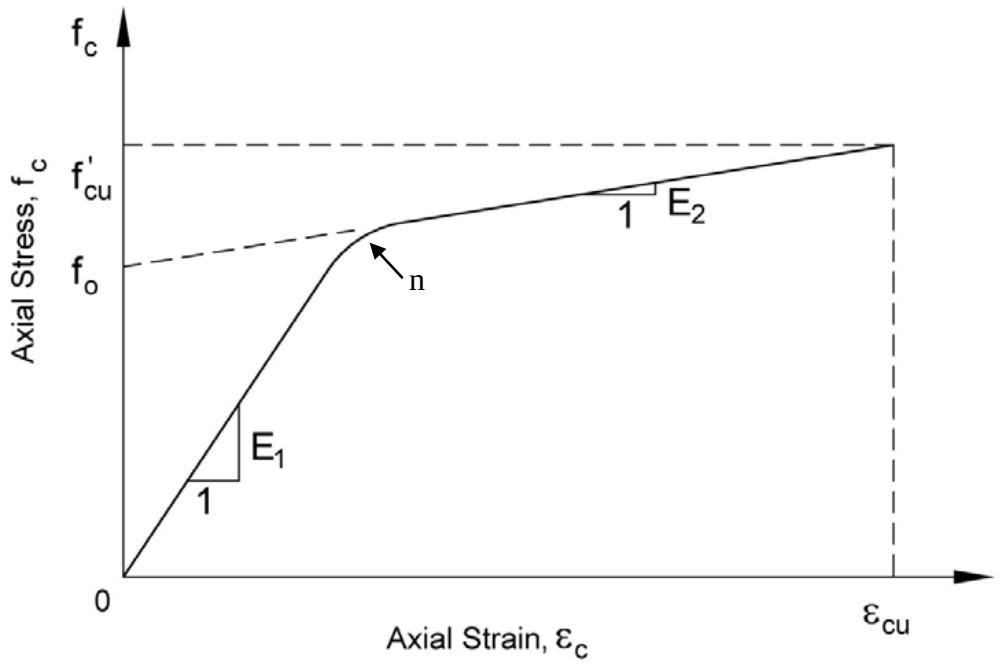

Figure 2.4 Richard and Abbot (1975) four parameter stress-strain curve

$$f_c = \frac{(E_1 - E_2)\varepsilon_c}{\left[\left(1+\left(\frac{(E_1-E_2)\varepsilon_c}{f_o}\right)^n\right)\right]^{1/n}} + E_2\varepsilon_c \qquad (2.12)$$

where ε_c and f_c are the axial strain and stress of confined concrete, respectively; E_1 and E_2 are first and second slopes; f_o is reference plastic stress at the intercept of the

second slope with the stress axis; and n is parameter controlling the transition from the first portion to the second portion of stress strain curve.

The Samaan et al. (1998) model was calibrated with experimental results of 30 concrete-filled FRP specimens conducted by the authors. Due to the advantage of the four-parameter curve, a number of models for FRP-confined concrete have been proposed using this expression (Campione and Miraglia 2003; Moran and Pantelides 2002; Xiao and Wu 2003).

The Lam and Teng (2003a) model developed based on an interpretation of a large test database. The model accounted for the actual hoop rupture strain and the effect of jacket strain capacity on the ultimate condition of FRP-confined columns. Details of the Lam and Teng (2003a) model are further discussed in Chapter 5, where theoretical interaction diagrams are developed on the basic of the model.

2.3.2 Analysis-oriented models

The analysis-oriented models have been developed based on an incremental iterative numerical approach, which considers the interaction between the concrete core and the confining of FRP (Chun and Park 2002; Fam and Rizkalla 2001; Mirmiran and Shahawy 1996; Spoelstra and Monti 1999). The basic for this type of model is a series of interdependent parameters including the hoop strain in FRP jacket, the corresponding axial strain, dilation of the concrete and FRP confining pressure. Due to the complex nature of these models, they not are suitable for manual design. However, they are most efficiently designed using computer analysis.

For CFRP-confined concrete, the Spoelstra and Monti's (1999) model performed better than other models. The model was proposed based on Popovics's (1973) active confinement model, which describes concrete confined at the constant confining pressure to failure. The lateral strain is determined using a simple constitutive model proposed by Pantazopoulou and Mills (1995), which describes the decrease of secant modulus of concrete with an increasing area strain/lateral strain.

2.4 Steel and FRP-confined concrete

While FRP has been used to retrofit and strengthen existing reinforced concrete structures. Most of the current models consider the confinement of FRP and ignore the contribution of transverse steel reinforcement. These models, therefore, do not

reflect the actual behavior of the structures. Some of the recent analytical models (Eid and Paultre 2008; Harajli et al. 2006; Ilki et al. 2008; Lee et al. 2010; Pellegrino and Modena 2010; Tastani et al. 2006) are taken into account the total confinement pressure resulting from external FRP jacket and internal transverse steel reinforcement. Figure 2.5 shows that with the same amount of FRP confinement, but a different amount of confinement transverse steel reinforcement, the strength and ductility of FRP-confined columns perform differently.

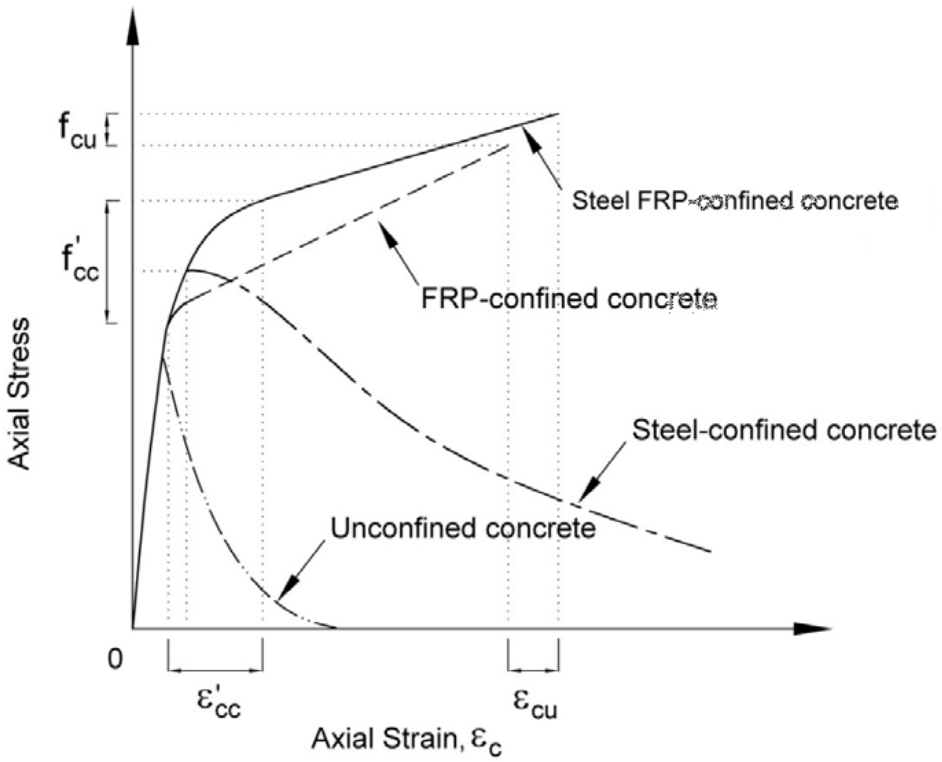

Figure 2.5 Stress-strain curves of FRP-confined concrete (Eid and Paultre 2008)

Harajli et al. (2006) firstly implemented the experimental and analytical methods to investigate the effect of internal steel reinforcement on the behaviour of FRP-confined concrete. The authors developed the model based on the confinement model proposed by (Richart et al. 1929; Richart et al. 1928). It is concluded that the stress-strain curve was not only influenced by the total amount of confining pressure, but by the relative confining pressure from each of the internal transverse steel reinforcement and FRP jacket.

Lee et al. (2010) developed the empirical model for confined concrete determining the effect of both FRP and transverse steel for circular columns as shown in Figure 2.6.

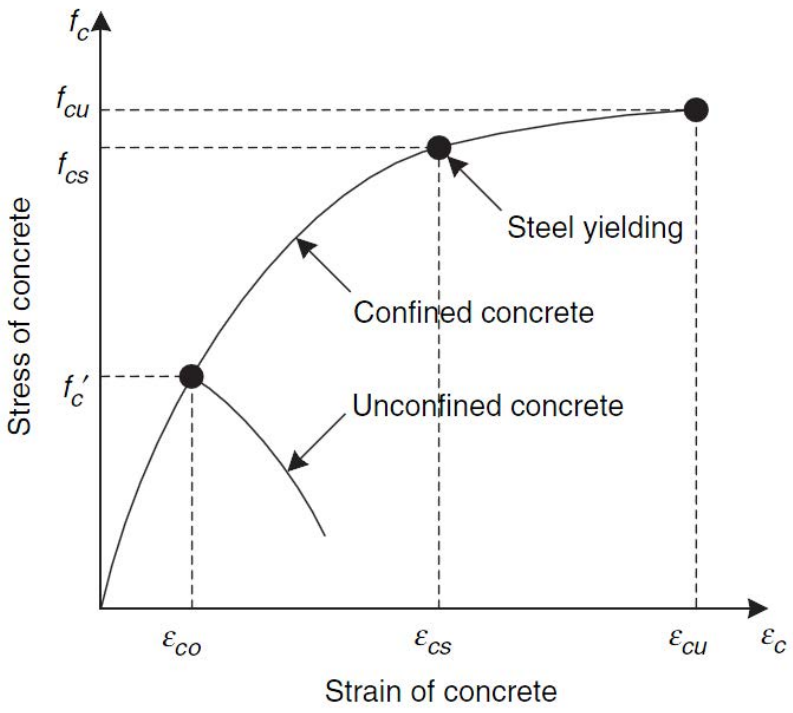

Figure 2.6 Stress-strain curve of concrete confined with steel spiral and FRP (Lee et al. 2010)

The stress-strain curve consists of three segments. The first one is the unconfined concrete model to predict the stress strain up to $\varepsilon = \varepsilon_{co}$ corresponding to the peak stress $f_c^{'}$ of unconfined concrete. The second and the third curves perform the stress and strain of confined concrete for strain ranging from ε_{co} to ε_{cs} and ε_{cs} to ε_{cu}, respectively.

The ultimate compressive strength f_{cu} corresponding to ultimate strain ε_{cu} were then proposed based on Lam and Teng (2003a) model as given in Equation (2.13) and (2.14)

$$f_{cu}^{'} = f_c^{'}(1 + 2\frac{f_{ls} + f_{lf}}{f_c^{'}}) \tag{2.13}$$

$$\varepsilon_{cu} = \varepsilon_{co}\,(1.75 + 5.25(\frac{k_s f_{ls} + k_f f_{lf}}{f_c^{'}})(\frac{\varepsilon_{f,rup}}{\varepsilon_{co}})^{0.45} \tag{2.14}$$

where

$k_s = 2 - f_{lf}\,/f_{ls}$ and $k_f = 1$ for $f_{lf} \leq f_{ls}$

$k_s = k_f = 1$ for $f_{lf} > f_{ls}$

$\varepsilon_{f,rup}$ is strain of FRP at rupture; f_{ls} is confining pressure from transverse steel; and f_{lf} is confining pressure from FRP.

Lee et al. (2010) proposed the model to determine the combined effect of transverse steel reinforcement and FRP on transverse confinement by presenting the parameters $k_s \; and \; k_f$. However, the model was not able to determine the lateral strain of confined concrete and developed based on the experimental results for circular columns.

Analytical model for FRP confined concrete with and without internal steel reinforcement was presented by Eid and Paultre (2008). Interaction mechanisms between internal steel reinforcement and external FRP showed the effect on FRP strain at rupture. Details of the Eid and Paultre (2008) model are further discussed in Chapter 5, where theoretical interaction diagrams are developed on the basic of the model.

2.5 Ductility of FRP-confined concrete

Ductility is the ability of a material to deform plastically without fracturing. Ductility of concrete member was proposed by several researchers for example (Bank 2006; and El-Dash and Ramadan 2006). Furthermore, the proposal more clearly defines the yield load and the corresponding deflection than others. The factor was calculated as the ratio of the deflection at 85% post-peak load (δ_u) and the yield load (δ_y) as given by:

$$\lambda = \frac{\delta_u}{\delta_y} \tag{2.15}$$

The deflection at 85% post-peak load was determined by the deflection corresponding to the axial load dropping to 85% of the peak load.

The deflection at yield load, the deflection at the limit of elastic behaviour, was determined as follow. A best-fit line to the linear portion of the axial load-carrying capacity and axial deflection curve for each specimen was obtained by linear regression analysis. This line was then extrapolated to intersect with the ultimate load sustained by the column.

2.6 FRP-confined concrete under eccentric loads

It should be noted that both the experimental studies and predictive models reviewed have been concerned with FRP-confined concrete columns subjected to concentric

loading. However, most columns are eccentrically loaded with their sections subjected to combined bending moment and axial compression. The performance of FRP-confined concrete columns under eccentric loading is different due to the non-uniform nature of FRP confinement across the column section.

Most existing studies (Bisby and Ranger 2010; Fam et al. 2003; Rocca et al. 2009; Saadatmanesh et al. 1994; Teng and Lam 2002) adopted the conventional section analysis approach with the assumption that the stress profile of FRP-confined concrete in the compression zone of an eccentrically loaded section can be described using the stress-strain relationship obtained from concentric compression tests. On the experimental side, some limited studies have been conducted on eccentrically FRP confined columns, but experimental data in this area is still limited.

Li and Hadi (2003) presented an experimental study on eccentrically loaded high strength concrete columns confined with different types of FRP including carbon FRP and e-glass FRP. The columns tested were circular with a diameter of 235 mm at the haunched ends and 150 mm in the middle. The height of the columns was 1400 mm. The columns were subjected to eccentric load of 42.5 mm eccentricity. The results indicated that wrapping the columns with FRP increased their strength and ductility. However, the strength benefits of FRP confinement were diminished with increasing load eccentricity. Meanwhile, CFRP confined columns achieved 30% higher ultimate load than GFRP confined columns, and the columns with internal reinforcement and CFRP achieved the highest level of ultimate load.

Hadi (2006) carried out a comparative study on the behaviour of FRP-columns to investigate under 42.5 mm eccentric load. Six circular concrete columns having similar geometry as reported by Li and Hadi (2003) were tested to failure to determine the effect of confinement on the performance of FRP-confined columns. The test results revealed that the additions of CFRP as an external confinement to CFRP-confined columns subjected to an eccentric load marginally obtained the strength. However, the ductility improvement was more distinctive than the gains in strength, particularly in the plain columns. It was also proven that the internal steel reinforcement increased both the strength and ductility of FRP-confined columns over columns without internal reinforcement.

Hadi (2007, 2009) continuously tested a series of circular columns confined with CFRP and GFRP under various loading conditions including concentric loading,

eccentric loading and flexural bending. It was shown that the CFRP-confined columns performed better than the GFRP-confined columns in terms of strength and ductility. The ultimate load decreased as the load of eccentricities increased.

Similar to Hadi (2007, 2009), Bisby and Ranger (2010) conducted an experimental study on circular FRP-confined concrete columns under different eccentric loading. The eccentricities ranged widely from 0 mm (concentric load), 5 mm, 10 mm, 20 mm, 30 mm, 40 mm to pure bending (infinite eccentricity). The results showed that reductions in load-carrying capacity due to load eccentricity were more pronounced for FRP-confined columns than for unconfined columns. The strain gradient caused by eccentric loading resulted in non-uniform FRP confinement in the hoop direction, with maximum hoop strains at the extreme compression fibre and negligible hoop strains at the extreme tension fibre.

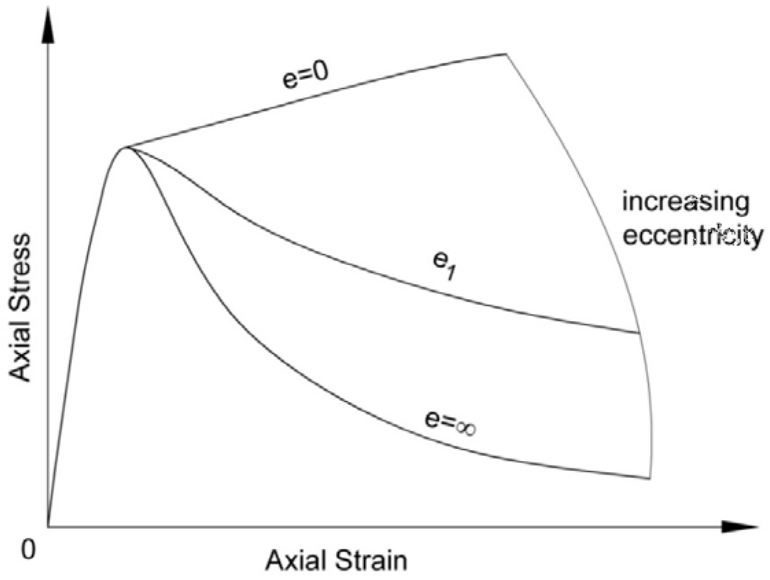

Figure 2.7 Stress-strain curves of FRP-confined concrete under various load eccentricties (Fam et al. 2003)

On the theoretical side, Fam et al. (2003) proposed a variable FRP confinement model to account for load eccentricity. The model was based on the assumption that a strain gradient that subjects a large part of the cross-section to tensile strain due to eccentric loading will decrease the level of confinement. The model also predicted an increasing axial compressive strain enhancement with increasing load eccentricity based on a Tsai-Wu biaxial failure criterion in the FRP material. It is important to recognize that the Fam et al. model can be implemented in conjunction with any

other available model that predicts the ultimate confined concrete compressive strength and strain. Figure 2.7 shows a stress-strain relationship under various load eccentricties. It is apparent that the load-carrying capacity of FRP-confined columns decreases significantly with increasing load of eccentricities.

Based on the research conducted to date, it is apparent that the benefits of FRP confinement diminish with increasing eccentricity resulting in reduction in strength and ductility. Although the available research on FRP-confined concrete columns subjected to eccentric loads has been carried out, further examination is required to quantify the enhancement in the strength and ductility of column wrapped with FRP under various eccentricities.

2.7 Shape modification of concrete columns

FRP jacket provides very effective confinement to circular columns, but is much less effective for rectangular columns. For these columns, more effective confinement can be achieved by modifying the column section into a circular or elliptical section as shown in Figure 2.8 before wrapping with FRP.

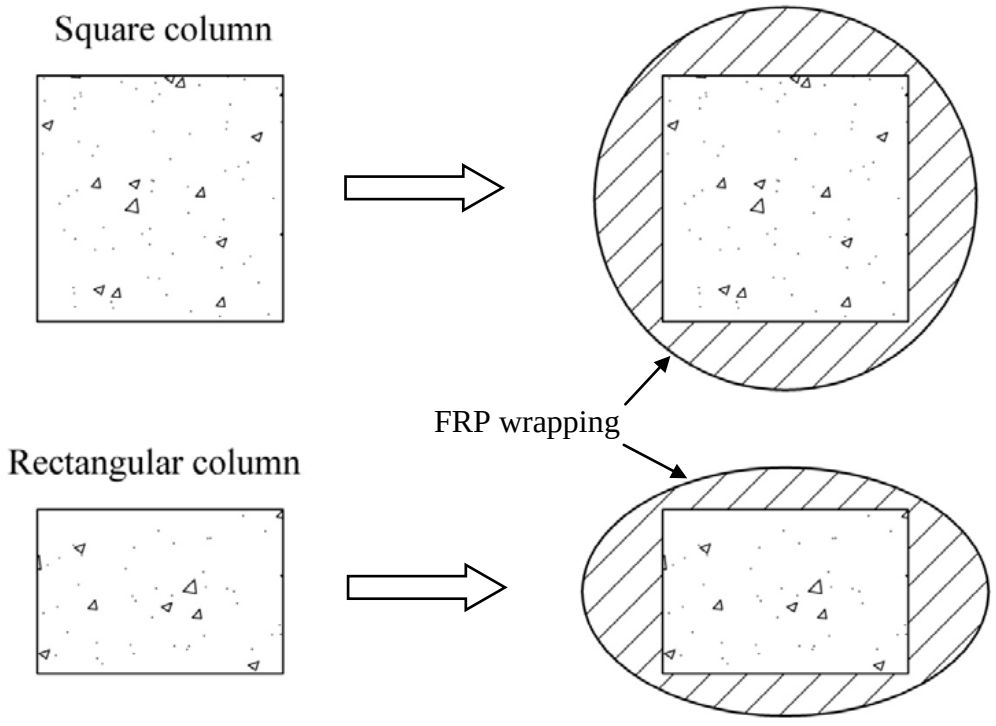

Figure 2.8 Retrofitting method by shape modification and FRP wrapping

Priestley and Seible (1995) were the first to modify square columns into circular or elliptical columns by adding concrete bolsters. It was found that the bending action in the CFRP jacket was reduced and the confining action increased effectively.

Yan et al (2006) conducted the experimental program to retrofit square and rectangular columns using the shape modification. The cross-section of columns was changed from a square to a circle and from a rectangular to an oval before wrapping with post-tensioned FRP composite shell. The expensive cement concrete was cast in the gap between the original concrete compression member and FRP shell. All specimens were tested under concentric compression loading. Their results proved the effectiveness of the shape modification method. Shape-modified columns confined with post-tensioned FRP shells achieved higher compressive strength, axial compressive strain and energy absorption compared to unconfined-columns. The stress-strain curve transformed from softening to hardening behaviour when the cross section of square or rectangular columns was modified into a circle or an oval. Yan and Pantelides (2006) also proposed a confinement model for shape-modified circular and elliptical sections confined with post-tensioned FRP shells. The model was implemented using an incremental approach, which accounted for the variable FRP confinement and dilation behaviour as compressive load increased.

Yan et al. (2007) and Yan and Pantelides (2011) carried out further tests to investigate the performance of shape-modified columns with other materials. Two methods were used to achieve shape modification, which included modifying the cross-section with non-shrink gout and wrapping with FRP; and filling the gap between the original column and FRP shell with various kinds of expansive cement concrete. Similar finding to the Yan and Pantelides (2006) study were found. The shape-modified columns achieved better performance than unmodified columns in terms of the enhancement of compressive strength and axial compressive strain. The modified specimens had a significant benefit of preventing buckling bars in the original column cross-section.

Overall, the shape modification method has been shown to be effective in retrofitting compression members with FRP. Early studies, however, did not consider the effect of eccentricity on column performance and the column with higher compressive strength. Therefore, further research must be carried out to address these issues.

2.8 FRP confinement

2.8.1 FRP confinement under concentric loading

The lateral confinement provided by an FRP jacket to concrete is passive in nature. The concrete has a tendency to dilate under axial compression. This dilation is confined by the FRP jacket, which is loaded in tension in the hoop direction. Different from steel-confined concrete in which the lateral confining pressure is constant following the yielding of steel, the confining pressure provided by the FRP jacket increases with the lateral strain of concrete because of the linear elastic stress-strain behaviour of FRP.

It is well known that the confinement pressure is uniform under concentric load (Hadi and Widiarsa 2012; Harries and Carey 2003; Lam and Teng 2003a; Yazici and Hadi 2009). The confining action in FRP-confined concrete can be schematically illustrated in Figure 2.9. The lateral confining pressure acting on the concrete core is given by:

$$\sigma_r = \frac{2\sigma_h t}{2R} \tag{2.16}$$

where σ_h is the tensile stress in the FRP jacket in the hoop direction, t is the thickness of the FRP jacket and R is the radius of the confined concrete core. If the FRP is loaded in the hoop tension only, then the hoop stress in the FRP jacket σ_h is proportional to the hoop strain ε_h due to the linearity of FRP and is given by:

$$\sigma_h = E_f \varepsilon_h \tag{2.17}$$

where E_f is the elastic modulus of FRP in the hoop direction.

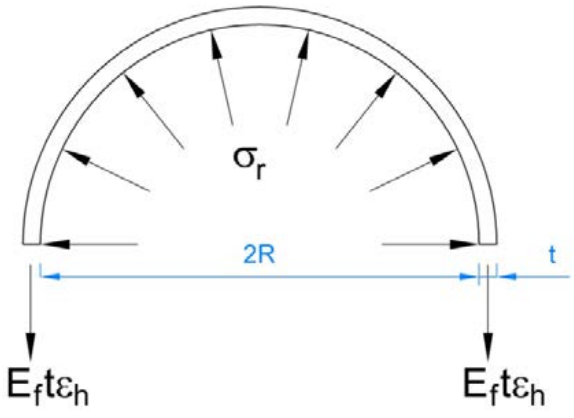

Figure 2.9 Confinement pressure of FRP under concentric loading

The lateral confining pressure reaches its maximum value f_l at the rupture of FRP

$$f_l = \frac{\sigma_{h,rup} t}{R} = \frac{E_f \varepsilon_{h,rup} t}{R} \tag{2.18}$$

where $\sigma_{h,rup}$ and $\varepsilon_{h,rup}$ are the hoop stress and strain of FRP at rupture, respectively, which are generally not the same as the ultimate tensile strength and the ultimate tensile strain of FRP obtained from flat coupon tests as discussed in Section 2.9.

The effectiveness of confinement is known to be greater for circular columns than for rectangular columns due to the singularity and stress concentration at the edges and the reduced confinement on the flat sides (Lam and Teng 2003b; Mirmiran et al. 1998; Parvin and Wang 2002; Rochette and Labossière 2000). Rectangular columns do not experience uniform confining pressure from FRP jacket. Dilation of the concrete section results in large confining pressure developed across the diagonals of rectangular sections. The jacket sides provide smaller levels of confinement since confining pressure of this location is engaged more by the flexural stiffness of the thin jacket rather than the tensile stiffness of the jacket. It has been reported that the cross-sectional area of effectively confined concrete for concentrically loaded columns consists of four parabolas within which the concrete is fully confined (Campione and Miraglia 2003; Lam and Teng 2003b; Wang and Restrepo 2001), as shown in Figure 2.10. The effectively confined area is a function of the dimensions of the rectangular columns and the radius of the corners.

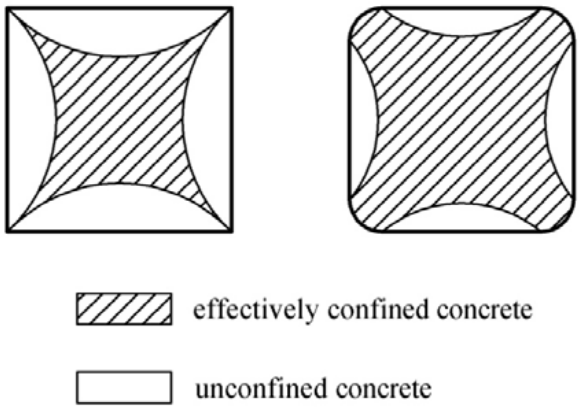

Figure 2.10 Effectively confined area of columns under concentric loading (Campione and Miraglia 2003)

2.8.2 FRP confinement under eccentric loading

For FRP-confined columns subjected to eccentric loading, the FRP confinement decreases with increasing load eccentricity (Hadi and Widiarsa 2012; Li and Hadi 2003; Maaddawy 2009). The FRP strain in the hoop direction of the eccentrically loaded columns was non-uniform, which is largest at the extreme fibre in the compression region of the columns, as shown in Figure 2.11.

Parvin and Wang (2001) studied the effect of FRP-jacketing system on small scale plain concrete subjected to eccentric loading. The FRP jacket thickness and the effects of various eccentricities were examined. It was concluded that the strain gradient caused non-uniform confining pressure, which reduced the efficiency of the FRP jacket under eccentric loading. The stiffness of the FRP composite fabric is a key parameter affecting the eccentrically loaded square columns.

In a study performed by Bisby and Ranger (2010), fourteen small scale circular RC columns with identical height-to-diameter ratios of 4 were tested to failure under monotonic, eccentric axial compressive load. The results indicated that for eccentric loading, the effective confining pressure was much less than for concentric loading. This can be explained by the hoop compressions of eccentrically loaded columns being higher than that of concentrically loaded columns, which reduces the likelihood of axial concrete cracks.

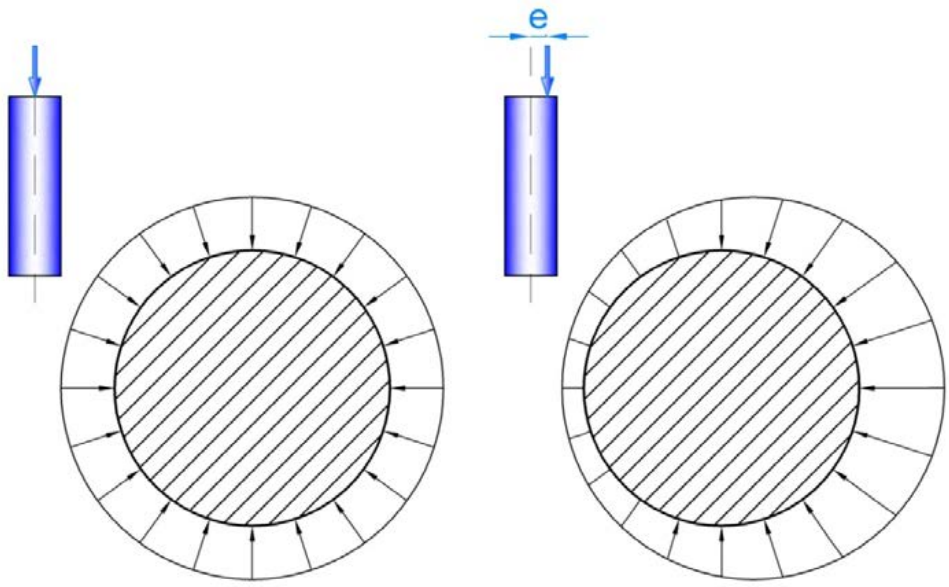

(a) Concentric loading (b) Eccentric loading

Figure 2.11 Confining pressure of FRP confined column

2.9 Ultimate condition of FRP

The ultimate condition of FRP is closely related to the confining pressure provided by the FRP jacket when it ruptures. Early researchers (Fardis and Khalili 1982; Saadatmanesh et al. 1994; Samaan et al. 1998; Toutanji 1999; Xiao and Wu 2000) commonly assumed that this confining pressure is equal to the tensile strength of the same FRP material obtained from flat tensile coupon tests. However, Pessiki et al. (2001) proved that the FRP rupture strains observed in tests of FRP-confined specimens is smaller than FRP material rupture strains determined from flat tensile coupon tests in accordance with ASTM D7565 (2010). The FRP strain efficiency factor was proposed to account for the premature failure of FRP confined columns. This phenomenon is possibly related to the multiaxial state of stress to which it is subjected to the pure axial tension used for material characterization. This factor is important for a stress-strain model to produce satisfactory results, which is the product of two components:

$$k_\varepsilon = k_{\varepsilon 1} k_{\varepsilon 2} \tag{2.19}$$

The strain localization factor,$k_{\varepsilon 1}$, is the ratio of the average strain in a jacket around it perimeter, ε_h, to the in situ jacket rupture strain, $\varepsilon_{h,rup}$, as:

$$k_{\varepsilon 1} = \frac{\varepsilon_h}{\varepsilon_{h,rup}} \tag{2.20}$$

The in situ properties factor, $k_{\varepsilon 2}$, is the ratio of the in situ jacket rupture strain, $\varepsilon_{h,rup}$, to the material strain capacity obtained from flat tensile coupon tests, ε_{fu}, as:

$$k_{\varepsilon 2} = \frac{\varepsilon_{h,rup}}{\varepsilon_{fu}} \tag{2.21}$$

When the strain in the jacket is uniform around the perimeter of the cross section,k_ε is equal to $k_{\varepsilon 2}$, as shown in Figure 2.12.

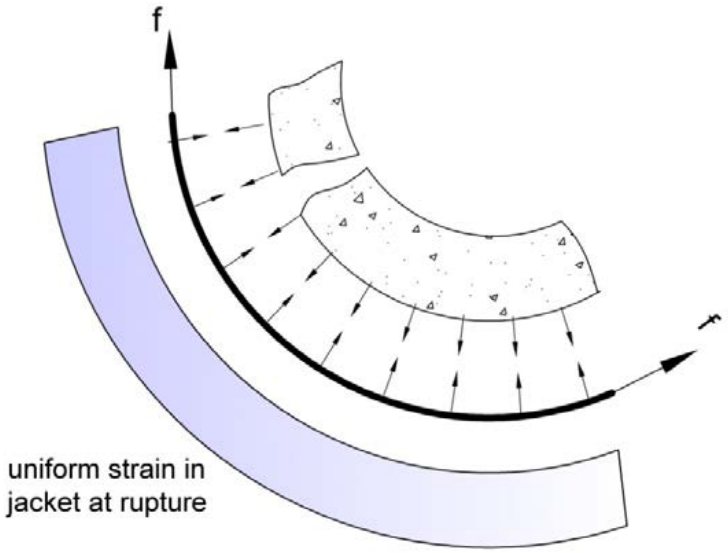

Figure 2.12 Uniform strain distribution in FRP jacket (Pessiki et al. 2001)

The author found that the FRP strain efficiency factor equalled to 0.6 and 0.42 for small-scale circular specimens and large circular specimens, respectively.

Lam and Teng (2004) investigated the rupture of FRP jacket. Three types of tests including flat coupon tensile tests, ring splitting tests and FRP-confined concrete cylinder compression tests were conducted and compared the ultimate tensile strains of both kinds of FRPs (Carbon FRP and Glass FRP). It was concluded that the FRP hoop rupture strain of FRP-confined cylinders was close to the ultimate tensile strain measured from ring splitting tests. Another observation was that the FRP hoop strain obtained from the overlap zone fell far below those measured outside the overlap zone. This is because the confining pressure is basically the same around the whole circumference, whereas the FRP jacket is thicker in the overlap zone, which can give rise to this phenomenon. To this end, the rupture strains in the FRP jacket are affected by the curvature of the FRP jacket, the non-uniformity of the deformation of concrete and overlap zone.

Based on experimental calibration using mainly CFRP-confined concrete specimens, an average value of 0.586 was computed for k_ε by Lam and Teng (2003a). Similarly, a database of 251 test results (Harries and Carey 2003) computed a value of $k_\varepsilon = 0.58$ while experimental tests on medium and large-scale columns resulted in values of $k_\varepsilon = 0.58$ and 0.61, respectively (Carey and Harries 2005).

2.10 Summary

This chapter has presented a review of existing studies on FRP-confined concrete and FRP-confined RC columns. This review has indicated that the stress-strain behaviour of FRP-confined concrete under concentric loading is much better understood than under eccentric loading. Therefore, further studies on these issues regarding experimental and theoretical methods are still needed. The work presented in the study is limited to the retrofitting method using CFRP subjected to various loading conditions including concentric loading, eccentric loading and flexural bending. The retrofitting method for square columns and the mechanics of FRP confinement are the focus of this study.

Chapter 3 presents the experimental program, which was carried out to evaluate the performance of the proposed retrofitting method using shape modification and CFRP wrapping.

CHAPTER 3. EXPERIMENTAL STUDY

3.1. Introduction

Chapter 2 presented a review of existing knowledge related to FRP-confined reinforced concrete (RC) columns. The efficiency of FRP confinement of square columns is significantly lower than circular columns. Therefore, the cross-section of RC columns needs to be changed from a square to a circle before wrapping them with FRP to maximise the confining pressure of FRP. This chapter presents a retrofitting method for square RC columns. The square RC columns were bonded with four pieces of segmental concrete covers to circularise the cross-section then confine them with CFRP.

All the tests in this study were conducted in the High Bay of the Civil Engineering Laboratory of the University of Wollongong.

3.2. Experimental Design of the Retrofitted Specimens

Sixteen square RC columns (150 mm in side length by 800 mm in height) were cast with 40 MPa concrete and divided into four groups. The specimens of the first group were tested without further modification and its four specimens served as a reference group. Each column from the remaining twelve square RC columns in the second, third and fourth groups were bonded with four pieces of segmental circular concrete covers, which had nominal compressive strengths of 40 MPa, 80 MPa and 100 MPa, respectively. The modified columns were then confined with three layers of CFRP. From each group, three of the four columns were tested under different eccentric loadings including 0 mm (concentric), 25 mm, and 50 mm eccentricity. The remaining specimen in each group was tested under flexural bending to failure.

The dimension of column core was 150 mm in sides and 800 in height. All the columns were made from normal strength concrete (NSC) with nominal compressive strength of 40 MPa. The longitudinal and transverse reinforcement of columns were designed in accordance with the Australian Standard (AS) 3600 (2009) with the adequate reinforcement requirements for columns. The purpose of this design ensured that the performance of specimens was similar to old deteriorated structures, which needed to be retrofitted. The longitudinal steel reinforcement consisted of four

12 mm (N12) deformed bars with a nominal tensile strength of 500 MPa tied inside by transverse steel reinforcement. The diameter of the plain transversal steel reinforcement was 6 mm (R6) with a nominal tensile strength of 250 MPa, which was placed at 60 mm spacing. The clearance between the steel reinforcement and the mould was maintained at 20 mm on each side, and at the top and bottom.

Twelve of the test specimens were modified by bonding four segmental circular plain concrete covers to each side. Segmental circular plain concrete covers were cast with different concrete grades from normal strength concrete to high strength concrete, with a nominal compressive strength of 40 MPa, 80 MPa and 100 MPa, respectively. The modified columns were then confined with three layers of CFRP. Figure 3.1 shows a detailed design of the existing columns.

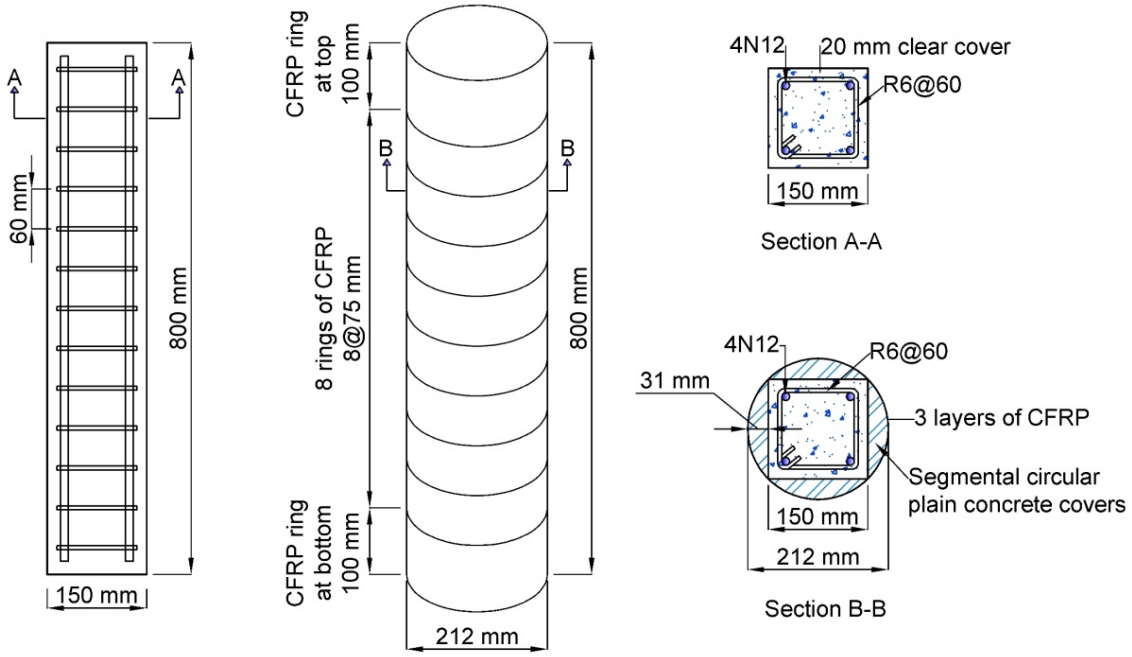

Figure 3.1 Design details of the specimens.

In total, sixteen RC columns were tested and subdivided equally into four groups. The first four square RC columns were tested without further modification and strengthening and served as a reference group. Each column from the twelve remaining square RC columns in the second, third and fourth groups were bonded with four pieces of segmental circular concrete covers, which had various compressive strengths. The modified columns were then confined with three layers of CFRP, as shown in Figure 3.1.

All the specimens were tested until failure to investigate the efficiency of the proposed method. Details of the specimens are presented in Table 3.1.

The labelling used for the specimens is composed of a combination of letters and numbers. The letters R and C denote the reference and modified columns from a square to a circle, respectively. The numbers 40, 80 and 100 indicating design concrete strengths, express the nominal compressive strength of segmental circular concrete covers bonded to the existing square RC columns. The letter F denotes the specimens, which were tested under flexural bending. The last number 0, 25 and 50 denote the eccentricity of axial loading. For example, Specimen C80-50 is the column which was modified by four pieces of segmental circular concrete covers of 80 MPa and tested under 50 mm eccentric load.

Table 3.1 Configuration of specimens

Column	Cross section	Strength of Segmental cover (MPa)	Internal reinforcement	Number of CFRP layers	Loading eccentricity (mm)
R-0 R-25 R-50 R-F	Square	-	4N12 and R6@60 mm	-	0 25 50 Bending
C40-0 C40-25 C40-50 C40-F	Circular	40	4N12 and R6@60 mm	3	0 25 50 Bending
C80-0 C80-25 C80-50 C80-F	Circular	80	4N12 and R6@60 mm	3	0 25 50 Bending
C100-0 C100-25 C100-50 C100-F	Circular	100	4N12 and R6@60 mm	3	0 25 50 Bending

3.3. Specimen Fabrication

3.3.1. Mixing High Strength Concrete (HSC)

Three different mixes were used to cast the existing square RC columns and segmental circular plain concrete covers. The NSC was supplied by a local supplier. However, the HSC was prepared in the High Bay laboratory of the University of Wollongong. Five trial batches of concrete were mixed and cast in cylindrical steel moulds with a 100 mm diameter by 200 mm height to examine the concrete compressive strength.

The following materials were used in this study:

1. Boral general purpose Portland complying with AS 3972 (2010) for type GP cement.

2. 10 mm aggregate, coarse sand and fine sand were chosen in accordance with the requirements of AS 1141.11.1 (2009). The maximum size of aggregates was 10 mm to ensure that concrete mixture had good workability. All these aggregates were supplied by Boral quarries in Dunmore, NSW, Australia.

3. Fly ash eraring and super fine fly ash (solid flow) from BASF (BASF n.d. 2012).

4. Admixtures consisted of super plasticizer (Glenium 27) and water reducer (Pozz 80) from BASF (BASF n.d. 2012).

5. Tap water.

Figure 3.2 Concrete mixer

Before mixing the HSC, 10 mm aggregate, coarse sand and fine sand were measured for the water content in order to control the water-cement ratio, which is an important parameter affecting the compressive strength of concrete. All mixes were prepared using a concrete mixer, as shown in Figure 3.2. The mixing procedures were carried out pertaining to AS 1012.2 (1994). The GP cement, 10 mm aggregate, coarse sand, fine sand, fly ash, and super fine fly ash were mixed for 1 min, then tap water and admixtures were added and mixed together for 2 min. After a rest of 2 min, all mixtures were mixed for another 2 min. The HSC was taken out to measure the concrete slump within 2 min according to AS 1012.2 (1994) (Figure 3.3). The procedure of adding tap water and admixtures for further 2 min was repeated until the design slump of the concrete was achieved.

Figure 3.3 Measuring HSC slump

The concrete was poured in cylindrical steel moulds. The specimens were left for 24 hours, after that they were taken out from the moulds and immersed in the water tank to maximise the hydration process of concrete.

Three concrete cylinders were tested at 7 days after casting and another three concrete cylinders were tested at 28 days. The cylinders were removed from the water tank and then capped them with a high strength plaster. These cylinders were tested to failure in the compression-testing machine under a constant strain rate of 17.5% (Figure 3.4). Details of concrete mix proportions and the compressive concrete strength are provided in Table 3.2.

Figure 3.4 Concrete cylinders after being tested to failure

Table 3.2 High strength concrete mix proportion for 1 m^3

Variable	Concrete trial number				
	1	2	3	4	5
Cement (kg)	529	450	550	540	505
Water (l)	193	140	184	187	190
Fly ash (kg)	-	-	30	60	35
10 mm aggregate (kg)	1180.3	1100	1085	1001.8	976.81
Coarse sand (kg)	339.6	685.6	619	397.38	427.19
Fine sand (kg)	150.5	129.4	117	75.02	189.58
Glenium 27 (l)	-	-	6	7.5	1.9
Solid Flow (super fine fly ash) (kg)	-	-	44	40	-
Pozz 80- Water reducer (ml/100 kg cementitious)	1228	1500	2345	670	720
Slump (mm)	110	120	40	50	150
$f_c^{'}$ MPa (7 days)	41	36	55	57	51
$f_c^{'}$ MPa (28 days)	52	54	78	85	75

3.3.2. Formwork preparation

Two wooden formworks for casting existing square columns and segmental circular covers in the experimental program were used. They were assembled in the High

Bay Laboratory of the University of Wollongong from rectangular wooden panels, which were provided by a local supplier. The wooden panels, which had internal cross-sections of 150 by 150 mm and 800 mm in height, were joined by screws to make the formworks for casting the existing columns, as illustrated in Figure 3.5. For casting the segmental circular concrete covers, the second formworks were similarly assembled from wooden form panels, which had internal cross-sections of 170 by 51 mm and 800 mm in height. Special forms were designed to fit inside the second formworks to prepare the segmental circular covers. These formworks are shown in Figure 3.6. In order to ensure that the formworks were stable while casting the concrete, timber bars were screwed into the formworks and bottom bases.

Figure 3.5 Formworks for the square columns

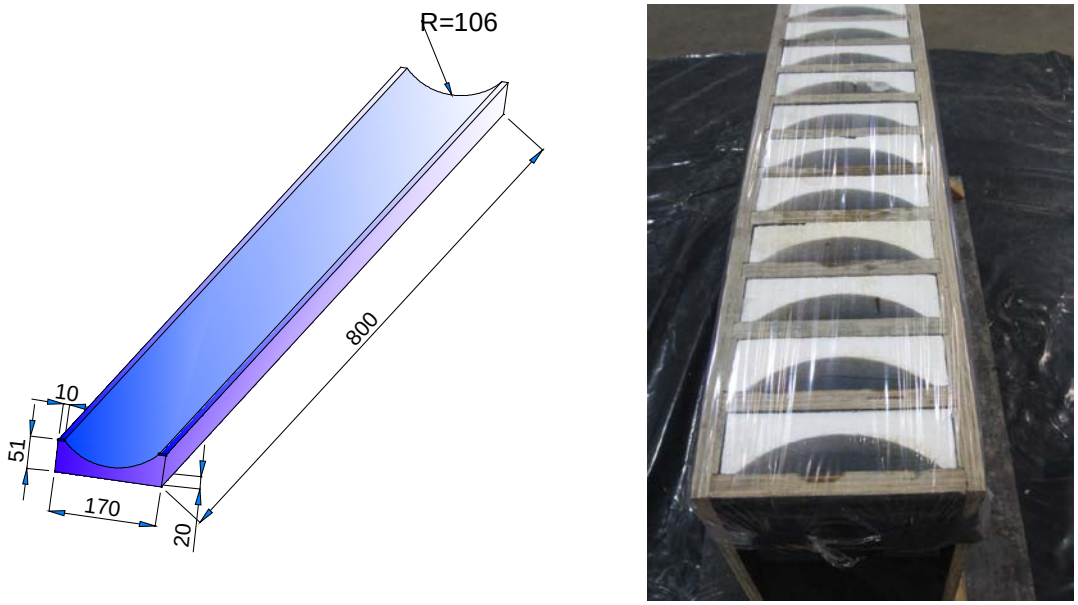

(a) (b)

Figure 3.6. Formworks for segmental circular covers:

(a) special forms (all dimension in mm) and (b) formworks prior to casting concrete

3.3.3. Steel cages

Each of the 16 specimens consisted of four N12 longitudinal bars and thirteen R6 hoop reinforcement. N12 longitudinal bars were cut in lengths of approximately 760 mm. R6 plain bars were cut in lengths of 500 mm and bent to form square steel ties. The square steel ties were placed on four N12 longitudinal bars and secured at each junction by the steel tie wires at 60 mm centre to centre spacing. Four pieces of 20 mm steel bars were welded at the bottom of each longitudinal bar to maintain a concrete clearance of 20 mm. Another four pieces of 20 mm steel bar were also welded on each side of the ties to ensure that the steel cages remained at the centre during casting of concrete. Details of the steel cages are described in Figure 3.7.

Before the steel cages were put into the formworks, an industrial vacuum machine was used to remove the dust from the formworks and oil was spread onto the inner surface for easy removal of the concrete columns after casting. The steel cages were then placed into the formworks.

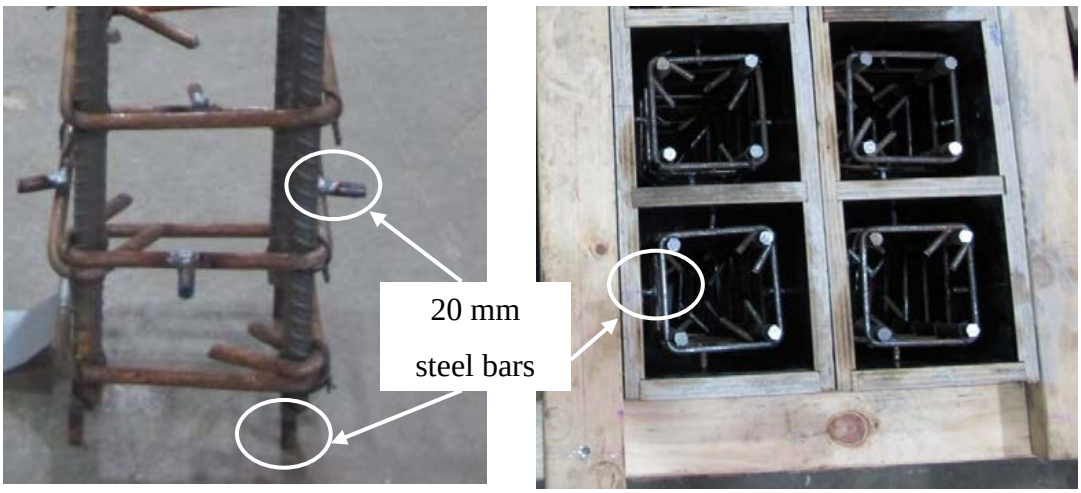

(a) (b)

Figure 3.7. Configuration of steel cages:

(a) before placing in the formworks and (b) after placing in the formworks

3.3.4. Concrete pouring and curing

NSC was supplied by a local supplier, while HSC was mixed in the High Bay Laboratory of the University of Wollongong, as presented in the Section 3.3.1. Before pouring the concrete, a slump test was conducted to ensure that the concrete had the adequate workability. The concrete was poured into the formworks and simultaneously compacted using two vibrators to produce homogeneous concrete (Figure 3.8a). When the concrete was compacted completely in the formworks, the column surface was leveled using trowels (Figure 3.8b). In order to maintain sufficient concrete hydration, moist hessian was used to cover all the specimens and keeping them wet. Figure 3.8 shows the casting concrete into the formworks in the laboratory.

The concrete was also cast into cylindrical steel moulds (100 mm in diameter by 200 mm in height) in two layers; each stage was compacted by a rod with 25 strokes of the rounded end of the rod pertaining to AS 1012.8.1 (2000), as presented in Figure 3.9.

(a) (b)

Figure 3.8. Casting concrete into formworks:

(a) pouring and vibrating concrete and (b) leveling column surface

(a) (b)

Figure 3.9 Preparing concrete cylinders for compressive strength test:

(a) concrete compaction using a rod and (b) concrete cylinders

3.3.5. Circularization Process

The segmental circular concrete covers were taken out of the formworks after 28 days. The contact surfaces between the segmental covers and the existing columns were ground using a wire brush and an electric grinder in order to achieve a smooth surface. Figure 3.10 shows the form removal on concrete covers and the segmental circular concrete covers.

(a) (b)

Figure 3.10 Fabrication of concrete covers

(a) form removal on concrete covers and (b) concrete covers

(a) (b)

Figure 3.11 Bonding concrete covers to square columns

(a) spreading adhesive on concrete covers and (b) bonded concrete covers

Four segmental circular concrete covers were then bonded to the square columns with an admixture, which was made from epoxy resin, slow hardener, and silica microsphere with a ratio of 5:1:10, as recommended by the manufacturer. This adhesive was spread on the surface of the concrete covers, which were then attached to the existing square column. In order to achieve the good contact between the column and the covers, four adjustable steel straps were used to tighten the covers on the column. The modified columns were left to dry before wrapping with CFRP.

3.3.6. CFRP wrapping of columns

The columns in the reference group were tested without the confining with CFRP; however, these columns were strengthened by three layers of CFRP at both ends to prevent premature failure of concrete during the applied loading.

The modified columns in the other groups were ground using an electric grinder to make smooth surfaces (Figure 3.12) to avoid local fracture of the CFRP jacket. These modified columns were then confined with three layers of CFRP. A wet lay-up method was applied to bond the CFRP to the columns with adhesive. The adhesive was prepared by mixing an epoxy resin (West system$^{@}$ 105 resin) and a slow hardener (West system$^{@}$206 slow hardener) with a ratio of 5:1, as specified by the supplier, West system Inc (West System n.d. 2012).

For the eight rings of the CFRP in the middle of the modified specimens, as shown in Figure 3.1, the adhesive was first spread on the surface of the column. A sheet of 2100 mm in length by 75 mm in width CFRP was then wrapped around the column in the hoop direction. After the first layer of CFRP was already attached on the column, the adhesive was then continuously spread on the surface of the first layer of CFRP and the second layer of CFRP was wrapped. The third layer was similarly prepared, but maintained a 100 mm overlap zone (Figure 3.13). Epoxy mixture was applied to the surface of the last layers of CFRP to harden the CFRP and ensure perfect bonding.

For the two rings of CFRP at both ends of the modified columns, as shown in Figure 3.1, instead of 3 CFRP layers was attached, 5 layers of CFRP were applied to prevent premature failure of the modified columns during load application. A sheet of 3450 mm in length and 75 mm in width CFRP were similarly wrapped as described above. A 100 mm overlap was also maintained to prevent debonding of CFRP. The modified columns after wrapping with the CFRP are shown in Figure 3.13.

Figure 3.12 Grinding the specimen surface

(a) (b)

Figure 3.13 Modified specimen after wrapping CFRP:

(a) first ring attached on the specimen and (b) modified specimen with CFRP

3.4. Materials used in the experiment

The materials used in the experiments consisted of normal strength concrete, high strength concrete, N12 deformed bars, R6 plain steel bars, and CFRP. The preliminary tests were conducted to determine the properties of all materials used the experimental program.

3.4.1. Concrete strength tests

All the column cores and the segmental circular covers in the second group were made from normal strength concrete of 40 MPa, which was supplied by a local supplier. Two of the five trial batches of high strength concrete were chosen to cast the segmental circular covers for the C80 and C100 groups, which were the trial batches of HSC, labelled No 4 and No 5 (Table 3.2), respectively.

The concrete including NSC and HSC was poured into the cylindrical steel moulds with 100 mm diameter and 200 mm height. Three concrete cylinders were tested in accordance with AS 1012.9 (1999) at 7 days, 28 days and the testing day of the columns. Details of the actual concrete compressive strength are presented in Table 3.3.

Table 3.3. Actual concrete compressive strength of the specimens

Testing day	Concrete compressive strength (MPa)			
	Column core	Covers of C40 group	Covers of C80 group	Covers of C100 group
7 days	23	23	51	57
28 days	37	37	77	82
Testing day of the reference group	44	-	-	-
Testing day of the C40 group	58	58	-	-
Testing day of the C80 group	59	-	98	-
Testing day of the C100 group	63	-	-	101

3.4.2. Tensile testing of steel bars

Tensile testing of steel bars was conducted in accordance with AS 1391 (2007). The test samples were taken from the steel bars used for reinforcement, which included

N12 deformed bars for longitudinal steel and R6 plain bars for transversal steel. The total length of the test sample was 500 mm, including 340 mm of extensometer gauge length and 80 mm of gauge length on each side (Figure 3.14).

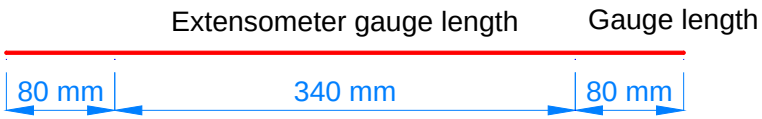

Figure 3.14 Dimension of the sample of steel reinforcement bars

Three samples of N12 deformed bars and R6 plain bars were tested under tensile load to failure (Figure 3.15). The test specimens were instrumented with one axial extensometer to measure the stress-strain response. Failure of specimen was characterized by gradual yielding, followed by necking of the cross-section within the gauge length and subsequent rupture of specimen was observed at the location of necking. The stress-strain relationship and the yield strength of N12 deformed bars and R6 plain bars are presented in Figure 3.16, 3.17 and Table 3.4, 3.5, respectively.

Figure 3.15 Tensile testing for the steel reinforcement

Table 3.4 Test results of N12 deformed bars

Property	Sample 1	Sample 2	Sample 3	Average
Yield Load (N)	60194	61302	62372	61289
Yield Strength (MPa)	532	542	551	542
Yield Strain (%)	0.297	0.303	0.308	0.303
Ultimate Strength (MPa)	637	648	646	644
Strain at Ultimate Strength (%)	10.70	10.63	10.67	10.67

Table 3.5 Test results of R6 plain bars

Property	Sample 1	Sample 2	Sample 3	Average
Yield Load (N)	15504	15514	15327	15448
Yield strength (MPa)	496	504	497	499
Yield strain (%)	0.31	0.33	0.32	0.32
Ultimate Strength (MPa)	557	563	554	558
Strain at Ultimate Strength (%)	7.06	7.03	7.05	7.04

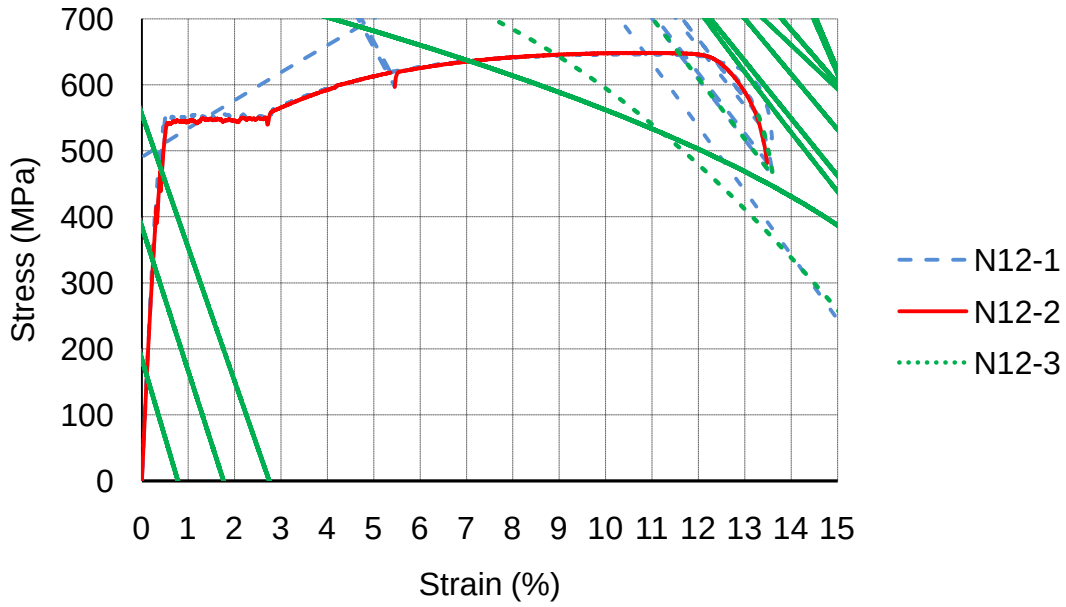

Figure 3.16 Stress-strain relationship of N12 deformed bars

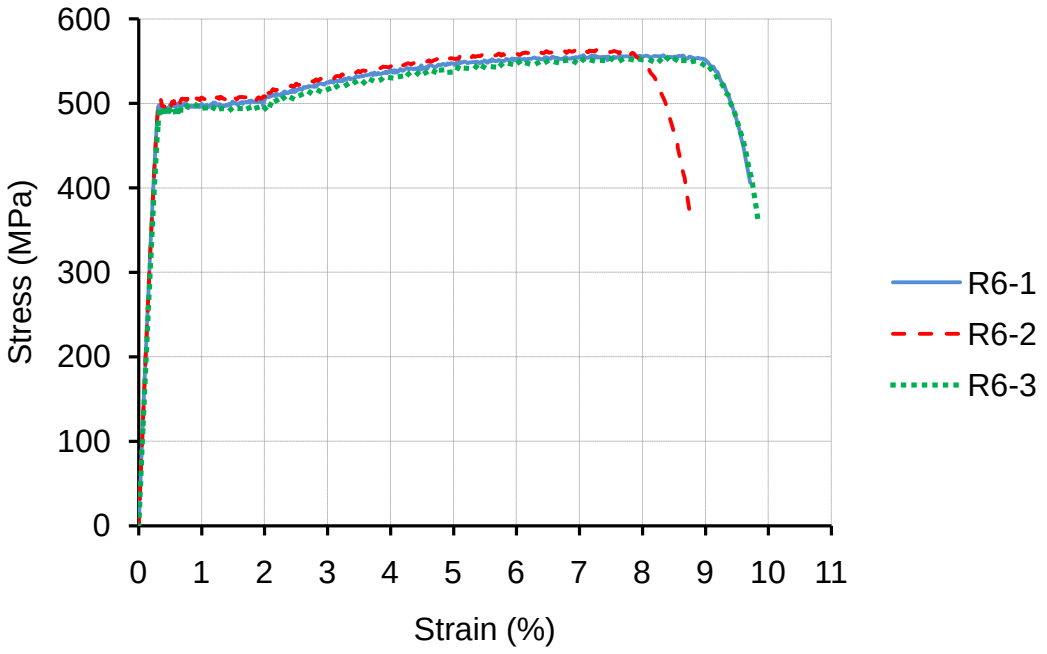

Figure 3.17 Stress-strain relationship of R6 plain bars

3.4.3. Coupon tests for Carbon Fibre Reinforced Polymer (CFRP)

The CFRP unidirectional laminates were available in the form of rolls, 50 m in length and 75 mm in width with a uni-directional fibre density of 340 g/m^2, as provided by the material manufacturer.

The CFRP was tested according to ASTM D7565 (2010) to determine its tensile strength. Three laminates of CFRP were glued together using the wet lay-up method with the adhesive. The coupons were capped at both ends by four pieces of aluminum plates. The dimension of the flat coupons was 25 mm in width and 250 in length, as shown in Figure 3.18.

Figure 3.18 CFRP flat coupons

After fabrication of CFRP coupons, their actual width dimensions were measured. To determine the strain of CFRP corresponding to the loading, each flat coupon was instrumented with one electrical resistance strain gauge. The test was conducted under tensile load, as shown in Figure 3.19.

Figure 3.19 CFRP coupon test under tensile load

According to D7565 (2010), the tensile force and elastic modulus per unit width was calculated, as presented in Figure 3.20 and Table 3.6.

Table 3.6 Test results for the 3 layers of CFRP flat coupons

Coupon	Strain at rupture (%)	Tensile Force per unit width at rupture (N/mm)
1	1.82	2282.28
2	1.55	2034.96
3	1.79	2049.05
4	1.72	1949.72
5	1.80	2210.53
Average	1.74	2105.31

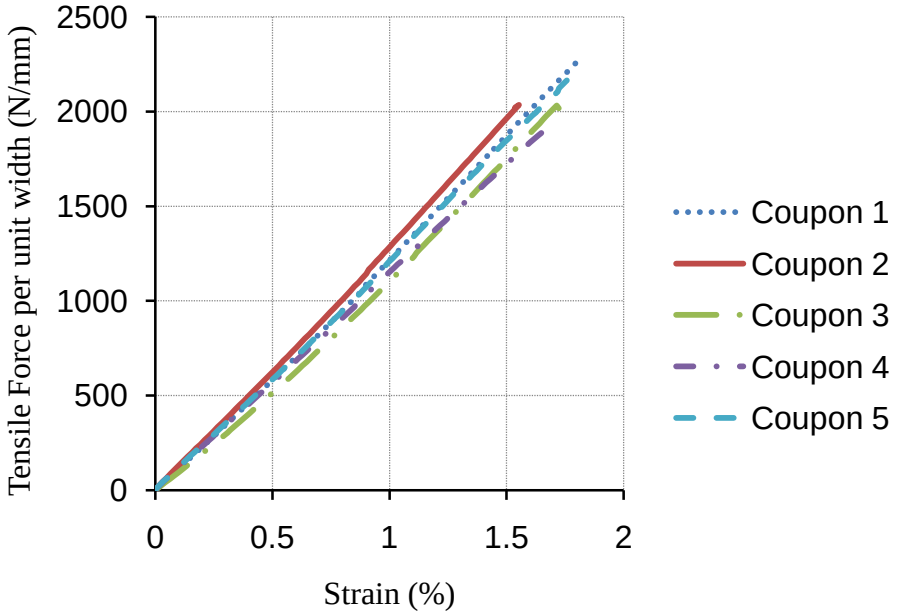

Figure 3.20 Tensile Force-Strain diagrams for the 3 layers of CFRP flat coupons

3.5. Instrumentation

The responses of the columns during the testing were measured and recorded, which include axial load, axial displacement, lateral deflection and CFRP strain in the hoop direction. The layout of instrumentation during the testing is shown in Figure 3.21.

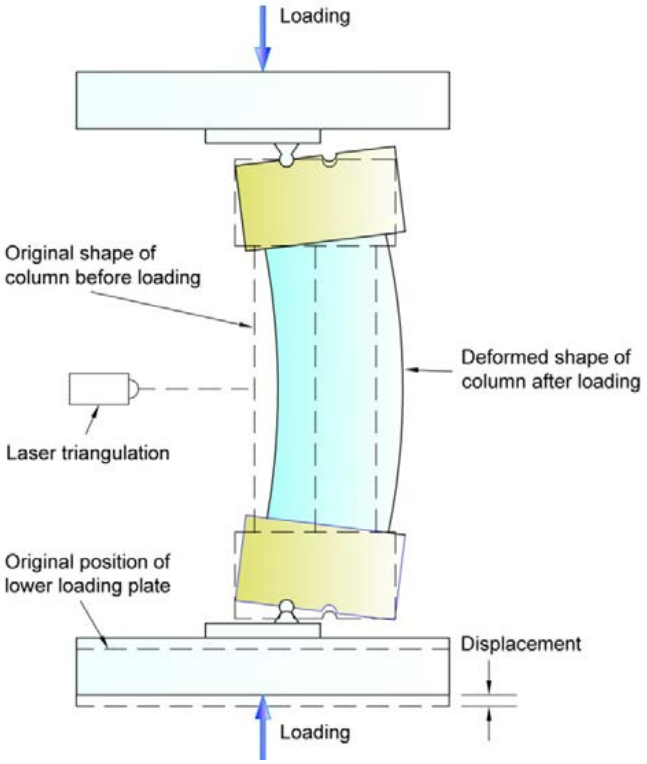

Figure 3.21 Equipment layout in the test

The axial load was measured by the load cell of the 5000 kN Denison Compression machine at the High Bay laboratory of the University of Wollongong. Two LVDTs were attached to the lower plate of the loading machine to measure the axial deflection of the columns. For columns that were subjected to eccentric loading (25 mm and 50 mm), a laser triangulation was set up at mid-height of the columns to record their lateral deflection. For testing the beams, a laser triangulation was placed on a hole, which was located at mid-span of the bottom loading frame. Details of the instrumentation are presented in Figure 3.22.

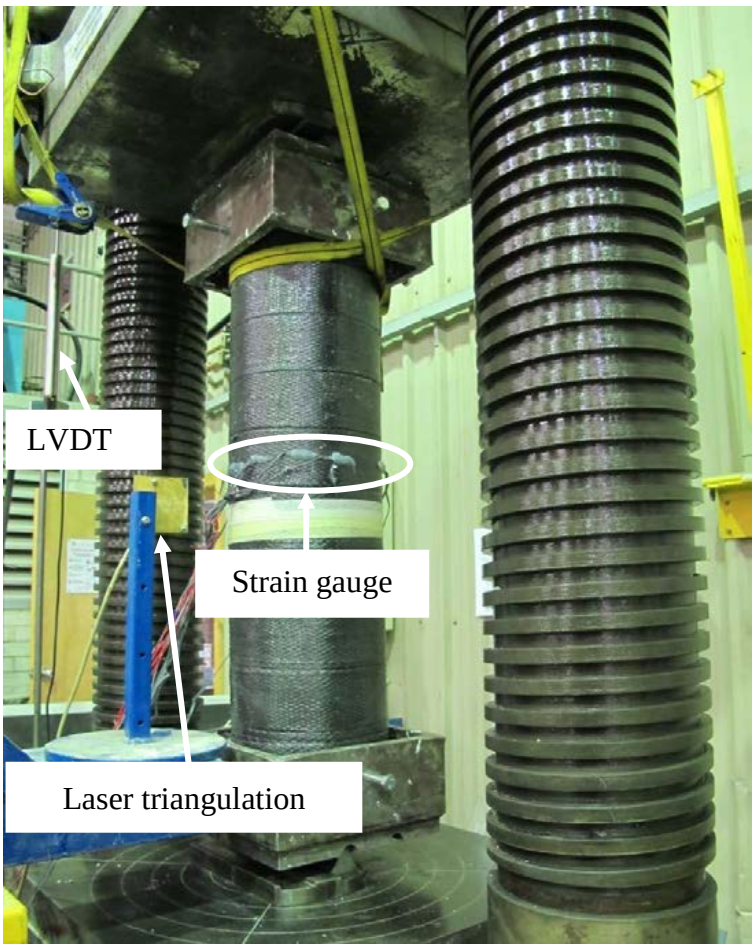

Figure 3.22 Measuring instruments arrangement

The electrical resistance strain gauges (SG) (UBF 20) were attached onto the surface of the middle CFRP ring (Figure 3.23) to investigate the strain of CFRP in the hoop direction. Four strain gauges were symmetrically bonded in all concentrically loaded columns while each eccentrically loaded column had ten strain gauges. More strain

gauges were installed in the compression region due to the largest confining pressure of the CFRP in this region. For beams, two strain gauges (SG) were attached at the compression and at the tension regions. All instrumental equipment were connected to a data-logger to record data during the testing at very two seconds.

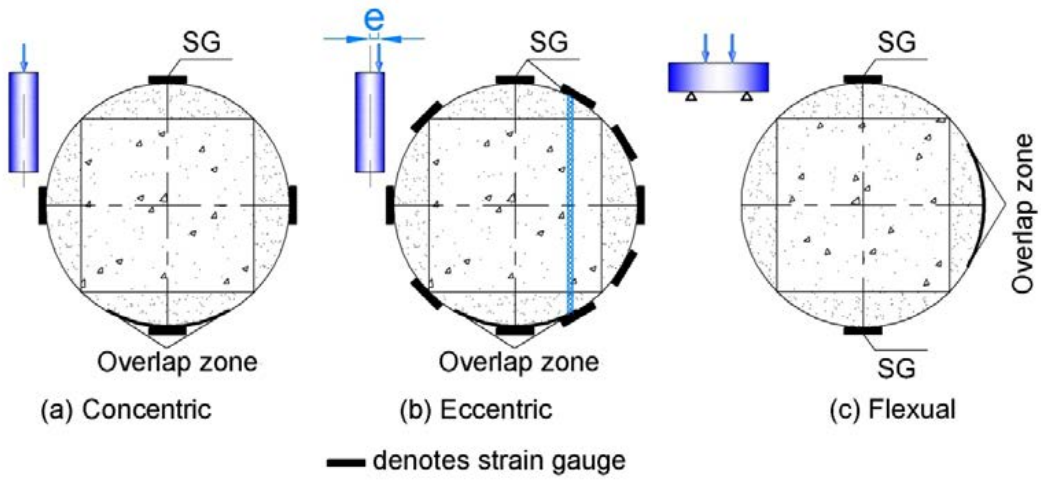

Figure 3.23 Strain gauge positions

3.6. Test setup and loading apparatus

All the columns including the four reference columns and twelve modified columns were tested using the 5000 kN Denison testing machine to failure. In order to transfer loading from the machine to the columns uniformly, each column was levelled by high strength plaster at both the top and bottom surfaces. The high strength plaster was poured on the first loading head. The column was then put on top of the first loading head and was calibrated with four bolts ϕ12 mm to ensure the column remained at the centre of the loading head. After that, the top column was filled with high strength plaster, then covered by the second loading head. The calibration at the centre of the second loading head was performed in a similar manner as above.

The eccentric loading was applied on the columns using the loading heads and the knife edges, as shown in Figure 3.24. These apparatus were made from high strength steel. The loading heads had two grooves, which were located at 25 mm and 50 mm from their centrelines. For 25 mm and 50 mm eccentric loading tests, the knife edges were placed at the groove position of 25 mm and 50 mm, respectively. For testing the beams, four-point loading system with a span of 700 mm was used (Figure 3.25).

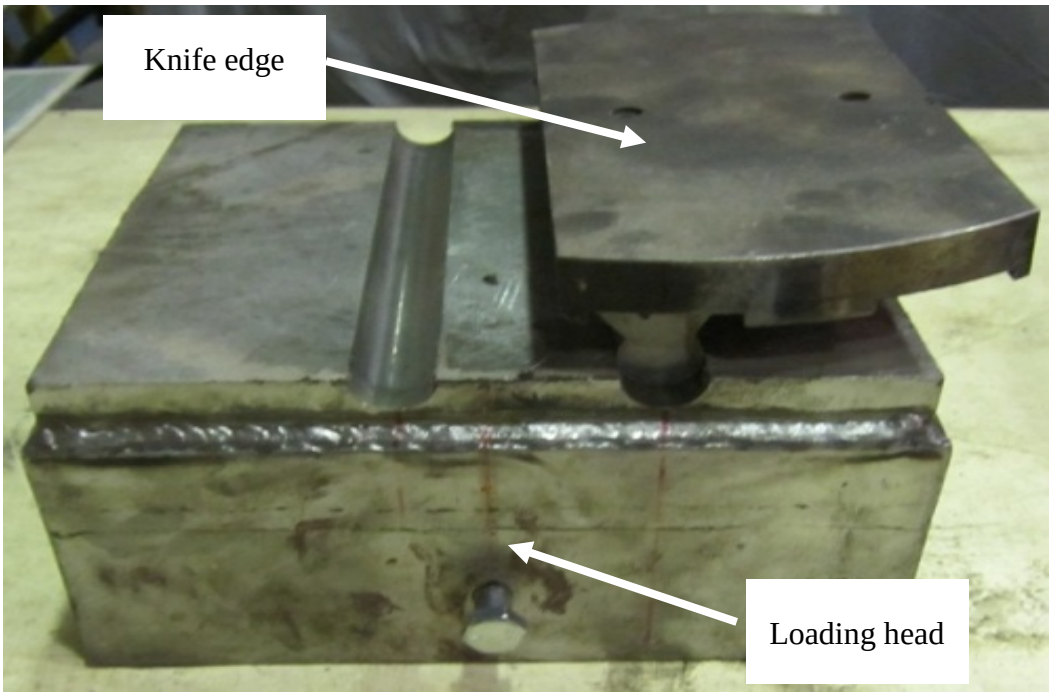

Figure 3.24 Loading head and knife edge used to apply eccentric loading

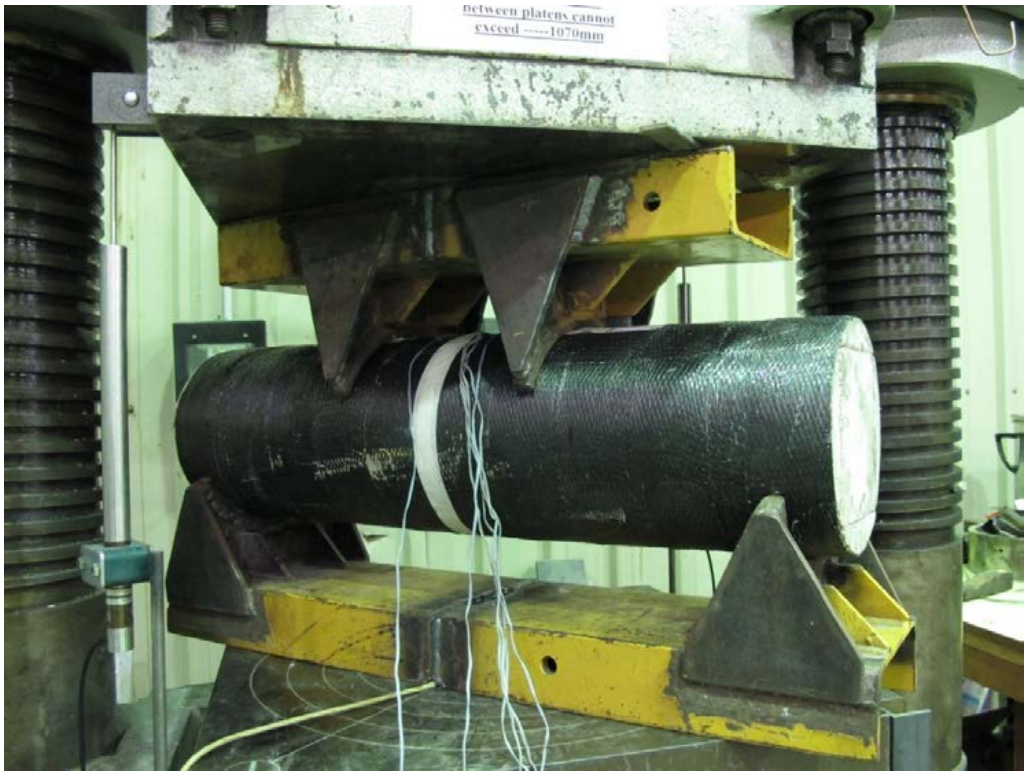

Figure 3.25 Four point loading regime for testing the modified specimens

3.7. Summary

This chapter presents the overall objectives of the experimental study and describes all the materials and procedures used in the High Bay laboratory of the University of Wollongong. Design and fabrication of the RC columns were introduced. The ancillary results of all material including normal strength concrete, high strength concrete, internal steel reinforcement, CFRP were analyzed. Finally, measuring equipment, test setup and loading apparatus were incorporated. The results of testing columns are presented in the next chapters.

CHAPTER 4. EXPERIMENTAL RESULTS

4.1 Introduction

This chapter presents the experimental results obtained from testing sixteen RC column specimens, twelve of which were confined with CFRP. All the columns were tested for their load-carrying capacity, axial and lateral displacement. In addition, the modified columns were tested for CFRP strain distribution in the hoop direction. These characteristics of the RC columns were observed under different loading conditions, including concentric loading, eccentric loading and flexural bending.

4.2 Behaviour of concentrically loaded columns

From each of the four groups of the prepared specimens described in Section 3.2, one specimen was tested under concentric loading to failure. The loading applied to these specimens was controlled with a displacement rate of 0.5 mm/min. The results of the experiments demonstrated that the CFRP plays an important role in enhancing the load-carrying capacity of the columns beyond their yield loads. Further, there was no debonding between the concrete core and the segmental circular concrete covers nor any failure of CFRP at the overlap zone.

4.2.1 Failure mechanism

The reference column, Specimen R-0, failed by crushing and spalling of the concrete cover at the upper height of the column. After the column achieved the ultimate load, the concrete cover began to spall, followed by the buckling outwards of the longitudinal reinforcement between two the ties at the mid-height of the column.

The confined columns, Specimens C40-0, C80-0 and C100-0, failed by the rupture of the CFRP, as illustrated in Figure 4.1. During testing, the relationship of applied load and axial deflection was linear until the unconfined compressive strength of the unconfined concrete covers and the core of the columns was achieved. At this point, the concrete began to crush but was restrained by the CFRP jacket. Here, there was a slight decrease in the load-carrying capacity as small ripples appeared on the sides of the columns, followed by a steady linear increase of the ultimate load carrying capacity where a snapping sound was heard and a small area of one CFRP ring near the mid-height of the columns ruptured. A sudden drop in the load carrying capacity

of the column was then observed. A second ring of CFRP at mid-height ruptured shortly afterwards, which created a loud noise. After the occurrence of this rupture, the concrete was completely crushed and the steel reinforcement buckled, as shown in Figure 4.1. In this study, the modified Specimens C100-0 and C80-0 had two types of concrete having different compressive strengths. These differences may lead to stress concentration on concrete covers, which had higher compressive strengths. As a result, the debonding at the interface between the two types of concrete may occur. As expected, there was no debonding between the concrete core and the segmental circular concrete covers nor any failure of the CFRP at the overlap zone.

4.2.2 Axial load and deflection responses

As can be seen in Figure 4.2, Specimen R-0 demonstrated a typical behaviour of steel-confined concrete; that is, the specimen increased to the peak load of 942 kN followed by a gradual descending branch to failure. The axial load-deflection diagrams of Specimens C40-0, C80-0 and C100-0 prove the effectiveness of CFRP due to the two distinct bilinear ascending responses with a sharp softening in the transition zone around the compressive strength of the unconfined concrete. The first branch of the axial load-axial deflection of the three retrofitted specimens was different because of the four segmental circular concrete covers, which were bonded to the existing core columns. These covers had various compressive strengths including 58 MPa, 98 MPa and 101 MPa. As a result, the yield load of Specimen C100-0 was 2418 kN, followed by C80-0 with 2452 kN and C40-0 with 2109 kN. The increase of yield load of 16% and 15% was achieved for Specimens C80-0 and C100-0 compared to Specimen C40-0, respectively. It is commonly assumed that the confinement effect caused by FRP is negligible at yield load. Thus, the increase of the yield load of Specimens C80-0 and C100-0 proved that the contribution of the high strength concrete of the segments. Furthermore, the yield loads of Specimens C40-0, C80-0 and C100-0 were higher than that of reference Specimen R-0 due to the cross-sectional enlargement and higher compressive strengths of the strengthened specimens. As a result, Specimens C100-0, C80-0 and C40-0 achieved 171%, 175% and 136% increase in yield load relative to reference Specimen R-0, respectively.

After reaching the yield load, the second branch of the load-deflection behaviour of these specimens was similar as the same amount of CFRP confinement was applied,

as shown in Figure 4.2. The axial load applied on the specimens increased linearly with the increase in the CFRP strain and achieved the ultimate load when the CFRP ruptured. Due to confinement effect of the CFRP jacket, the ultimate loads of Specimens C100-0, C80-0 and C40-0 increased by 1216 kN, 1010 kN and 1291 kN compared to their yield loads, respectively. The results revealed that the compressive strengths of concrete cover could have a negligible effect on CFRP confinement.

The experimental results, as shown in Figure 4.2, Figure 4.3 and Table 4.1, reveal the effectiveness of the retrofitting method. Specimen C100-0 achieved the highest ultimate load, which was 386% of Specimen R-0. This was followed by 368% and 361% in the ultimate load increase for Specimens C80-0 and C40-0, respectively, compared to that of Specimen R-0.

The concrete of the column cores and the segmental covers has differences in the axial concrete stiffness and the axial strain. These differences lead to inconsistency in transferring the applied load to the core and the covers. The experimental results revealed that the two concrete components worked as a composite material to failure. Therefore, the cross-sectional stress is calculated as the axial load divided by the gross cross-sectional area. As can be seen in Figure 4.3, the ultimate axial stress of Specimen R-0 was close to the cylinder compressive strength of concrete at testing day. However, the ultimate axial stress of CFRP-confined specimens was larger than the cylinder compressive strength of concrete at testing day. It was proven that the effect of CFRP confinement on the load-carrying capacity of the confined-specimens.

Table 4.1 Test results of the concentrically loaded columns

Specimen	R-0	C40-0	C80-0	C100-0
Yield Load (kN)	892	2109	2452	2418
Corresponding Axial Deflection (mm)	3.88	2.57	3.39	3.85
Ultimate Load (kN)	942	3400	3462	3634
Corresponding Axial Deflection (mm)	4.75	13.75	12.0	17.99
Ductility*	1.48	5.45	4.05	4.03

*Refer to Section 2.5 for ductility definition

(a) Specimen R-0

(b) Specimen C40-0

(c) Specimen C80-0

(d) Specimen C100-0

Figure 4.1 Failure modes of concentrically loaded columns

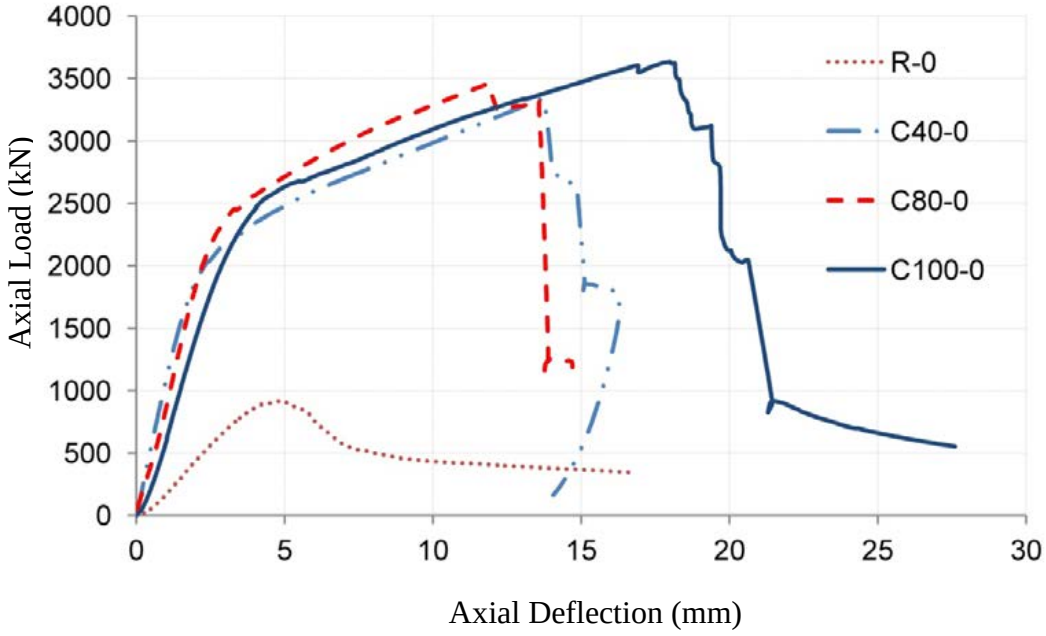

Figure 4.2 Axial Load- Deflection diagrams for concentric loading tests

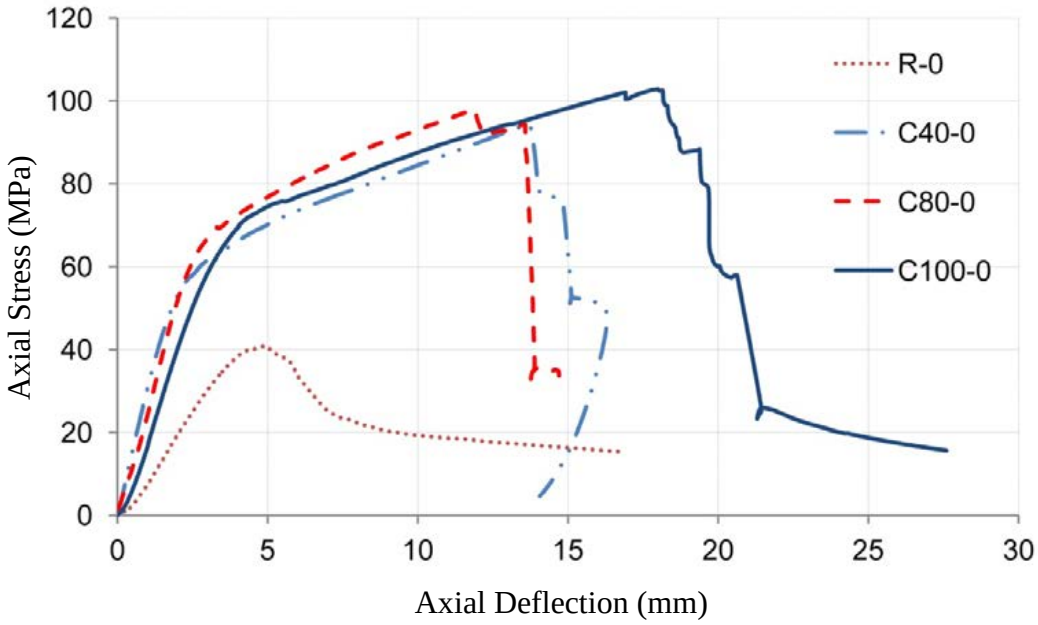

Figure 4.3 Axial Stress- Deflection diagrams for concentric loading tests

4.3 Behaviour of the eccentrically loaded columns

From each of the four groups of the prepared specimens described in Section 3.2, two specimens were tested under eccentric loading of 25 mm and 50 mm eccentricity to failure. The loading applied to these specimens was controlled with a displacement

rate of 0.5 mm/min. This testing demonstrated that the shape of load-deflection diagrams of the eccentrically loaded columns is different from those under concentric loading.

4.3.1 Failure mechanism

Specimen R-25 and Specimen R-50 failed by crushing and spalling of concrete covers in the compression side. The longitudinal steel in the compression side also buckled between the two ties at the mid-height of the columns.

The failure of the modified specimens under 25 mm and 50 mm eccentric loadings was generally characterised by crushing of concrete and rupture of CFRP at the extreme compression region, either at the peak compressive axial load, or at a lower post-peak load. When increasing the load, cracking of the concrete at the tension fibre between two rings of CFRP at the mid-height was first observed. Some CFRP ripples then appeared on the column sides followed by a snapping sound when the small area of one CFRP ring near the mid-height of the columns ruptured. At failure, the concrete in the compression region of the specimens completely crushed and the steel reinforcement buckled at the compression side of the specimens. There were also big cracks between two rings of CFRP at the mid-height in the tension side. The bond of the existing concrete columns and the segmental circular concrete covers was not destroyed proving that the proposed modification method is effective. Details of the failure modes of the modified specimens under eccentric loading of 25 mm and 50 mm eccentricity are shown in Figure 4.4 and Figure 4.5.

(a) Specimen R-25

(b) Specimen C40-25

(c) Specimen C80-25

(d) Specimen C100-25

Figure 4.4 Failure modes of the 25 mm eccentrically loaded specimens

(a) Specimen R-50

(b) Specimen C40-50

(c) Specimen C80-50

(d) Specimen C100-50

Figure 4.5 Failure modes of the 50 mm eccentrically loaded specimens

4.3.2 Axial load and deflection responses

As can be seen in Figure 4.6, Figure 4.7, Figure 4.8, Figure 4.9, Table 4.2 and Table 4.3, the specimens under 50 mm eccentric loading had a lower ductility and load-carrying capacity than that of 25 mm eccentric loading. The results of these specimens proved the effectiveness of the modification.

For Specimen R-25 and Specimen R-50, as shown in Figure 4.6 and Figure 4.8, the axial load versus deflection diagram was linear until the yield load was reached. This linearity was followed by a sudden drop, leading to crushing the concrete in the compression region and cracks in the tension region. The specimens deflected extensively before failure occurred.

Figure 4.6 shows the load-deflection diagrams for the 25 mm eccentrically loaded Specimens C40-25, C80-25 and C100-25. The slopes of the axial load versus deflection were ascending until reaching the ultimate load. Due to crushing of concrete, the load-carrying capacity of the specimens decreased slightly. At this time, the CFRP confinement became active. After the rupture of CFRP at mid-height, there was a steep drop in the load-carrying capacity of the specimens to failure. The ultimate load of Specimens C100-25, C80-25 and C40-25 was 264%, 260% and 231% that of the reference Specimen R-25, respectively.

The axial load-deflection diagrams of the specimens under 50 mm eccentricity (Specimens C40-50, C80-50 and C100-50) were nearly similar to that of the specimens under 25 mm eccentricity (Specimens C40-25, C80-25 and C100-25). However, after achieving the ultimate load, the load-carrying capacity of the specimens under the 50 mm eccentric load decreased quicker than that of the 25 mm eccentric load, as shown in Figure 4.6 and Figure 4.8. This phenomenon explained why the ductility of 50 mm eccentrically loaded specimens was smaller than that of 25 mm, as shown in Table 4.2 and Table 4.3.

For the specimens under 50 mm eccentric load, Specimen C100-50 achieved the highest ultimate load, which was 260% that of Specimen R-50. This was followed by 255% and 229% in the ultimate load enhancement for Specimens C80-50 and C40-50 compared to that of Specimen R-50.

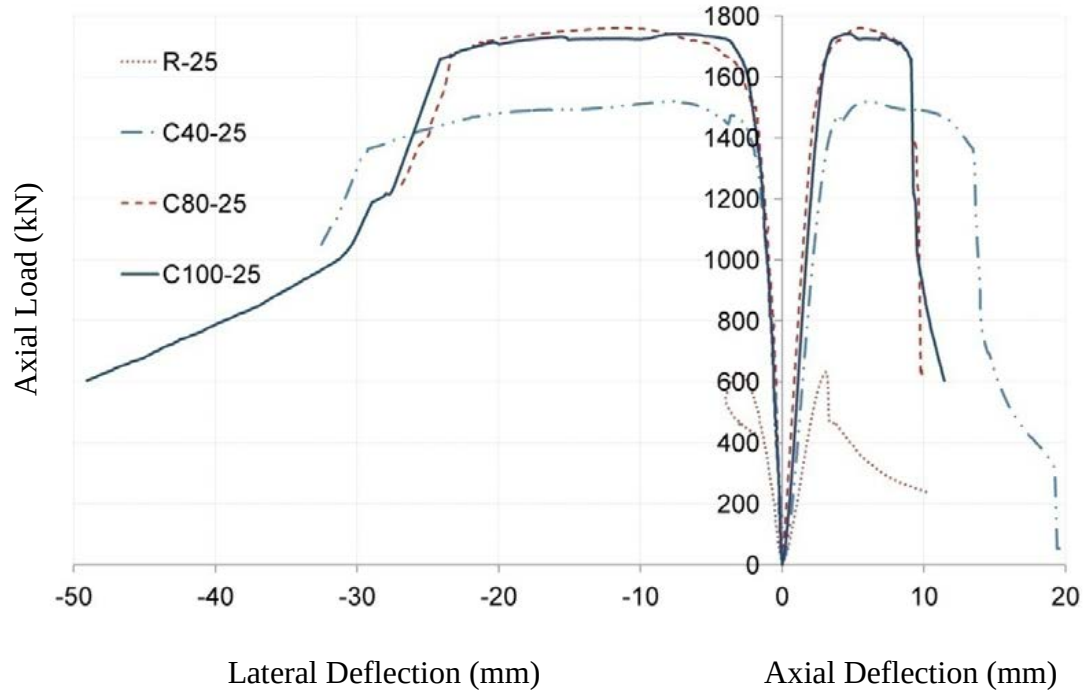

Figure 4.6 Axial Load- Deflection diagrams for 25 mm eccentric loading tests

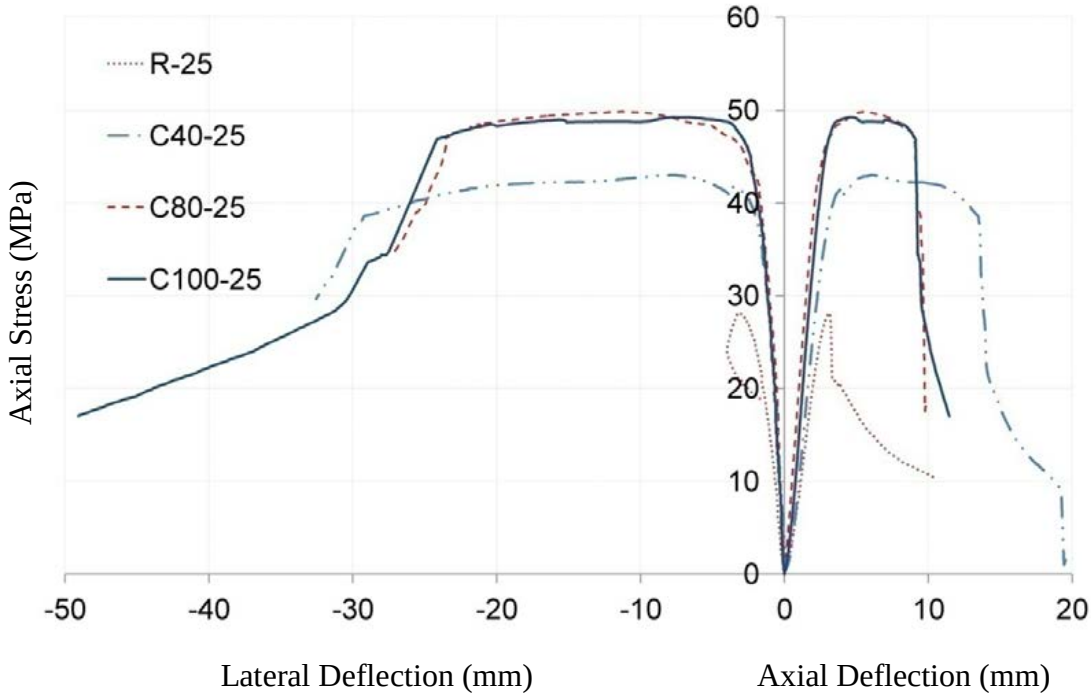

Figure 4.7 Axial Stress- Deflection diagrams for 25 mm eccentric loading tests

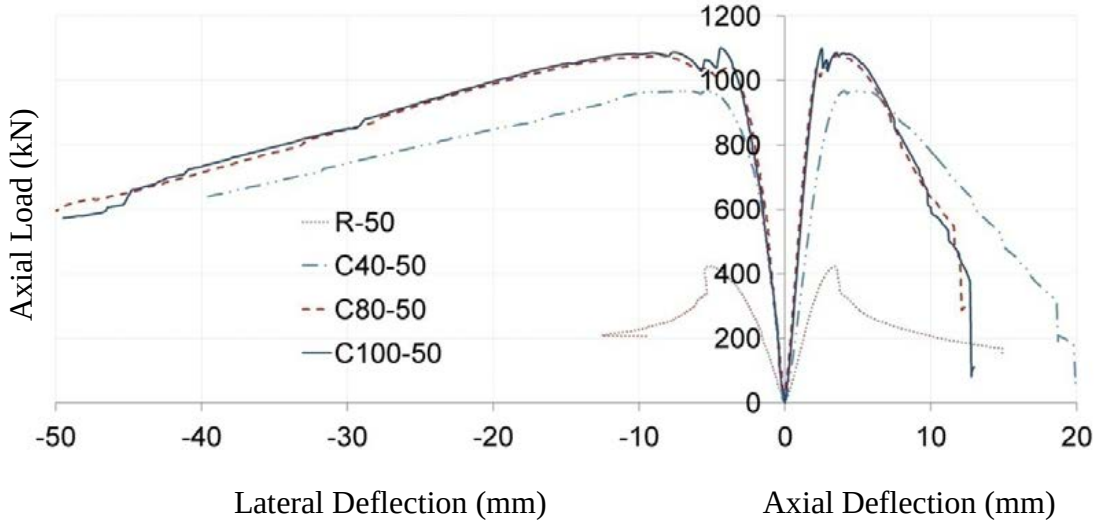

Figure 4.8 Axial Load- Deflection diagrams for 50 mm eccentric loading tests

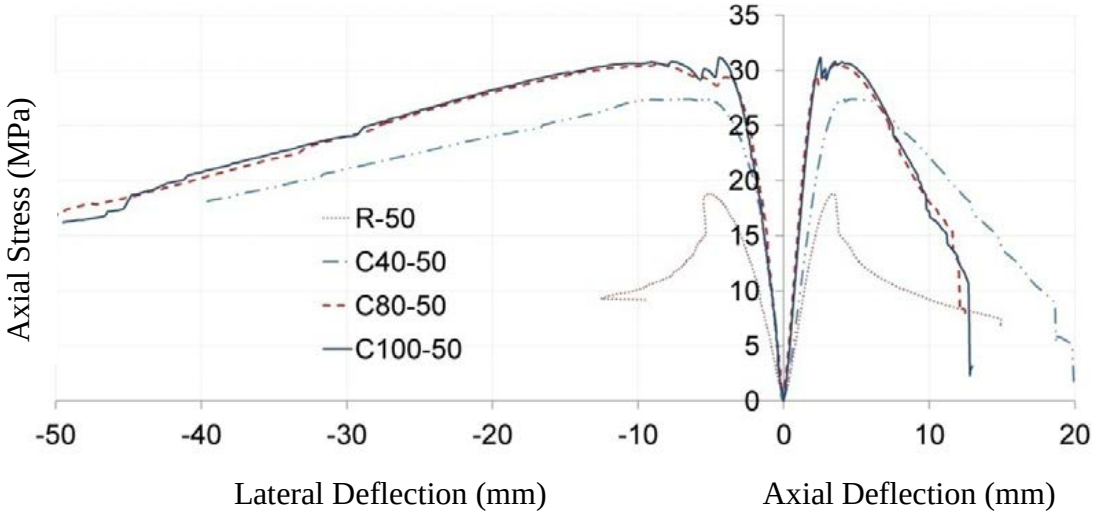

Figure 4.9 Axial Stress- Deflection diagrams for 50 mm eccentric loading tests

Table 4.2 Test results of 25 mm eccentrically loaded specimens

Specimen	R-25	C40-25	C80-25	C100-25
Yield Load (kN)	615	1421	1603	1624
Corresponding Axial Deflection (mm)	2.84	3.43	2.72	2.93
Ultimate Load (kN)	633	1519	1762	1741
Corresponding Axial Deflection (mm)	3.13	6.03	5.52	4.79
Corresponding Lateral Deflection (mm)	3.20	7.60	11.27	7.76
Ductility*	1.15	3.97	3.37	3.16

*Refer to Section 2.5 for ductility definition

Table 4.3 Test results of 50 mm eccentrically loaded specimens

Specimen	R-50	C40-50	C80-50	C100-50
Yield Load (kN)	416	905	1020	1095
Corresponding Axial Deflection (mm)	3.09	3.19	2.50	2.47
Ultimate Load (kN)	423	968	1080	1101
Corresponding Axial Deflection (mm)	3.40	4.05	3.57	2.54
Corresponding Lateral Deflection (mm)	5.13	5.27	8.63	4.39
Ductility*	1.22	2.88	2.78	2.79

*Refer to Section 2.5 for ductility definition

4.4 Behaviour of the beams

From each of the four groups of prepared specimens described in Section 3.2, one specimen was tested under four-point loading regime. The loading applied to these specimens was controlled with a displacement rate of 0.5 mm/min. The results of the experiments demonstrated that these modified beams had higher load carrying capacity than the reference beam owing to the larger compression section and CFRP confinement effect on the modified beams.

4.4.1 Failure mechanism

The reference beam, Specimen R-F, failed by crushing the concrete in the compression side and the fracture of the longitudinal reinforcement in the tension region. The vertical cracks first occurred as a result of flexural stresses under the applied load. Those cracks started at the bottom of the beam where the flexural stresses were the largest. As the load increased, additional cracks formed closer to the supports and some of the cracks became slightly inclined towards the load. The inclined cracks at the ends of the beam are due to the combination of shear and flexure. The compression strut in the beam appeared and the beam completely failed, as shown in Figure 4.10a.

The three retrofitted beams, Specimens C40-F, C80-F and C100-F behaved in a similar manner as Specimen R-F. However, these retrofitted specimens achieved the higher yield load and ultimate load capacity than the reference specimen due to the larger compression region of the concrete in the tension side and the CFRP confinement effect. The first vertical crack occurred between two CFRP rings at the midspan of these beams. As the load increased, these cracks propagated towards both ends as shown in Figure 4.10b.

4.4.2 Load and midspan deflection responses

Figure 4.11 and Figure 4.12 respectively show the load- midspan deflection diagrams and the maximum bending stress-midspan deflection diagrams for the specimens tested under four-point loading regime. The maximum bending stress of beams is calculated as the maximum bending moment divided by the section modulus for cross-section of the beams. The reference beam, Specimen R-F increased steadily before achieving the ultimate load. At this time, the concrete in the beam reached the

ultimate strain. The specimen deformed extensively before complete failure. This is because the internal steel reinforcing bars carried the majority of tensile force in the tension region.

The load-midspan deflection diagrams of Specimens C40-F, C80-F and C100-F included two stages with two different slopes, as shown in Figure 4.11. The ultimate load of Specimens C100-F, C80-F and C40-F was 223%, 291% and 282% that of the reference Specimens R-F.

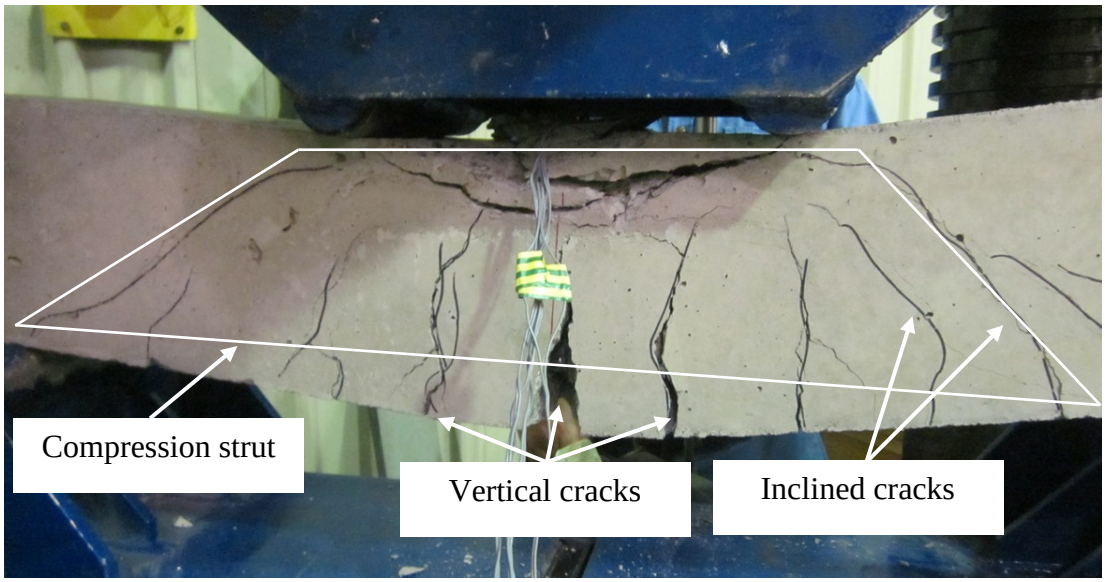

(a) Specimen R-F

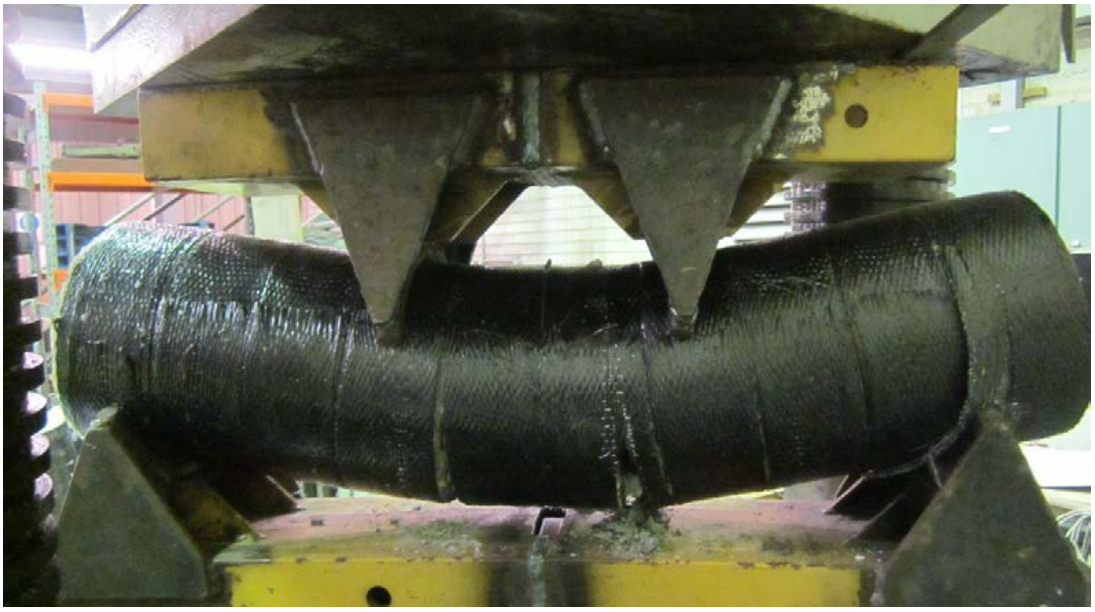

(b) Specimen C80-F

Figure 4.10 Failure modes of the beams

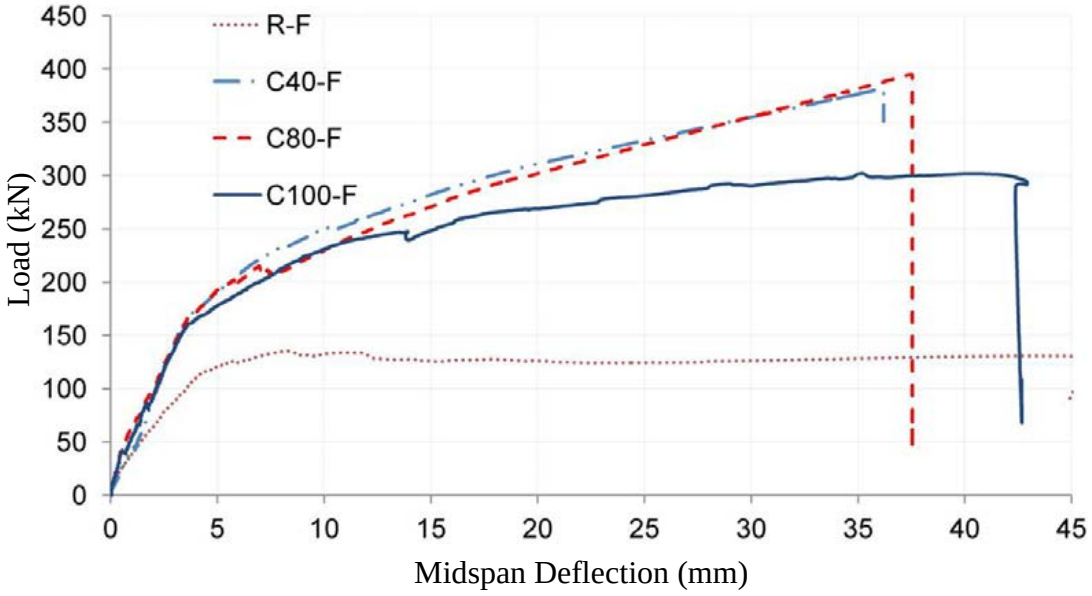

Figure 4.11 Load - Midspan deflection diagrams of the beams

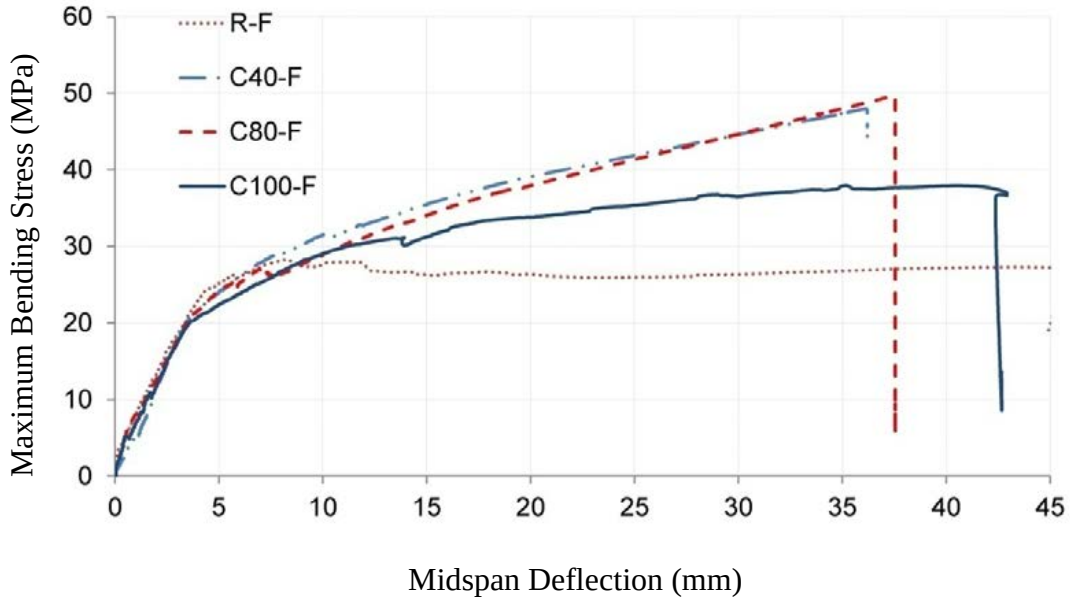

Figure 4.12 Maximum Bending Stress - Midspan deflection diagrams of the beams

Table 4.4 Test results of beams under four-point loading regime

Specimen	R-F	C40-F	C80-F	C100-F
Yield Load (kN)	122	178	187	182
Corresponding Midspan Deflection (mm)	5.24	4.30	4.73	5.36
Ultimate Load (kN)	136	382	395	302
Corresponding Midspan Deflection (mm)	8.23	36.15	37.49	35.193
Ductility*	8.64	8.42	7.93	7.91

*Refer to Section 2.5 for ductility definition

4.5 Distribution of CFRP hoop strain under different loading conditions

The CFRP strain in hoop direction (out of the overlap zone) of the concentrically loaded columns was almost uniform. However, the CFRP hoop strain became the largest at the extreme fibre in the compression region of the columns under the eccentric loading. The strain gauge layout, as described in Section 3.5, was used to measure the hoop strain of the CFRP jacket at the mid-height under concentric loading and eccentric loading (25 mm and 50 mm).

4.5.1 Concentrically loaded columns

The CFRP of concentrically loaded columns ruptured at the ultimate load. The CFRP hoop strain at rupture was calculated from the average values from the strain gauges outside the overlap zone.

The average hoop strains in the CFRP at failure were approximately 1.29%, 1.05% and 1.08% for Specimens C40-0, C80-0 and C100-0, respectively. These results proved that the compressive strength of concrete covers had a negligible effect on the confinement of CFRP. In addition, the smallest strain was always found within the

overlap zone, which was about 75% of the average strain in CFRP at rupture. This is because the thickness of CFRP within the overlap zone was thicker than outside the overlap zone. The strain in the jacket is inversely proportional to the thickness of the jacket for the same confinement pressure.

As stated in Section 3.4.3, the average ultimate strain from flat coupon tests was 1.74%. The CFRP strain efficiency factors of these specimens, defined as the ratio of the actual hoop rupture strain to the ultimate strain of CFRP from flat coupon tests, are given in Table 4.5.

Table 4.5 Results of CFRP strain at rupture for concentrically loaded columns

Specimen	C40-0	C80-0	C100-0
Ultimate Load (kN)	3343	3462	3634
CFRP strain at rupture (%)	1.29	1.05	1.08
CFRP strain in overlap zone at failure (%)	1.01	0.81	0.77
Strain efficiency factor	0.74	0.60	0.62

*Refer to Section 2.6 for CFRP strain efficiency factor

4.5.2 Eccentrically loaded columns

The CFRP rupture of eccentrically loaded columns did not simultaneously occur when these columns reached the ultimate load, as shown in Figure 4.13. Therefore, the CFRP strain distributions of these specimens were obtained at the ultimate load and at CFRP rupture.

The CFRP strain was the highest at the extreme compression fibre, whereas the smallest strain arose at the extreme tension fibre of the columns. The CFRP strain decreased gradually from the extreme compression fibre to the extreme tension fibre, as shown in Figure 4.14. This figure also shows the effect of the overlap zone on the hoop strain distribution over the columns' circumference. The CFRP strains within the overlap zone were always lower than outside the overlap zone. The strains at the

extreme compression fibre were 5.3 and 3.3 times higher than those at the extreme tension fibre when Specimen C80-25 achieved the ultimate load and CFRP ruptured, respectively. Furthermore, these ratios were 10.8 and 9.3 respectively for Specimens C80-50. The results demonstrate that the disproportion between the CFRP strain at the extreme compression fibre and at the extreme tension fibre increased when the columns were subjected to higher eccentricity.

The strain efficiency factor of CFRP under eccentric load is defined as the ratio of CFRP strain at the extreme compression fibre at the ultimate load to the ultimate strain of CFRP from flat coupon tests. The higher eccentricity led to the lower strain efficiency factor. For example, the strain efficiency factors were 0.65, 0.4 and 0.26 for the columns under concentric loading, 25 mm eccentric loading and 50 mm eccentric loading.

Table 4.6 presents results of the CFRP rupture strains in the hoop direction at the extreme compression fibre, which were quite similar to the value of CFRP rupture strain under concentric loading. It is believed that the CFRP ruptured when the maximum CFRP hoop strain reached about 0.68% of the ultimate strain of CFRP from flat coupon tests.

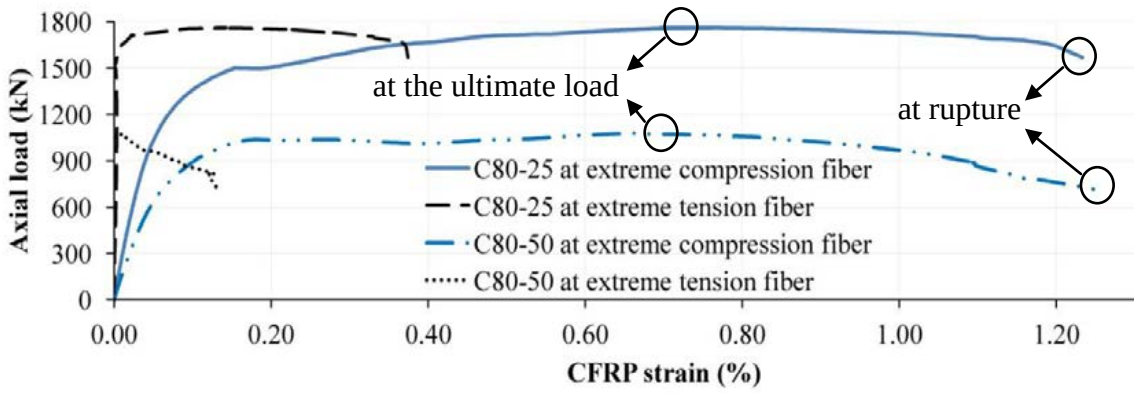

Figure 4.13 Axial load- CFRP strain diagrams of specimens subjected eccentric load

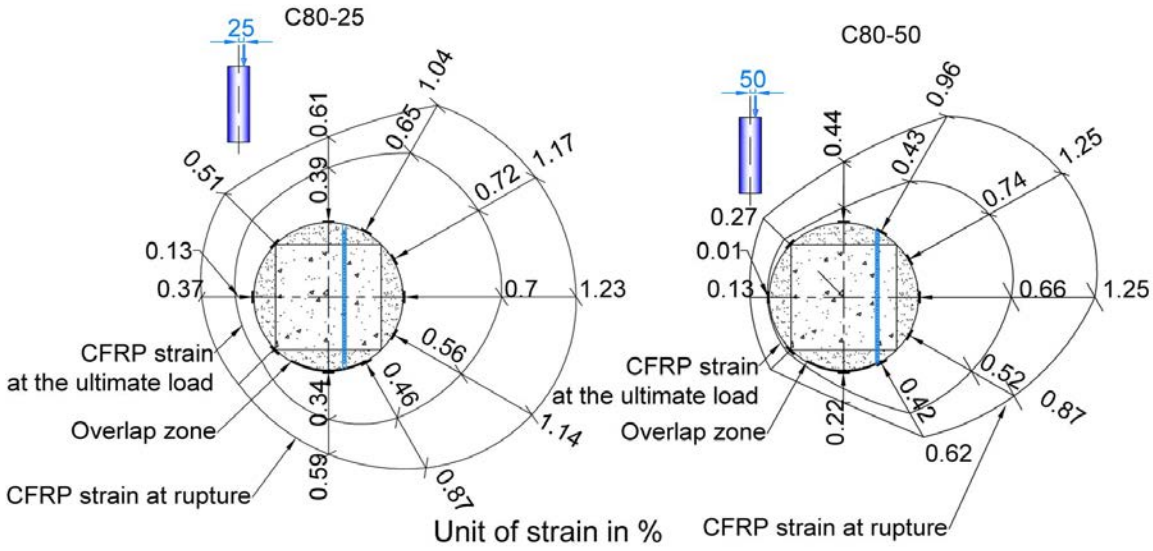

Figure 4.14 CFRP hoop strain distribution over the columns' circumference

Table 4.6 CFRP hoop strain of the columns at extreme compression fibre at rupture

Eccentricity	CFRP hoop strain of the columns		
	C40 group	C80 group	C100 group
Concentric load	1.29%	1.05%	1.08%
25 mm Eccentric load	1.13%	1.23%	1.16%
50 mm Eccentric load	1.22%	1.25%	-

4.6 Axial load-Moment Interaction Diagrams

The specimens in this experimental program were tested under different loading conditions including concentric loading, eccentric loading (25 mm and 50 mm) and flexural bending. An axial load-bending moment interaction diagram visualizes the different combinations of axial load and bending moment of these specimens. The diagrams were constructed based on four points:

(1) The column subjected to the concentric load.

(2) The column subjected to the 25 mm eccentric load.

(3) The column subjected to the 50 mm eccentric load.

(4) The beam tested under four-point loading regime.

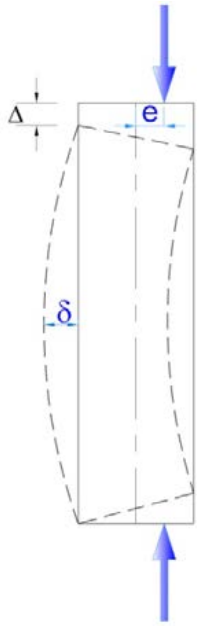

Figure 4.15 Deflection of the eccentrically loaded column

The moments of the eccentrically loaded columns incorporate the moments as results of the initial load eccentricity, P.e, as well as the second-order effect, as shown in Figure 4.15. The moment capacities including the secondary moments were calculated as follows:

$$M = P(e + \delta) \tag{4.1}$$

where P = the ultimate axial load; e = initial load eccentricity and δ = lateral deflection at the ultimate load.

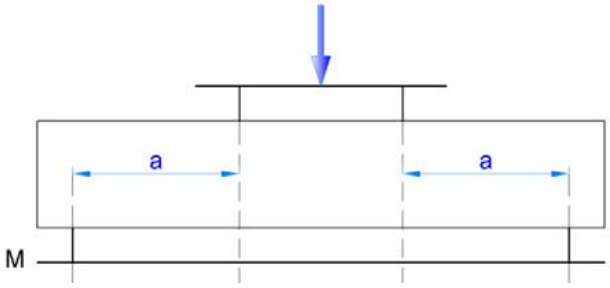

Figure 4.16 Testing specimens under four-point loading regime

The bending moment capacity of the investigated specimens is reported in Table 4.7 and the experimental P-M interaction diagrams are plotted in Figure 4.17. It can be seen that the retrofitted specimens achieved both the higher load-carrying capacity and bending moment compared to the reference specimens, even for the specimens subjected to highly eccentric loading. There were strength reductions in the range of 49% to 55% for CFRP confined columns with an eccentricity-to-diameter (e/D) ratio

of 0.12 (25 mm eccentricity) and in the range of of 69% to 71% with e/D of 0.24 (50 mm eccentricity).

Table 4.7 Summary of test results for P-M diagrams

Specimen	Eccentricity mm	Ultimate load kN	Lateral deflection mm	Bending moment kNm
R-0	0	942.00	0.00	0.00
R-25	25	633.00	3.20	17.85
R-50	50	423.00	5.13	23.32
R-F	Flexural	0.00	8.23	15.98
C40-0	0	3400.00	0.00	0.00
C40-25	25	1519.00	7.60	49.52
C40-50	50	968.00	5.27	53.50
C40-F	Flexural	0.00	36.15	44.89
C80-0	0	3462.00	0.00	0.00
C80-25	25	1762.00	11.27	63.91
C80-50	50	1080.00	8.63	63.32
C80-F	Flexural	0.00	37.49	46.41
C100-0	0	3634.00	0.00	0.00
C100-25	25	1741.00	7.76	57.04
C100-50	50	1101.00	4.39	59.88
C100-F	Flexural	0.00	35.19	35.49

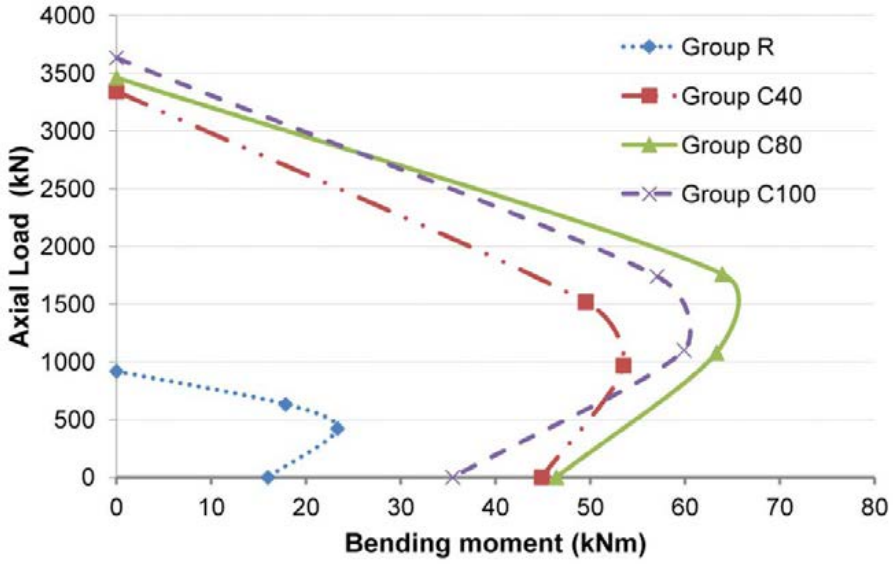

Figure 4.17 Experimental P-M diagrams

4.7 Summary

This chapter presented and discussed the results of the reference and the retrofitted columns under concentric loading, eccentric loading (25 mm and 50 mm) and flexural bending. On the basis of the test observation in the experimental program, the following conclusions can be drawn:

1. The proposed retrofitting method was used effectively in terms of improving the axial load-carrying capacity and ductility of the columns under all loading conditions. The load-carrying capacity of the modified columns was about 3.6 to 4 times higher than that of the reference columns under concentric loading and about 2.3 to 2.6 times higher under eccentric loading.
2. There was no debonding between the concrete core and the segmental circular concrete covers nor any failure of CFRP at the overlap zone. This observation proves that the two concrete components worked as a composite material to failure.
3. The effect of segmental concrete cover compressive strength on CFRP confinement could be neglected due to the similar second portion of the stress-strain curve of the retrofitted columns.
4. The experimental results revealed that CFRP confinement was less effective when columns subjected to higher eccentric loading. After reaching the ultimate load, the stress-strain curves of 50 mm eccentrically columns decreased faster than that of 25 mm and concentric loaded columns.
5. Columns subjected to high eccentricity had lower ductility due to CFRP confinement effect under eccentric loading. The ductility was about 2.8 and 3.5 for 50 mm and 25 mm eccentrically loaded columns, respectively.
6. The CFRP strain efficiency factors were 0.653, 0.4 and 0.26 for the specimens under concentric loading, 25 mm eccentric loading and 50 mm eccentric loading, respectively.
7. The CFRP rupture strains at the extreme compression fibre under eccentric loading were quite similar to the value of CFRP rupture strain under concentric loading.
8. The disproportion between the CFRP strain at the extreme compression fibre and at the extreme tension fibre increased when the columns were subjected to higher eccentricity.

The experimental results proved the effectiveness of the proposed method in enhancing the load-carrying capacity and ductility of CFRP confined square column under all loading conditions. A theoretical study is conducted in the following chapter to generate a theoretical axial load-bending moment diagram model.

CHAPTER 5. ANALYTICAL MODELING OF COLUMNS

5.1 Introduction

RC columns are generally subjected to axial compressive loads as well as bending moments. The bending moments may be caused by misalignment of the load on the columns, or may result from the column resisting a portion of the moments at the ends of the beams that are supported by the columns. Therefore, the evaluation of the axial load-bending moment plays an important role in the design and analysis of the columns.

An axial load-bending moment (P-M) interaction diagram can be constructed based upon strain compatibility and force equilibrium. The only difference for establishing a P-M interaction diagram of CFRP confined columns is the use of a CFRP confined stress-strain curve to replace the stress-strain curve of unconfined concrete (Concrete Society 2012; ACI 440.2R 2008; Bank 2006; Hadi et al. 2013; Hadi and Widiarsa 2012; Rocca et al. 2009). The stress-strain relationship of the unconfined concrete is based upon Popovics (1973) model. The stress-strain relationship of the CFRP-confined concrete is established using two models proposed by Lam and Teng (2003a) and Eid and Paultre (2008). The Eid and Paultre (2008) model accounts for the interaction between the internal lateral steel reinforcement and the external CFRP jackets while the Lam and Teng (2003a) model considers the confinement effect of CFRP. Finally, the design guidelines currently being proposed by ACI-440.2R (2008) are adopted to construct the P-M interaction diagram.

The following sections present the details of how the interaction diagrams were computed. The results obtained from the analytical methods were then validated by the experimental results.

5.2 Assumptions

The relationship needed to compute the various points on the P-M interaction diagrams are derived using strain compatibility and force equilibrium and satisfies the following assumptions:

1. Sections that are plane before bending remain plane after bending. That is, the strain at each point of the cross-section is proportional to its distance from the neutral axis.

2. The strain in the reinforcement is equal to the strain in the concrete at the same level. This assumption ensures a perfect bond between the concrete and the steel reinforcement.

3. The stress in the concrete and reinforcement can be computed from the strains using the stress-strain curves for concrete and steel.

4. The tensile strength of concrete is ignored in flexural-strength calculations. The strength of the concrete in tension is roughly one-tenth of the compressive strength and the tensile force in the concrete below the zero strain axis is small compared with the tensile force in the steel. Hence, the contribution of the tensile stresses in the concrete to the load-carrying capacity is small and can be ignored.

5. The concrete is assumed to fail when the maximum compressive strain reaches:

- ✓ 0.003 for unconfined concrete.
- ✓ 0.01 or maximum axial strain, whichever is less for CFRP confined concrete.

Limiting the maximum value of ultimate axial strain to 0.003 for unconfined concrete and 0.01 for CFRP-confined concrete is intended to prevent excessive cracking and the resulting loss of concrete integrity. Additionally, the limiting values of maximum compressive strain are consistent with the recommendations from the Concrete Society in the Technical Report 55 (2012) and ACI-440.2R (2008).

6. CFRP in hoop and axial direction is assumed to have no stiffness under compression and has a linear elastic response to failure in tension.

5.3 Stress-strain behaviour of confined concrete

5.3.1 Lam and Teng's Model

Lam and Teng's design-oriented stress-strain model (Lam and Teng 2003a) has been common in practical applications and adopted by the latest ACI 440.2R (2008) for FRP-confined concrete. The stress-strain model of FRP-confined concrete is

designed based on five basic assumptions: (i) the stress-strain curve consists of a parabolic first portion and a straight line second portion, as shown in Figure 5.1; (ii) the slope of the initial slope is the same as the elastic modulus of unconfined concrete ; (iii) the nonlinear part of the first portion is affected to some degree by the presence of an FRP jacket; (iv) The parabolic first portion meets the linear second portion smoothly; (v) the linear second portion ends at a point where both the FRP confined compressive strength and the ultimate axial strain of the FRP confined concrete are reached.

Based on these assumptions, the proposed stress-strain model for FRP-confined concrete is described by the following expressions:

$$\sigma_c = E_c\varepsilon_c - \frac{(E_c - E_2)^2}{4f'_{co}}\varepsilon_c^2 \text{ for } 0 \le \varepsilon_c \le \varepsilon_t \tag{5.1}$$

$$\sigma_c = f'_{co} + E_2\varepsilon_c \text{ for } \varepsilon_t \le \varepsilon_c \le \varepsilon_{cu} \tag{5.2}$$

where σ_c and ε_c are the axial stress and the corresponding axial strain, E_c is the elastic modulus of unconfined concrete, E_2 is the slope of the linear second portion and f'_{co} is the compressive strength of unconfined concrete.

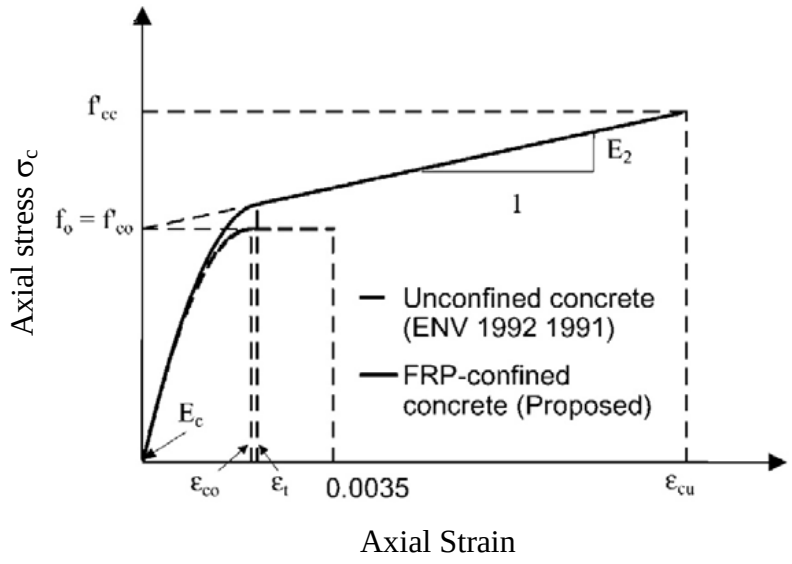

Figure 5.1 Stress-strain model for FRP-confined concrete (Lam and Teng 2003a)

The transition strain (ε_t) between the parabolic fist portion and the linear second portion and the slope of the linear second portion E_2 are presented:

$$\varepsilon_t = \frac{2 f_{co}^{'}}{(E_c - E_2)} \tag{5.3}$$

The slope of the linear second portion E_2 is given by:

$$E_2 = \frac{f_{cc}^{'} - f_o}{\varepsilon_{cu}} \tag{5.4}$$

where $f_{cc}^{'}$ and and ε_{cu} are the compressive strength and ultimate axial strain of confined concrete.

Lam and Teng (2003a) proposed the following equations to predict compressive strength ($f_{cc}^{'}$), which can be calculated as

$$f_{cc}^{'} = f_{co}^{'} + 3.3 f_l \tag{5.5}$$

where f_l is the effective confining pressure of FRP, which can be estimated by

$$f_l = \frac{2 f_{fu} t_f k_\varepsilon}{D} \tag{5.6}$$

where f_{fu} and t_f are respectively the rupture stress and the thickness of FRP, *D* is the diameter of a column and k_ε is the FRP strain efficiency factor calculated as

$$k_\varepsilon = \frac{\varepsilon_{fe}}{\varepsilon_{fu}} \tag{5.7}$$

where ε_{fe} is the actual FRP hoop rupture strain in FRP-confined concrete and ε_{fu} is the FRP rupture strain from flat coupon tests.

The ultimate axial strain (ε_{cu}) of FRP-confined concrete can be expressed as

$$\varepsilon_{cu} = \varepsilon_{co}\left(1.75 + 12\frac{f_l}{f_{co}^{'}}\left(\frac{\varepsilon_{fe}}{\varepsilon_{co}}\right)^{0.45}\right) \tag{5.8}$$

It should be remembered that a significant strength enhancement can only be expected with an actual confinement ratio $f_l^{'}/f_{co}^{'} \geq 0.07$. For the case of FRP-confined concrete with $f_l^{'}/f_{co}^{'} < 0.07$, no strength enhancement suggested by Spoelstra and Monti (1999) is assumed.

It can be seen that the proposed models (Lam and Teng 2003a, 2003b) compared well with the results of test data of other studies in circular section, as shown in Figure 5.2.

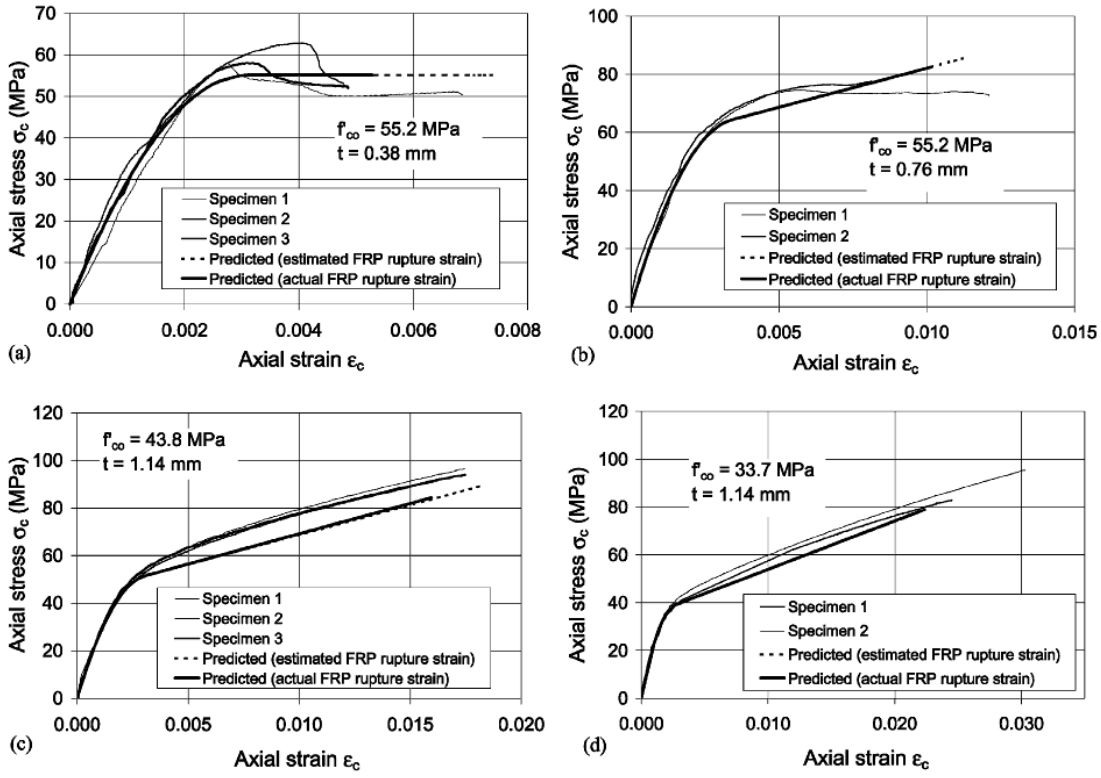

Figure 5.2 Comparison between proposed model and test stress-strain curves for circular section (Lam and Teng 2003a)

5.3.2 Eid and Paultre's model

According to structural design codes (American Concrete Institute (ACI) 318-08; Australian Standard the (AS) 3600 (2009)), the concrete columns should include a minimum amount of the transverse steel reinforcement. Therefore, the retrofitted concrete column confined with FRP is under dual confinement of the FRP and the transverse steel reinforcement. The first ascending branch of the stress-strain curve for the FRP-steel-confined concrete is similar to that of the FRP-confined concrete and the steel-confined concrete. However, the stiffness of the second branch for the

FRP-steel-confined concrete is higher than others due to the higher confinement, as shown in Figure 5.3.

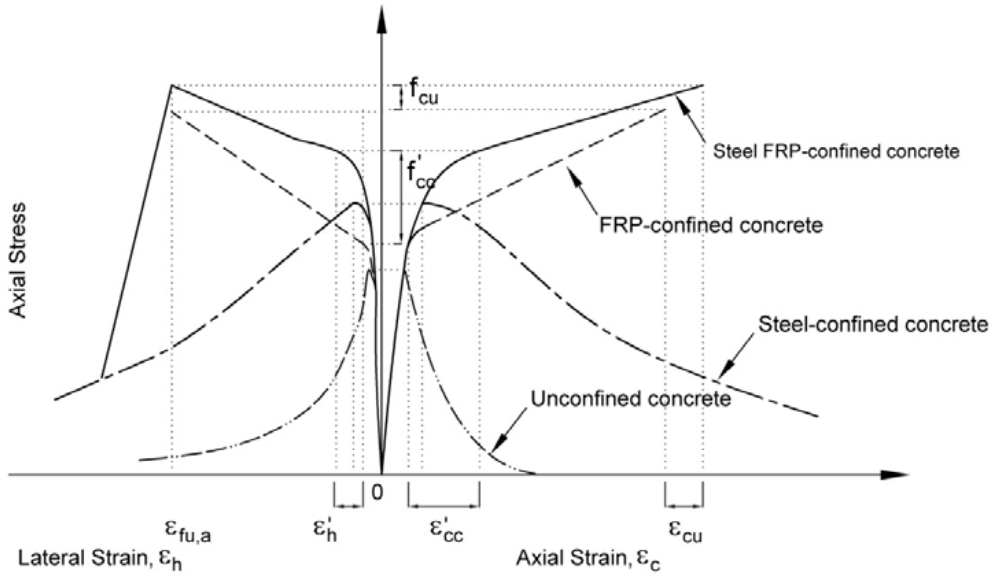

Figure 5.3 Stress-strain curves for FRP-steel-confined concrete (Eid and Paultre 2008)

The ultimate concrete strain and the ultimate concrete strength of Eid and Paultre's (2008) model were modified from Lam and Teng's (2003a) model and calibrated based on a set of 117 experimental results of normal and high strength FRP and FRP-steel-confined concrete columns.

$$f'_{cc} = f'_{co} + 3.3(f_l + f'_l) \tag{5.9}$$

$$\varepsilon_{cu} = \varepsilon_{co}\left(1.56 + 12\left(\frac{f_l + f'_l}{f'_{co}}\right)\left(\frac{\varepsilon_{fe}}{\varepsilon_{co}}\right)^{0.45}\right) \tag{5.10}$$

where f'_l is the effective confining pressure of transverse steel reinforcement in accordance with AS 3600 (2009).

The lateral- to- axial relationship was developed from the elastic constitutive Hooke's law, as follows

$$\varepsilon_l = \frac{\nu_c \varepsilon_c}{1+(m_{sl}+m_{sf})(1-\nu_c-2\nu_c^2}} \tag{5.11}$$

where m_{sl} and m_{sf} are the modulus ratio of transverse steel and concrete and the modulus ratio of FRP and concrete, ν_c is the concrete secant Poisson's ratio.

5.4 Column design under axial load- bending moment

The unconfined and CFRP confined axial load-bending moment (P-M) diagrams can be constructed by four points (Bank 2006; Rocca et al. 2009), as shown in Figure 5.4, where four points on the curve are determined:

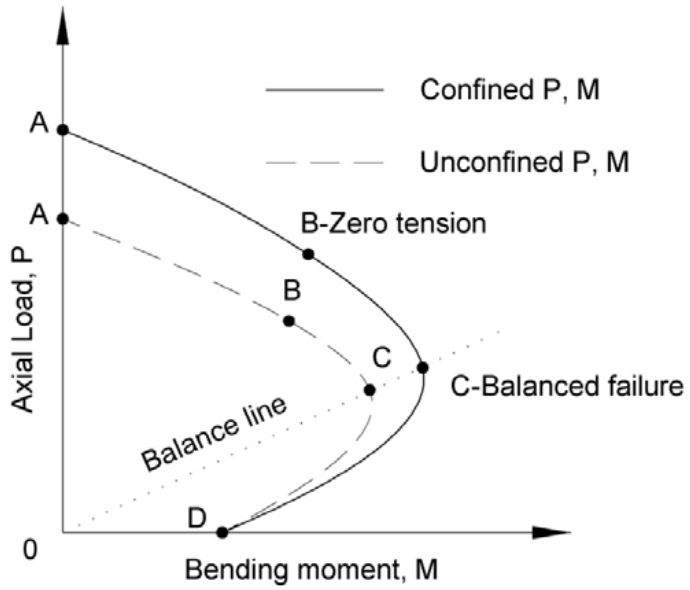

Figure 5.4 Axial load- bending moment interaction diagrams (Rocca et al. 2009)

1. Point A- Pure axial load. The corresponding strain distribution represents uniform axial compression without moment, sometimes referred to as pure axial load.

2. Point B- Zero tension. The strain distribution corresponds to the axial load and bending moment at the onset of crushing of the concrete just as the strain in the reinforcement steel on the opposite face of the column reaches zero.

3. Point C- Balanced failure, compression- controlled limit strain. This point occurs when the tension reinforcement steel yields at the same time that the concrete reaches its maximum strain.

4. Point D: Pure bending. This point corresponding to the pure bending moment and zero axial force.

5.4.1 Point A: Squash Load

The symmetrical columns are subjected to concentric axial loads causing the longitudinal steel and the concrete to deform uniformly. The forces in the concrete and steel are equal to the stresses multiplied by the corresponding areas. Therefore, the axial load capacity of the column is

$$P_u = \alpha_1 f_c^{'}\left(A_g - A_{st}\right) + f_y A_{st} \tag{5.12}$$

where f_y and A_{st} is the yield strength and the total area of the longitudinal reinforcement, respectively; A_g is the gross area of the concrete and α_1 is the reduction factor in accordance with AS 3600-2009 which is calculated as

$$\alpha_1 = 1 - 0.003\, f_c^{'} \text{ within the limit } 0.72 \leq \alpha_1 \leq 0.85 \tag{5.13}$$

$f_c^{'}$ is the compressive strength of the concrete which can be taken as the 28 day cylinder strength $f_{co}^{'}$ for unconfined concrete and $f_{cc}^{'}$ is the confined concrete strength which described in the previous sections.

The value of $f_{co}^{'}$ is the average strength over the entire cross-section including the original concrete and the additional concrete as follows:

$$f_{co}^{'} = \frac{f_{co1}^{'} A_1 + f_{co2}^{'} A_2}{A_1 + A_2} \tag{5.13'}$$

where f'_{co1} and f'_{co2} are respectively the confined concrete strength of the column core and the segmental covers, and A_1 and A_2 are the cross sectional area of the column core and the total cross sectional area of the segmental covers

5.4.2 Points B and C: under eccentric load

For columns subjected to combined bending and axial compression, complete composite action between the concrete and the FRP is assumed and tensile strength of the concrete is ignored. The stress in the concrete in the compression zone is used by the Whitney stress block to transfer non-uniform compressive confined concrete stresses to rectangular distribution of stresses in accordance with AS 3600 (2009) and Bank (2006). The equivalent stress block can be described by two factors, the magnitude of the compressive stress $(\beta f_{cc}^{'})$ and the depth of the equivalent rectangular stress block (γd_n), as shown in Figure 5.5.

$$\beta = 1 - 0.003 f_{cc}^{'} \text{ within the limit } 0.67 \leq \alpha_1 \leq 0.85 \tag{5.14}$$

$$\gamma = 1.05 - 0.007 f_{cc}^{'} \text{ within the limit } 0.67 \leq \alpha_1 \leq 0.85 \tag{5.15}$$

The axial load capacity for the assumed strain distribution is the summation of the axial forces:

$$P = C_c + C_s - T_s \tag{5.16}$$

where C_c is the compressive force in the concrete, C_s is the compressive force in the compression reinforcement and T_s is the tensile force in the tension reinforcement.

For circular columns, the compression zone is a segment of a circle having depth (γd_n), as shown in Figure 5.6. To compute the compressive force, it is necessary to determine the area and centroid of the compression zone. The area of the segment is:

$$A = d^2(\frac{\theta - sin\theta cos\theta}{4}) \tag{5.17}$$

where θ is expressed in radian. The angle can be calculated as:

$$\theta = \text{acos}\left(1 - \frac{2\gamma d_n}{d}\right) \; for \; \gamma d_n \leq \frac{d}{2}; \; \theta \leq 90^0 \tag{5.18}$$

$$\theta = 180 - \text{acos}\left(\frac{2\gamma d_n}{d} - 1\right) \; for \; \gamma d_n > \frac{d}{2}; \; \theta > 90^0 \tag{5.19}$$

Therefore, the compressive load C_c of CFRP-confined concrete for circular columns can be calculated as:

$$C_c = \beta f_{cc}^{'} A \tag{5.20}$$

To calculate the compressive force the compression reinforcement, the strain in the steel can be calculated using the similar triangles, as shown in Figure 5.5:

$$\varepsilon_{sc} = \varepsilon_{cu}(1 - \frac{d_0}{d_n}) \tag{5.21}$$

where ε_{cu} is the ultimate strain taken as 0.003 for unconfined columns and the ultimate strain of FRP-confined concrete defined in Equation 5.8 and 5.10, d_0 is the distance between the extreme tension layer and the centre of the compression reinforcement and d_n is the depth of the neutral axis. Thus, the stress in the compression reinforcement would be:

$$\sigma_{sc} = E_s \varepsilon_{sc} \; for \; \varepsilon_{sc} < \varepsilon_{sy} \tag{5.22}$$

$$\sigma_{sc} = f_{sy} \; for \; \varepsilon_{sc} \geq \varepsilon_{sy} \tag{5.23}$$

where ε_{sy}, f_{sy} and E_s are the yield strain, yield stress and the elastic modulus of the steel. Therefore, the compression force in the compression reinforcement would be:

$$C_s = \sigma_{sc} A_{sc} \tag{5.24}$$

in which A_{sc} is the area of the compression reinforcement. Similarly, the tensile strain and tensile force in the tension reinforcement would be:

$$\varepsilon_{st} = \varepsilon_{cu}(\frac{d^{'}}{d_n} - 1) \tag{5.25}$$

$$T_s = \sigma_{st} A_{st} \tag{5.26}$$

where d' is the distance between the extreme tension layer and the centre of the tension reinforcement and σ_{st}, A_{st} is the tensile stress and the area of the tension reinforcement.

The moment capacity M_n is found by summing the moments of all the internal forces about the centroid of the columns. In this study, the symmetrical columns with symmetrical reinforcement can be calculated as:

$$M = C_c\left(\frac{d}{2} - \frac{\gamma d_n}{d}\right) + C_s\left(\frac{d}{2} - d_0\right) + T\left(d' - \frac{d}{2}\right) \quad (5.27)$$

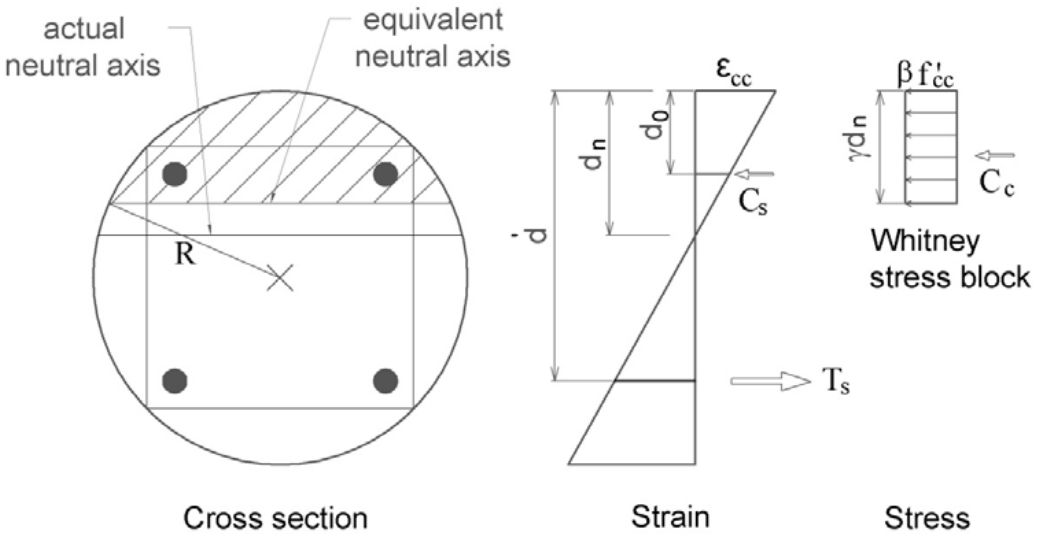

Figure 5.5 Stress and strain over eccentrically loaded column depth

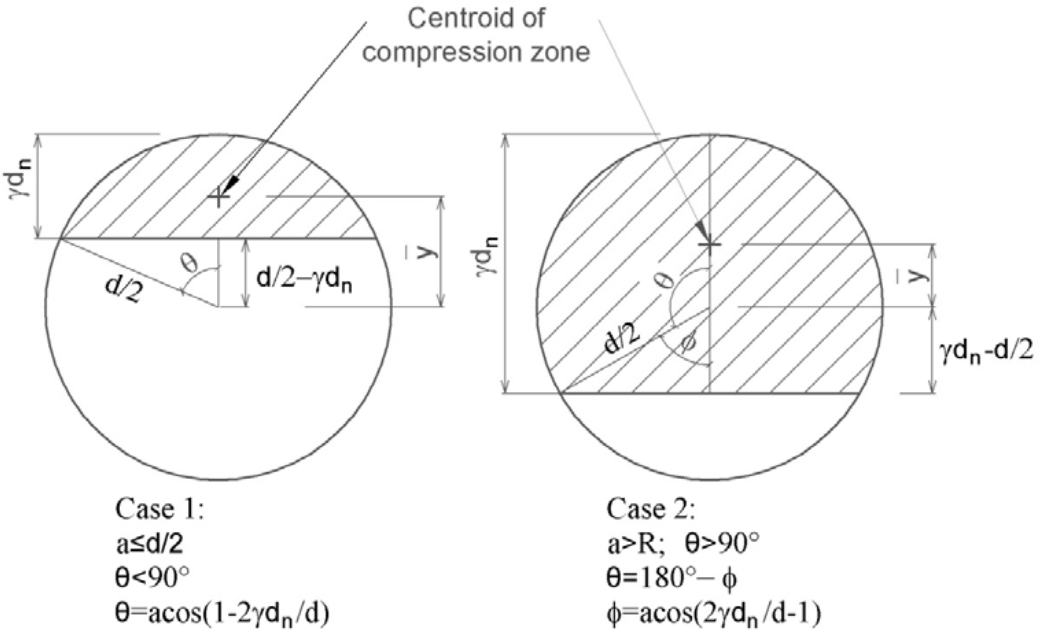

Figure 5.6 Compression zone of circular columns under eccentric loading

5.4.3 Point D: pure bending

For columns under flexural bending, the axial load equals zero. Therefore, a trial and error process (Nawy 2003) is used to determine a specific depth of neutral axis d_n, under which the axial load calculated using Equation 5.16 approaches zero. Then the bending moment of the column under the pure bending load can be computed using the specific d_n.

5.5 Theoretical axial load-bending moment interaction diagram

The theoretical P-M interaction diagrams for the columns can be constructed as described above. For CFRP-confined columns, two models including Lam and Teng (2003a) and Eid and Paultre (2008) were adopted to calculate the compressive strength and corresponding maximum compressive strain of the unconfined concrete. The model of Lam and Teng (2003a) originally features a value of 1.75 instead of 1.5, which for the case of the unconfined concrete yields an ultimate axial strain to 0.0035. This change to 1.5 was necessary to limit the axial strain of the unconfined concrete to 0.003 consistent with ACI-440.2R (2008) and AS 3600 (2009).

The FRP strain efficiency factor is a ratio of the effective strain level in the FRP jackets at failure to the material ultimate tensile strain obtained from the flat coupon tensile tests. Based on experimental results by Xiao and Wu (2000), Pessiki et al (2001), Lam and Teng (2003a, 2004), Carey and Harries (2005), Matthys et al (2005) and Ilki et al. (2008), the FRP strain efficiency factor ranges widely from 0.46 to 0.9 for the concentrically loaded FRP-confined circular specimens. For the case of eccentrically loaded FRP-confined circular columns, very little research on this factor has been concerned due to the non-uniform nature of the CFRP confinement in such columns under eccentric loading. According to ACI-440.2R (2008), the effective strain in the FRP jacket should not be greater than 0.4% to ensure shear integrity of the confined concrete. It is clear that the value of the CFRP efficiency factor is unstable. For these reasons, the experimental program in this study focused on the CFRP strain efficiency factors, as stated in Section 4.7. These factors were 0.653, 0.4 and 0.26 for the specimens under concentric loading, 25 mm eccentric loading and 50 mm eccentric loading, respectively.

The axial load and bending moment was calculated using the aforementioned procedures for all the specimens in the experimental program. Table 5.1 and Figure 5.7 show the theoretical results based upon the Lam and Teng (2003a) model. The results of axial load versus bending moment based upon Eid and Paultre (2008) model are shown in Table 5.2 and Figure 5.8. It can be seen that the retrofitted columns had both a higher axial load-carrying capacity and bending moment than the reference columns. The columns of the C100 group achieved the highest axial load-carrying capacity and bending moment among the four groups, followed by the columns of the C80 group and the C40 group.

Table 5.1 Summary of theoretical results based on Lam and Teng (2003a) model

Group	Point	Ultimate load (kN)	Bending moment (kNm)
R	Point A- Pure axial load	1070	0.00
	Point B- Zero tension	590	19.59
	Point C- Balanced failure	219	22.14
	Point D- Pure bending	0	13.17
C40	Point A- Pure axial load	3269	0.00
	Point B- Zero tension	1165	55.66
	Point C- Balanced failure	758	55.54
	Point D- Pure bending	0	30.39
C80	Point A- Pure axial load	3685	0.00
	Point B- Zero tension	1327	63.51
	Point C- Balanced failure	848	62.43
	Point D- Pure bending	0	30.44
C100	Point A- Pure axial load	3833	0.00
	Point B- Zero tension	1379	66.01
	Point C- Balanced failure	876	64.42
	Point D- Pure bending	0	30.62

Table 5.2 Summary of theoretical results based on Eid and Paultre (2008) model

Group	Point	Ultimate load (kN)	Bending moment (kNm)
R	Point A- Pure axial load	1070	0.00
	Point B- Zero tension	590	19.59
	Point C- Balanced failure	219	22.14
	Point D- Pure bending	0	13.17
C40	Point A- Pure axial load	3420	0.00
	Point B- Zero tension	1234	59.02
	Point C- Balanced failure	943	63.92
	Point D- Pure bending	0	30.39
C80	Point A- Pure axial load	3833	0.00
	Point B- Zero tension	1397	66.87
	Point C- Balanced failure	1220	71.70
	Point D- Pure bending	0	30.44
C100	Point A- Pure axial load	3983	0.00
	Point B- Zero tension	1449	69.37
	Point C- Balanced failure	1270	74.19
	Point D- Pure bending	0	30.62

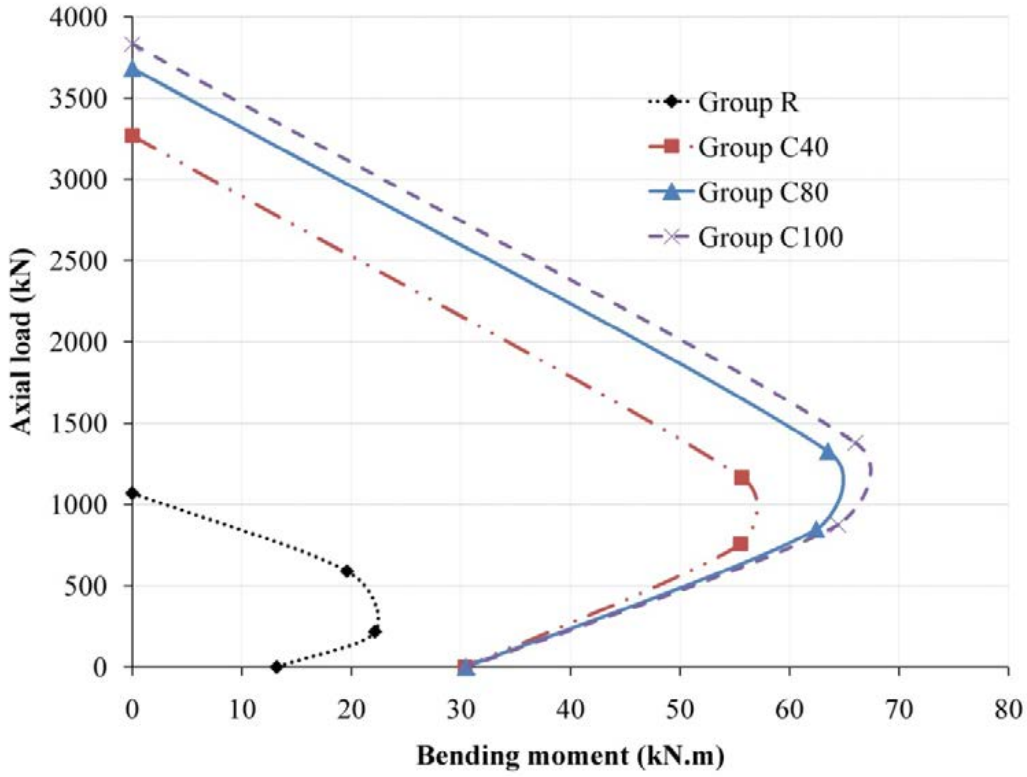

Figure 5.7 Theoretical P-M diagrams of columns based on Lam and Teng (2003a) model

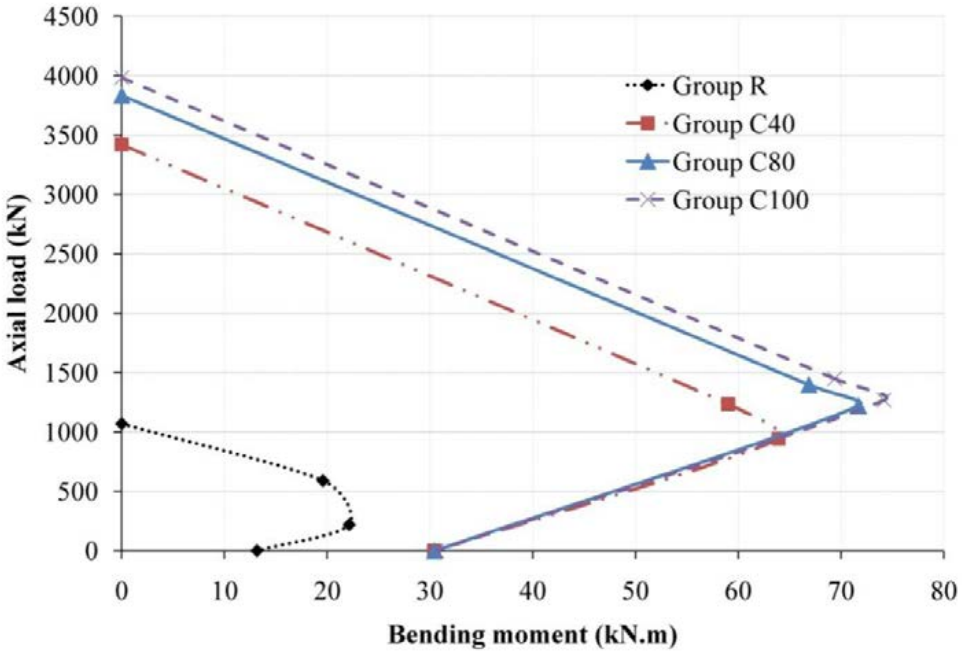

Figure 5.8 Theoretical P-M diagrams of columns based on Eid and Paultre (2008) model

Figure 5.9, Figure 5.10 and Figure 5.11 demonstrate the comparison of the predicted analysis of the retrofitted columns in this experimental program from the models proposed by Lam and Teng (2003a) and Eid and Paultre (2008). The axial load-carrying capacity and bending moment capacity proposed by Eid and Paultre (2008) were always higher than those of the other. The discrepancy between these two models in relation to axial load-carrying capacity for the concentrically loaded columns is 3.92% to 4.59%, respectively. This is because the model of Eid and Paultre (2008) considers the dual confinement of both the transverse steel reinforcement and the CFRP jacket. However, the Lam and Teng (2003a) model does not consider the confining pressure of the transverse steel reinforcement on the performance of retrofitted columns.

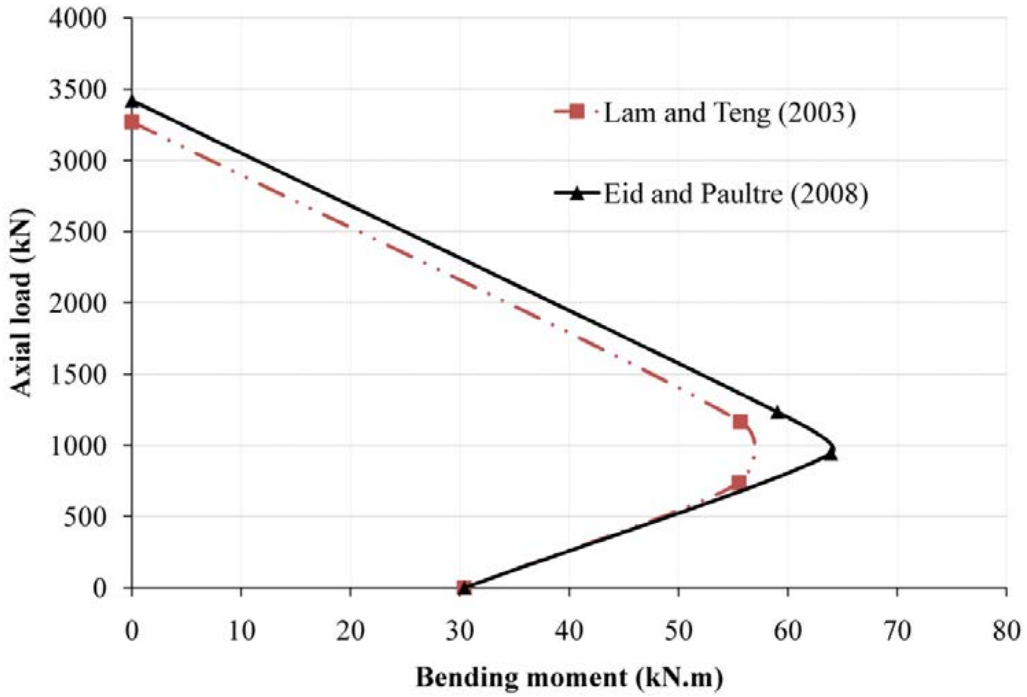

Figure 5.9 Theoretical P-M diagrams of C40 columns

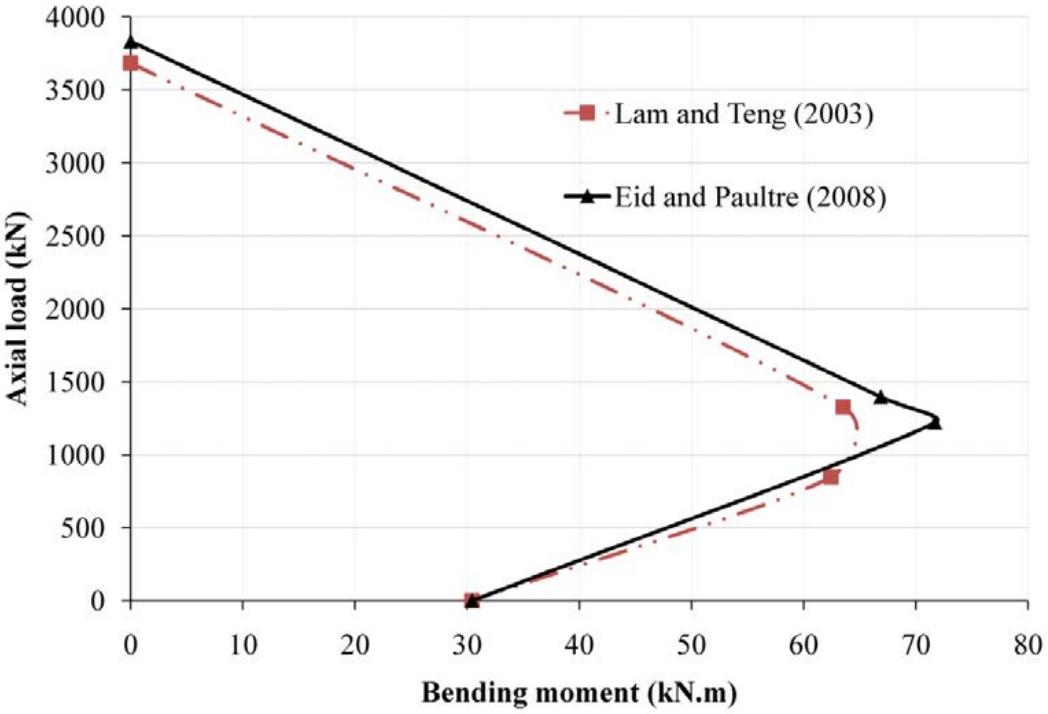

Figure 5.10 Theoretical P-M diagrams of C80 columns

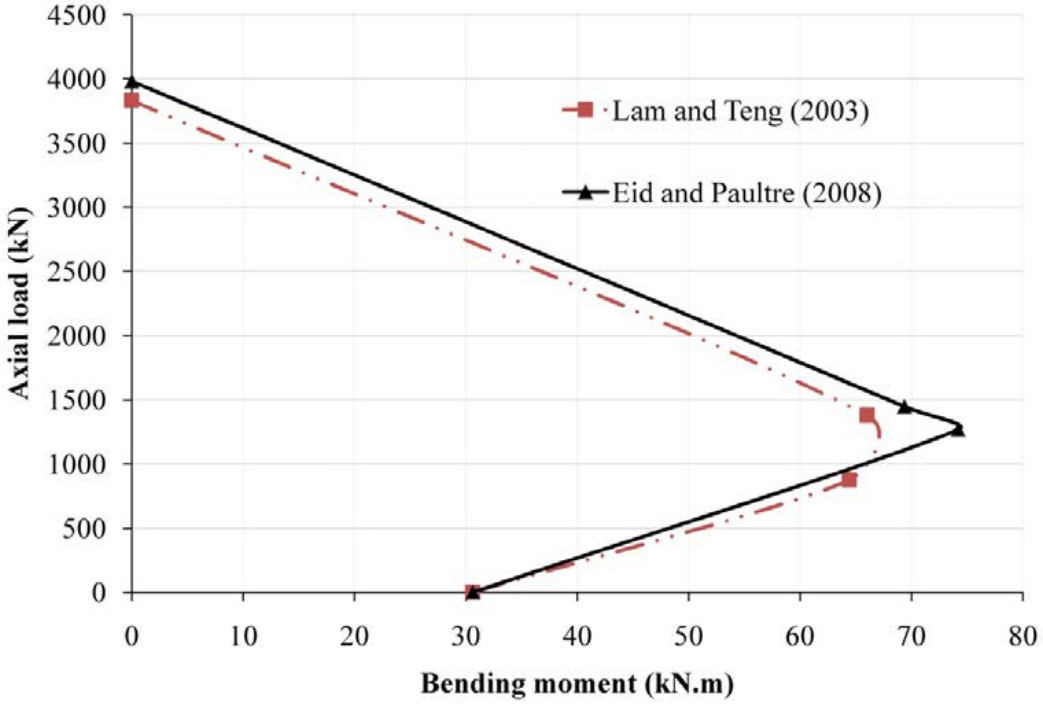

Figure 5.11 Theoretical P-M diagrams of C100 columns

5.6 Validation with experimental results

The aforementioned approach was adopted to carry out the P-M interaction diagrams, which were used to verify the experimental results. Therefore, the theoretical P-M diagrams were constructed based on four points: (a) the pure axial condition; (b) 25 mm eccentric load; (c) 25 mm eccentric load; and (d) the pure flexural condition.

Table 5.3 and Table 5.4 present the predicted results of the tested columns based on the models proposed by Lam and Teng (2003a) and Eid and Paultre (2008), respectively. For better comparison, the theoretical and experimental values are shown separately for each group, as given in Figure 5.12, Figure 5.13, Figure 5.14 and Figure 5.15. As can be seen from the graphs, the estimation was consistently conservative when compared against the experimental results for the columns under concentric, eccentric loading of 25 mm and 50 mm eccentricity. For the columns subjected to pure bending, there was a gap in predicting the columns' performance, up to 34 % discrepancy. This is because the specimen wrapped with CFRP under flexural tests failed in a manner of a combination of flexure and shear as described in Chapter 4. The compression strut in the specimens appeared which resulted in the bending moment capacity. Furthermore, the calculation did not consider the tensile strength of FRP-confined concrete may be effect the results.

Figure 5.13 compares the theoretical value and experimental results of C40 columns. The predicted axial load-carrying capacity for Specimen C40-0 based on Lam and Teng (2003a) model was 2.2% lower than the experimental result, while the estimation based on Eid and Paultre (2008) was 2.3 % higher. For Specimen C40-F, the predicted bending moment values based on both models were underestimated around 32%. For Specimen C80-0, there were 6.4% and 10.7% overestimation of the axial load capacity based on Lam and Teng (2003a) and Eid and Paultre (2008), respectively as shown in Figure 5.14. In general, the analytical predictions based on Lam and Teng (2003a) model were quite closer to the experimental values than that of Eid and Paultre (2008).

Table 5.3 Summary of theoretical results of the tested columns based on Lam and Teng (2003a) model

Specimen	Eccentricity m	Ultimate load (kN)	Bending moment (kN.m)
R-0	0	1070	0.00
R-25	25	688	17.20
R-50	50	425	21.32
R-F	Flexural	0	13.17
C40-0	0	3269	0.00
C40-25	25	1781	44.51
C40-50	50	1117	55.87
C40-F	Flexural	0	30.39
C80-0	0	3685	0.00
C80-25	25	2043	50.83
C80-50	50	1270	63.67
C80-F	Flexural	0	30.44
C100-0	0	3833	0.00
C100-25	25	2120	53.02
C100-50	50	1320	66.14
C100-F	Flexural	0	30.62

Table 5.4 Summary of theoretical results of the tested columns based on Eid and Paultre (2008) model

Specimen	Eccentricity m	Ultimate load kN	Bending moment kNm
R-0	0	1070	0.00
R-25	25	688	17.20
R-50	50	425	21.32
R-F	Flexural	0	13.17
C40-0	0	3420	0.00
C40-25	25	1887	47.24
C40-50	50	1199	60.03
C40-F	Flexural	0	30.39
C80-0	0	3833	0.00
C80-25	25	2147	53.65
C80-50	50	1358	67.93
C80-F	Flexural	0	30.44
C100-0	0	3983	0.00
C100-25	25	2227	55.70
C100-50	50	1406	70.52
C100-F	Flexural	0	30.62

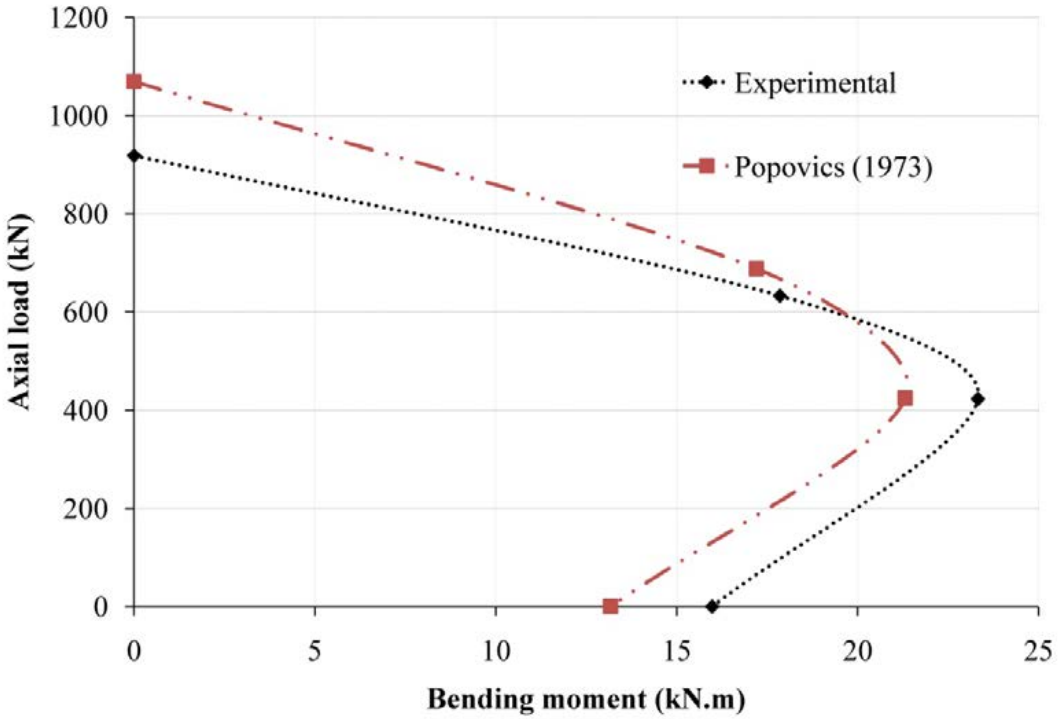

Figure 5.12 Experimental and theoretical P-M diagrams of R columns

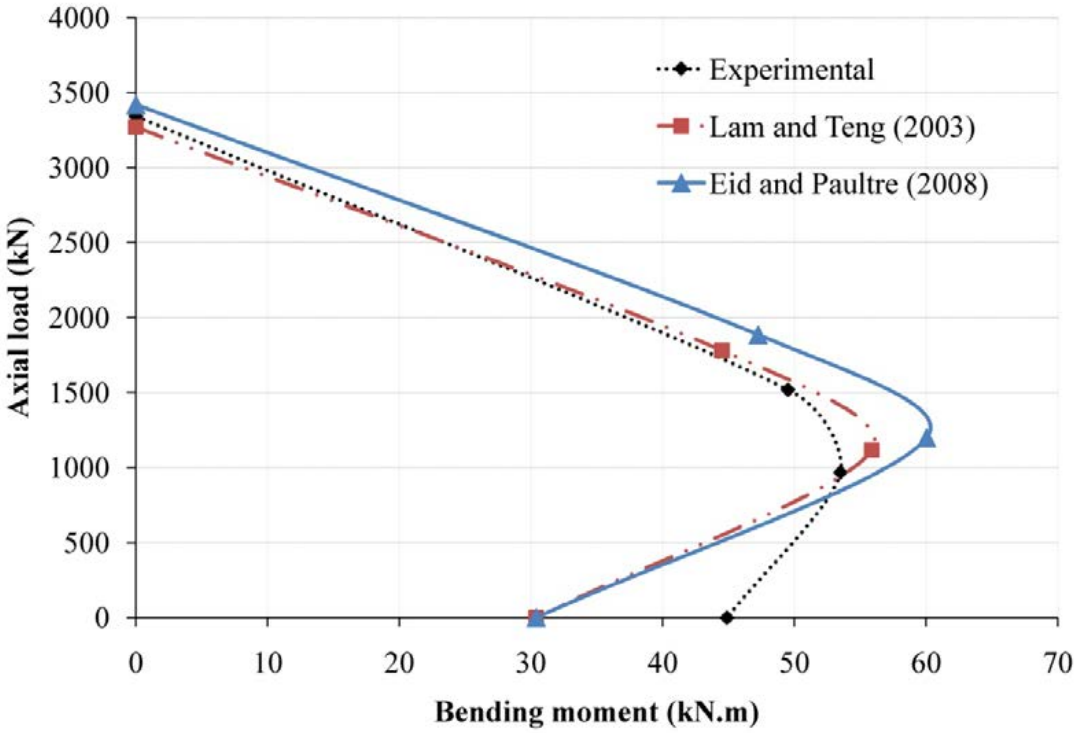

Figure 5.13 Experimental and theoretical P-M diagrams of C40 columns

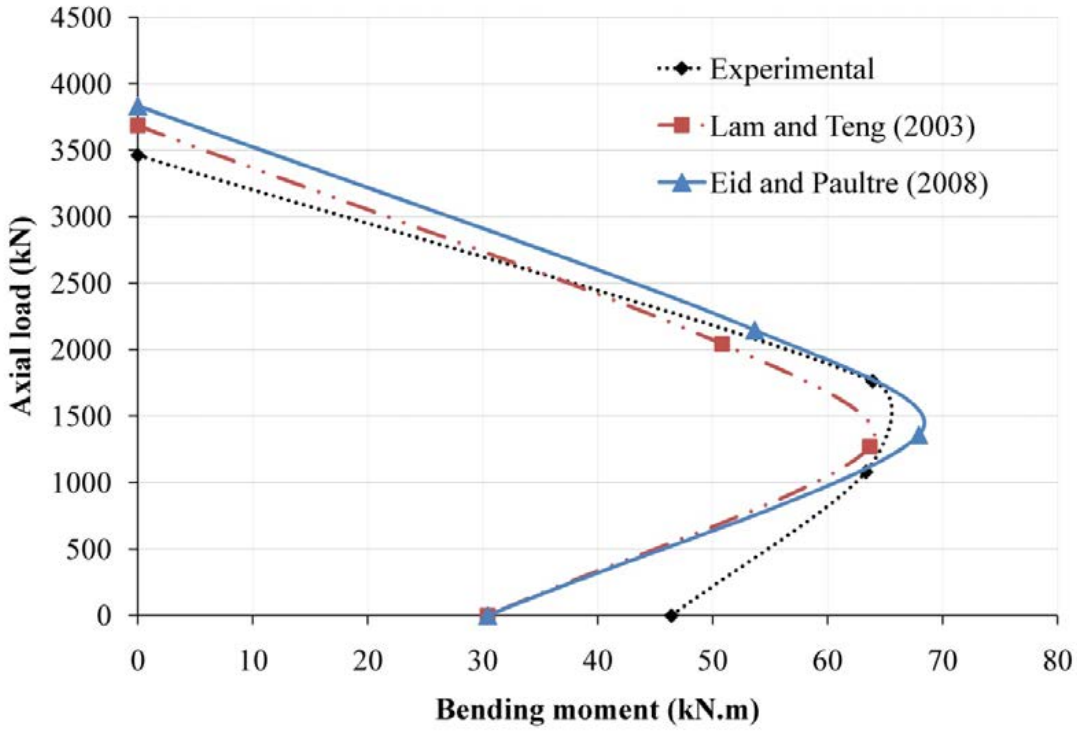

Figure 5.14 Experimental and theoretical P-M diagrams of C80 columns

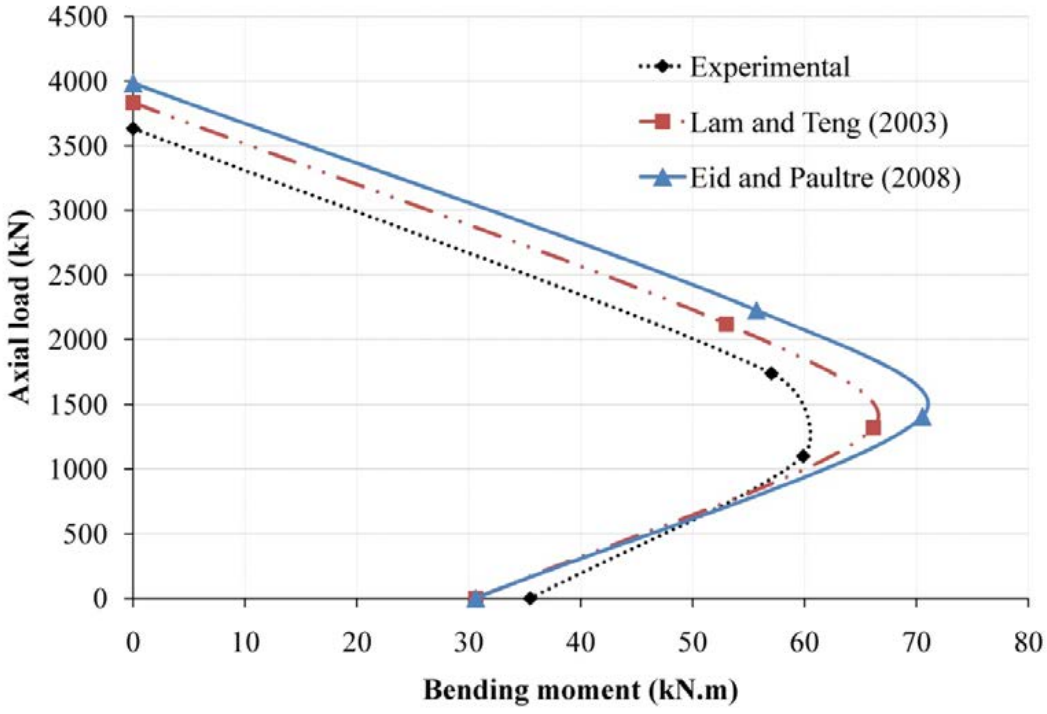

Figure 5.15 Experimental and theoretical P-M diagrams of C100 columns

5.7 Effect of circulation

In this study, the proposed strengthening technique was used effectively in terms of improving the axial load-carrying capacity and ductility of the columns under pure axial load, eccentric loads and flexural bending. The bonding of the original concrete core and segmental circular concrete covers was perfect to failure, as shown in Figure 5.16. Furthermore, the calculated theoretical values were close to the experimental results for different compressive strengths of concrete covers, as stated above. These phenomena proved that the retrofitted columns work as conventional circular columns.

The compressive strengths of concrete covers had the influence on the load-carrying capacity of the columns under concentric loading and eccentric loading. The columns circularised with the higher compressive strength concrete covers achieved a higher load-carrying capacity. The C100 columns (C100-0, C100-25 and C100-50) reached the highest ultimate axial load, followed by the C80 columns and the C40 columns. However, the concrete cover strengths had a negligible effect on the CFRP confinement. The similar second branch of the stress-strain curve of the retrofitted columns proved the same CFRP confinement.

(a) Specimen C80-25 (b) Specimen C100-0

Figure 5.16 Perfect bonding between concrete covers and original core to failure

5.8 Effect of eccentricity

The theoretical results and experimental results of this study have shown that the axial load capacity of both the unconfined and CFRP-confined concrete columns decreased as the loading eccentricity increased. As can be seen in Figure 5.17, the ultimate load of CFRP-confined columns dropped sharply with the increase of eccentricity compared to the unconfined columns. The CFRP-confined columns with an eccentricity of 25 mm demonstrated a 52% drop in their ultimate axial load capacity whereas the unconfined columns demonstrated only a 31% drop. This indicates that the CFRP-confined columns are more sensitive to eccentricity than the unconfined columns.

It is apparent from the results that the effective confinement of CFRP decreased significantly when the columns were subjected to eccentric loading, as shown in Figure 4.14. Under eccentric loading, CFRP confinement was non-uniform and most highly activated near the extreme compression fibre of the cross-section. Under high eccentricity of the load, the confinement provided by the CFRP jacket was less activated and is thus less effective than for the pure axial load.

It was shown that the CFRP ruptured when the maximum CFRP hoop strain reached about 0.68% of the ultimate strain of CFRP from flat coupon tests in the case of both concentrically and eccentrically loaded columns. The concentrically loaded columns confined with CFRP reached the ultimate axial load and CFRP rupture simultaneously. In the case of eccentrically loaded columns confined with CFRP, however, the CFRP rupture did not simultaneously occur when the columns reached the ultimate load, as shown in Figure 4.13. The ultimate axial load of CFRP-confined concrete columns occurred when the CFRP strain at the extreme tension fibre achieved 0.4% (25 mm of eccentricity) and 0.26% (50 mm of eccentricity) of the ultimate strain of CFRP from flat coupon tests. These results show a good agreement with the theoretical study.

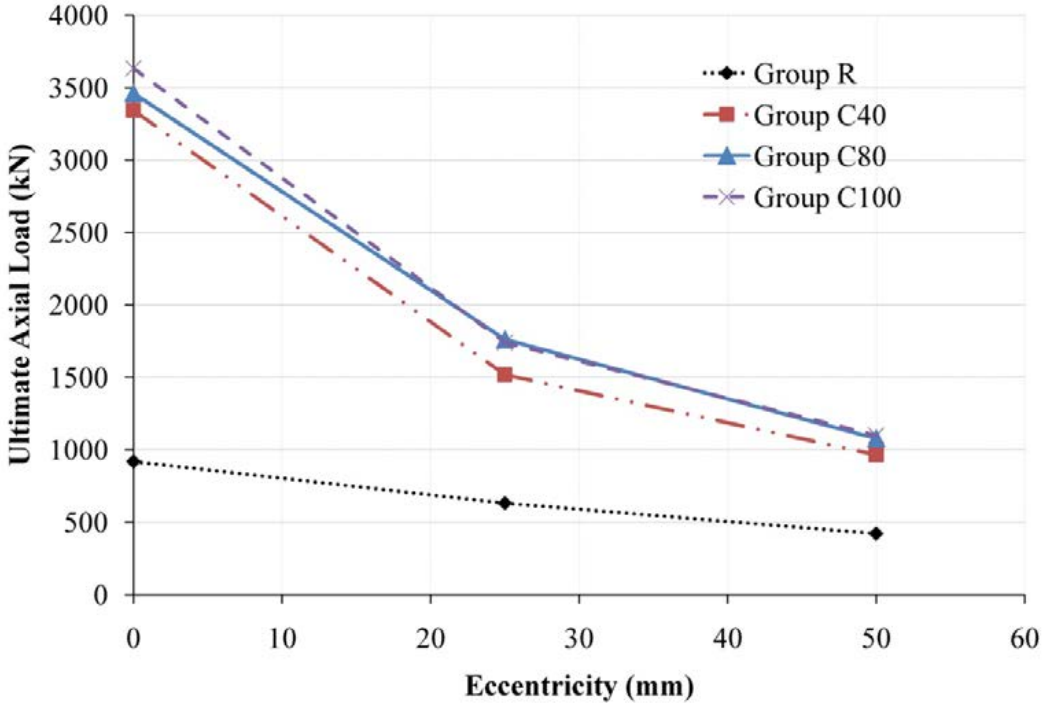

Figure 5.17 Ultimate Axial Load versus Eccentricity diagrams

Both the experimental results and analytical results indicated that the specimens confined with CFRP in the hoop direction had a small effect on the bending moment capacity, which could be consistent with Concrete Society 2012; ACI 440.2R 2008. The retrofitted beams had the higher bending moment than that of reference beams due to the larger cross-sectional area. The analytical values were unpredicted the bending moment capacity because of the failure mode of the beams. The specimens under flexural tests failed in a manner of the combination of shear and flexure resulting in a compression strut, as shown in Figure 4.10. This resulted in some arching action, which tended to increase the bending moment capacity as observed. This phenomenon may be related to the shear span to depth ratio of the specimens less than 2.

5.9 Summary

Theoretical analysis on the P-M behaviour of both the unconfined and FRP-confined concrete columns was carried out in this chapter.

The proposed approaches adopting the Lam and Teng (2003a) and Eid and Paultre (2008) models appeared to be highly conservative for the specimens under concentric

loading and eccentric loading. For the case of the beams, the theoretical results were both shown to underestimate the bending moment capacity. Although the Eid and Paultre (2008) model took into consideration the interaction between the internal lateral steel reinforcement and the external FRP jacket, the results based on Lam and Teng (2003a) showed better prediction of the axial load-carrying capacity and the bending moment capacity.

The next chapter concludes this study and gives a summary of the implication of this study together with the possible future studies.

CHAPTER 6. SUMMARY AND CONCLUSIONS

6.1 Introduction

This thesis has presented a systematic study proposing a retrofitting method for square reinforced concrete columns. The cross-section of RC columns was changed from a square to a circle before wrapping with Carbon Fiber Reinforcement Polymer (CFRP) to maximise their axial load- carrying capacity.

Sixteen specimens, which included the reference columns and modified columns, were tested in this study to understand and compare the performance of the unconfined concrete and FRP-confined concrete columns. The mechanics of confinement provided by the FRP and the failure modes of both the unconfined and confined-FRP specimens subjected to increasing eccentricities have been studied, presented and discussed in detail.

In addition to the experimental program, an analytical approach adopting the Lam and Teng (2003a) and Eid and Paultre (2008) models was developed to predict the axial load-carrying capacity and bending moment interaction diagrams of the sixteen specimens. Both models were compared with the tested data for validation purposes.

In this chapter, the findings of the research and future direction are finally given.

6.2 Conclusions

Based on the experimental and analytical investigations presented in this study, the following conclusions can be drawn:

1. The proposed retrofitting method was used effectively in terms of improving the axial load-carrying capacity and ductility of the columns subjected to concentric loading, eccentric loading and flexural bending. The load-carrying capacity of the modified columns was up to 4 times higher compared to the reference columns.

2. The bonding of the original concrete core and segmental circular concrete covers was perfect. This observation proves that the two concrete components worked as a composite material to failure.
3. The effect of segmental concrete cover compressive strength on CFRP confinement is insignificant. The similar second branch of the stress-strain curve of the retrofitted columns proved the same CFRP confinement.
4. The performance of CFRP-confined columns was sensitive to eccentricity of loads due to the CFRP confinement mechanism. The axial load-carrying capacity and ductility of columns decreased significantly under eccentric loading.
5. The CFRP strain measured from the overlap zone is lower than from outside the overlap zone. The CFRP rupture strains at the extreme compression fibre under eccentric loading were quite similar to the value of CFRP rupture strain under concentric loading. At the ultimate axial load, however, the ratio of CFRP strain at the extreme compression fibre and the ultimate strain of CFRP from flat coupon tests decreased with increasing load eccentricities.
6. The disproportion between the CFRP strain at the extreme compression fibre and at the extreme tension fibre increased when the columns were subjected to higher eccentricity.

Overall, the proposed method has been shown to be effective in enhancing the load-carrying capacity and ductility of CFRP confined square column under all loading conditions. It has also been found that the value of the CFRP strain efficiency factor is different under different eccentricities.

6.3 Recommendations for future research

The focus of the experimental and analytical aspects of this study was examined the performance of shape-modified columns confined with CFRP under various loading conditions. It has been shown that circularisation maximises the FRP confining pressure resulting in the improvement of the load-carrying capacity and ductility of confined columns. Despite these encouraging findings, the behaviour of FRP-

confined concrete columns subjected to eccentric loading still remain unclear. Below are recommendation for future research:

1. Extending the proposed technique to larger cross-section columns and taller columns, which may affect the behaviour of FRP-confined concrete. The load-carrying capacity and ductility of these columns can be investigated by both experimental program and numerical analysis.

2. Investigating the FRP strain efficiency factor for various cross-section columns including square, elliptical and circular columns under loading of different eccentricities. Understanding about the FRP confining pressure would modify the FRP stress-strain model in case of FRP-confined concrete at various load eccentricities.

3. Further investigating the interaction of internal steel reinforcement and FRP jacket. The amount of internal steel reinforcement may have an influence on the rupture of FRP in confined columns, which leads to an accurate stress-strain model for design use.

REFERENCES

ACI 440.2R-08 (2008). “Guide for the Design and Construction of Externally Bonded FRP Systems for Strengthening Concrete Structures.” American Concrete Institute.

AS 3600 (2009). “Concrete Structures.” Australian Standard 3600:2009, SAI Global database.

ASTM (2010). "Determining Tensile Properties of Fiber Reinforced Polymer Matrix Composites Used for Strengthening of Civil Structures." D7565/D7565M – 10, United States

Bank, L. C. (2006). *Composites for construction: structural design with FRP materials*, John Wiley & Sons, Hoboken, N.J, USA.

Bisby, L., and Ranger, M. (2010). "Axial-flexural interaction in circular FRP-confined reinforced concrete columns." *Construction and Building Materials*, 1672-1681.

Campione, G., and Miraglia, N. (2003). "Strength and strain capacities of concrete compression members reinforced with FRP." *Cement and Concrete Composites*, 25(1), 31-41.

Carey, S. A., and Harries, K. A. (2005). "Axial behavior and modeling of confined small-, medium-, and large-scale circular sections with carbon fiber-reinforced polymer jackets." *ACI Structural Journal*, 102(4), 596-604.

Cedolin, L., Crutzen, Y. R. J., and Dei Poli, S. (1977). "Triaxial stress-strain relationship for concrete." *ASCE J Eng Mech Div*, 423-439.

Chun, S. S., and Park, H. C. (2002). "Load carrying capacity and ductility of RC columns confined by carbon fiber reinforced polymer." *Proc., 3rd Int. Conf. on Composites in Infrastructure (CD-Rom).*

Csuka, B., and Kolla´r, L. P. (2011). "FRP-confined circular columns subjected to eccentric loading." *Journal of Reinforced Plastics and Composites*, 30(14), 1167-1178.

Csuka, B., and Kollár, L. P. (2012). "Analysis of FRP confined columns under eccentric loading." *Composite Structures*, 94(3), 1106-1116.

Concrete Society Technical Report 55 (2012). "Design guidance for strengthening concrete structures using fibre composite materials." The Concrete Society, Camberley, UK.

Cusson, D., and Paultre, P. (1995). "Stress-strain model for confined high-strength concrete." *Journal of structural engineering New York, N.Y.*, 121(3), 468-477.

De Lorenzis, L., and Tepfers, R. (2003). "Comparative study of models on confinement of concrete cylinders with fiber-reinforced polymer composites." *Journal of Composites for Construction*, 7(3), 219-237.

Eid, R., and Paultre, P. (2007). "Plasticity-based model for circular concrete columns confined with fibre-composite sheets." *Engineering Structures*, 29(12), 3301-3311.

Eid, R., and Paultre, P. (2008). "Analytical Model for FRP-Confined Circular Reinforced Concrete Columns." *Journal of Composites for Construction*, 12(5), 541.

Fam, A., Flisak, B., and Rizkalla, S. (2003). "Experimental and analytical modeling of concrete-filled fiber-reinforced polymer tubes subjected to combined bending and axial loads." *ACI Structural Journal*, 100(4), 499-509.

Fam, A. Z., and Rizkalla, S. H. (2001). "Confinement model for axially loaded concrete confined by circular fiber-reinforced polymer tubes." *ACI Structural Journal*, 98(4), 451-461.

Fardis, M. N., and Khalili, H. (1981). "Concrete encased in fiberglass-reinforced plastic." *ACI Journal*, 78(6), 440-446.

Fardis, M. N., and Khalili, H. H. (1982). "FRP-Encased Concrete as a Structural Material." *Magazine of Concrete Research*, 34(121), 191-202.

Guan, H., Wang, Q., and Ruan, B. (2011). "Experimental Investigation and Analytical Modeling of Eccentrically Loaded Composite Short Columns Confined with Glass Fiber-Reinforced Polymer Tube."Guangzhou, 143-151.

Hadi, M., Pham, T., and Lei, X. (2013). "New Method of Strengthening Reinforced Concrete Square Columns by Circularizing and Wrapping with Fiber-Reinforced Polymer or Steel Straps." *Journal of Composites for Construction*, 17(2), 229-238.

Hadi, M. N. S. (2006). "Behaviour of FRP wrapped normal strength concrete columns under eccentric loading." *Composite Structures*, 72(4), 503-511.

Hadi, M. N. S. (2007). "Behaviour of FRP strengthened concrete columns under eccentric compression loading." *Composite Structures*, 77(1), 92-96.

Hadi, M. N. S. (2009). "Behaviour of eccentric loading of FRP confined fibre steel reinforced concrete columns." *Construction and Building Materials*, 23(2), 1102-1108.

Hadi, M. N. S. (2010). "Behaviour of reinforced concrete columns wrapped with fibre reinforced polymer under eccentric loads." *Australian Journal of Structural Engineering*, 169.

Hadi, M. N. S., and Widiarsa, I. B. R. (2012). "Axial and Flexural Performance of Square RC Columns Wrapped with CFRP under Eccentric Loading." *Journal of Composites for Construction*, 244.

Harajli, M. H., Hantouche, E., and Soudki, K. (2006). "Stress-strain model for fiber-reinforced polymer jacketed concrete columns." *ACI Structural Journal*, 103(5), 672-682.

Harries, K. A., and Carey, S. A. (2003). "Shape and “gap” effects on the behavior of variably confined concrete." *Cement and Concrete Research*, 33(6), 881-890.

Hognestad, E. (1951). "Study of combined bending and axial load in reinforced concrete members." *University of Illinois. Engineering Experiment Station. Bulletin ; no. 399*.

Ilki, A., Peker, O., Karamuk, E., Demir, C., and Kumbasar, N. (2008). "FRP retrofit of low and medium strength circular and rectangular reinforced concrete columns." *Journal of Materials in Civil Engineering*, 20(2), 169-188.

Imran, I., and Pantazopoulou, S. J. (1996). "Experimental study of plain concrete under triaxial stress." *ACI Materials Journal*, 93(6), 589-601.

Lam, L., and Teng, J. G. (2003a). "Design-oriented stress-strain model for FRP-confined concrete." *Construction and Building Materials*, 17(6-7), 471-489.

Lam, L., and Teng, J. G. (2003b). "Design-oriented stress-strain model for FRP-confined concrete in rectangular columns." *Journal of Reinforced Plastics and Composites*, 22(13), 1149-1186.

Lam, L., and Teng, J. G. (2004a). "Ultimate condition of fiber reinforced polymer-confined concrete." *Journal of Composites for Construction*, 8(6), 539-548.

Lan, S. G., and Guo, Z. H. (1997). "Experimental investigation of multiaxial compressive strength of concrete under different stress paths." *ACI Materials Journal*, 94(5), 427-434.

Lee, J. Y., Yi, C. K., Jeong, H. S., Kim, S. W., and Kim, J. K. (2010). "Compressive Response of Concrete Confined with Steel Spirals and FRP Composites." *Journal of Composite Materials*, 44(4), 481-504.

Légeron, F., and Paultre, P. (2003). "Uniaxial confinement model for normal- and high-strength concrete columns." *Journal of Structural Engineering*, 129(2), 241-252.

Li, J., and Hadi, M. N. S. (2003). "Behaviour of externally confined high-strength concrete columns under eccentric loading." *Composite Structures*, 62(2), 145-153.

Maaddawy, T. E. (2009). "Strengthening of Eccentrically Loaded Reinforced Concrete Columns with Fiber-Reinforced Polymer Wrapping System: Experimental Investigation and Analytical Modeling." *Journal of Composites for Construction*, 13(1), 13-24.

Madas, P., and Elnashai, A. S. (1992). "A new passive confinement model for the analysis of concrete structures subjected to cyclic and transient dynamic loading." *Earthquake Engineering & Structural Dynamics*, 21(5), 409-431.

Mander, J. B., Priestley, M. J. N., and Park, R. (1988a). "Theoretical stress-strain model for confined concrete." *Journal of Structural Engineering New York, N.Y.*, 114(8), 1804-1826.

Mander, J. B., Priestley, M. J. N., and Park, R. (1988b). "Observed stress-strain behavior of confined concrete." *Journal of Structural Engineering New York, N.Y.*, 114(8), 1827-1849.

Matthys, S., Toutanji, H., Audenaert, K., and Taerwe, L. (2005). "Axial load behavior of large-scale columns confined with fiber-reinforced polymer composites." *ACI Structural Journal*, 102(2), 258-267.

Mirmiran, A., and Shahawy, M. (1996). "A new concrete-filled hollow FRP composite column." *Composites Part B: Engineering*, 27(3-4), 263-268.

Mirmiran, A., and Shahawy, M. (1997). "Behavior of Concrete Columns Confined by Fiber Composites." *Journal of Structural Engineering*, 123(5), 583.

Mirmiran, A., Shahawy, M., Samaan, M., Echary, H. E., Mastrapa, J. C., and Pico, O. (1998). "Effect of Column Parameters on FRP-Confined Concrete." *Journal of Composites for Construction*, 2(4), 175.

Moran, D. A., and Pantelides, C. P. (2002). "Stress-strain model for fiber-reinforced polymer-confined concrete." *Journal of Composites for Construction*, 6(4), 233-240.

Nawy, E. G. (2003). *Reinforced concrete: a fundamental approach*, Prentice Hall, New Jersy.

Pantazopoulou, S. J., and Mills, R. H. (1995). "Microstructural aspects of the mechanical response of plain concrete." *ACI Structural Journal*, 92(6), 605-616.

Parvin, A., and Wang, W. (2001). "Behavior of FRP Jacketed Concrete Columns under Eccentric Loading." *Journal of Composites for Construction*, 5(3), 146-152.

Parvin, A., and Wang, W. (2002). "Concrete columns confined by fiber composite wraps under combined axial and cyclic lateral loads." *Composite Structures*, 58(4), 539-549.

Pellegrino, C., and Modena, C. (2010). "Analytical model for FRP confinement of concrete columns with and without internal steel reinforcement." *Journal of Composites for Construction*, 14(6), 693-705.

Pessiki, S., Harries, K. A., Kestner, J. T., Sause, R., and Ricles, J. M. (2001). "Axial behavior of reinforced concrete columns confined with FRP jackets." *Journal of Composites for Construction*, 5(4), 237-245.

Pessiki, S., and Pieroni, A. (1997). "Axial load behavior of large-scale spirally-reinforced high-strength concrete columns." *ACI Structural Journal*, 94(3), 304-314.

Popovics, S. (1973). "A numerical approach to the complete stress-strain curve of concrete." *Cement and Concrete Research*, 3(5), 583-599.

Priestley, M. J. N., and Seible, F. (1995). "Design of seismic retrofit measures for concrete and masonry structures." *Construction and Building Materials*, 9(6), 365-377.

Priestley, M. J. N., Seible, F., and Calvi, G. M. (1996). *Seismic design and retrofit of bridges*, Wiley, New York.

Richard, R. M., and Abbott, B. J. (1975). "Versatile elastic-plastic stress-strain formula." *J. Struct. Engrg., ASCE*, 101(4), 511-515.

Richart, F. E., Brandtzæg, A., and Brown, R. L. (1929). *The failure of plain and spirally reinforced concrete in compression*, Engineering Experiment Station,

University of Illinois, Urbana, bulletin 190.

Richart, F. E., Brandtzaeg, A., and Brown, R. L. (1928). "A study of the failure of concrete under combined compressive stresses." *Engineering Experiment Station*, University of Illinois, Urbana, bulletin 185.

Rocca, S., Galati, N., and Nanni, A. (2009). "Interaction diagram methodology for design of FRP-confined reinforced concrete columns." *Construction and Building Materials*, 23(4), 1508-1520.

Rochette, P., and Labossière, P. (2000). "Axial testing of rectangular column models confined with composites." *Journal of Composites for Construction*, 4(3), 129-136.

Saadatmanesh, H., Ehsani, M. R., and Li, M. W. (1994). "Strength and ductility of concrete columns externally reinforced with fiber-composite straps." *ACI Structural Journal*, 91(4), 434-447.

Samaan, M., Mirmiran, A., and Shahawy, M. (1998). "Model of concrete confined by fiber composites." *Journal of Structural Engineering-ASCE*, 124(9), 1025-1031.

Sfer, D., Carol, I., Gettu, R., and Etse, G. (2002). "Study of the behavior of concrete under triaxial compression." *Journal of Engineering Mechanics*, 128(2), 156-163.

Sheikh, S. A., and Uzumeri, S. M. (1980). "Strength and Ductility of Tied Concrete Columns." *ASCE J Struct Div*, 106(5), 1079-1102.

Silva, M. A. G. (2011). "Behavior of square and circular columns strengthened with aramidic or carbon fibers." *Construction and Building Materials*, 25(8), 3222-3228.

Spoelstra, M. R., and Monti, G. (1999). "FRP-Confined Concrete Model." *Journal of Composites for Construction*, 3(3), 143.

Tastani, S. P., Pantazopoulou, S. J., Zdoumba, D., Plakantaras, V., and Akritidis, E. (2006). "Limitations of FRP jacketing in confining old-type reinforced concrete members in axial compression." *Journal of Composites for Construction*, 10(1), 13-25.

Teng, J. G., and Lam, L. (2002). "Compressive behavior of carbon fiber reinforced polymer-confined concrete in elliptical columns." *Journal of Structural Engineering*, 128(12), 1535-1543.

Toutanji, H., Han, M., Gilbert, J., and Matthys, S. (2010). "Behavior of large-scale rectangular columns confined with FRP composites." *Journal of Composites for Construction*, 14(1), 62-71.

Toutanji, H. A. (1999). "Stress-strain characteristics of concrete columns externally confined with advanced fiber composite sheets." *ACI Structural Journal*, 96(3), 397-404.

Wang, Y. C., and Restrepo, J. I. (2001). "Investigation of concentrically loaded reinforced concrete columns confined with glass fiber-reinforced polymer jackets." *ACI Structural Journal*, 98(3), 377-385.

William, K. J., and Warnke, E. P. (1975). "Constitutive model for the triaxial behaviour of concrete " *Proc., Int. Assoc. Bridge Structural Eng., 19, pp. 1-30*.

Wu, Y. F., and Jiang, C. (2012). "Effect of load eccentricity on the stress-strain relationship of FRP-confined concrete columns." *Composite Structures*.

Xiao, Y., and Wu, H. (2000). "Compressive behavior of concrete confined by carbon fiber composite jackets." *Journal of Materials in Civil Engineering*, 12(2), 139-146.

Xiao, Y., and Wu, H. (2003). "Compressive behavior of concrete confined by various types of FRP composite jackets." *Journal of Reinforced Plastics and Composites*, 22(13), 1187-1202.

Yan, Z., and Pantelides, C. P. (2006). "Fiber-Reinforced Polymer Jacketed and Shape-Modified Compression Members: II-Model." *ACI Structural Journal*, 103(6), 894.

Yan, Z., and Pantelides, C. P. (2011). "Concrete column shape modification with FRP shells and expansive cement concrete." *Construction and Building Materials*, 25(1), 396-405.

Yan, Z., Pantelides, C. P., and Reaveley, L. D. (2006). "Fiber-Reinforced Polymer Jacketed and Shape-Modified Compression Members: I-Experimental Behavior." *ACI Structural Journal*, 103(6), 885.

Yan, Z., Pantelides, C. P., and Reaveley, L. D. (2007). "Posttensioned FRP Composite Shells for Concrete Confinement." *Journal of Composites for Construction*, 11(1), 81-90.

Yazici, V., and Hadi, M. N. S. (2009). "Axial Load-Bending Moment Diagrams of Carbon FRP Wrapped Hollow Core Reinforced Concrete Columns." *Journal of Composites for Construction*, 13(4), 262-268.